2014

Structure-Property Relationships in Polybenzimidazole Materials for Gas Separation and Fuel Cell Applications

Xin Li
University of South Carolina - Columbia

STRUCTURE-PROPERTY RELATIONSHIPS IN POLYBENZIMIDAZOLE MATERIALS FOR GAS SEPARATION AND FUEL CELL APPLICATIONS

by

Xin Li

Bachelor of Science
Nankai University, 2009

Submitted in Partial Fulfillment of the Requirements

For the Degree of Doctor of Philosophy in

Chemistry

College of Arts and Sciences

University of South Carolina

2014

Accepted by:

Brian C. Benicewicz, Major Professor

Chuanbing Tang, Committee Member

Thomas Vogt, Committee Member

John W. Weidner, Committee Member

Lacy Ford, Vice Provost and Dean of Graduate Studies

DEDICATION

This dissertation is dedicated to my loving parents, Yanjing Xing and Wenjun Li, and also my grandfather, Fuhe Li. Without your unconditional love and support, none of this would be possible.

I also dedicate this work to my dear wife, Nan Jiang. Thank you for being with me all the time through the good and the bad. You encouragement, support and love are always my motivation.

ACKNOWLEDGEMENTS

First and foremost I want to express my deepest thanks to my Ph.D. advisor, Dr. Brian Benicewicz; for his tremendous encouragement and support on my graduate study. He has taught me, both consciously and unconsciously, how a scientific problem is analyzed and solved and how good chemistry is done. More importantly, I always enjoyed our conversations on a variety of topics, within and beyond the science, which broadened my understanding of the world and taught me how to be a better person. I am always very proud of being a part of Benicewicz group.

Then I would like to thank my collaborators from Los Alamos National Laboratory, Dr. Kathryn Berchtold and Dr. Rajinder Singh, for their tremendous discussions and guidance on my work. I also appreciate the opportunity to visit their lab in 2012, which is a great memory in my life.

I also thank the other members of my thesis committee - Dr. Chuanbing Tang, Dr. Thomas Vogt, and Dr. John Weidner - for their advice and encouragement throughout my candidacy.

Finally, it is my honor to have worked with all the current and former members from Benicewicz group. Guoqing, Kayley, Max, Anand, Alex, Junting, and Lei – thank everyone for helping me complete my doctorate and I enjoyed the time working with you.

ABSTRACT

The central theme of my research lies in the investigation of novel polybenzimidazole (PBI)-based materials for different energy related applications ranging from proton exchange membrane fuel cells (PEMFC) to high temperature gas separation. With the aid of a deeper understanding of the structure-property relationships in this class of materials, a better control on PBI chemistry - from monomer structure to polymer morphology to membrane/film processing method was able to be performed in order to achieve greater performance in targeted applications.

In Chapter 1, the overall background of two energy related applications - fuel cells and gas separation was first introduced as well as their recent developments based on polymeric materials. Next, the history of PBI materials and the role they are playing in these two main areas were briefly discussed. Major research objectives of my doctoral study were described in the end.

The first section of the dissertation, on the synthesis and characterization of novel PBI materials for fuel cell uses was provided in Chapter 2 and Chapter 3. In Chapter 2, the synthesis and characterization of phenylindane-containing PBI for high-temperature polymer electrolyte membrane fuel cells was described. The introduction of a bulky, rigid, and bent phenylindane moiety into the PBI background help the PBI achieve greater solubility in organic solvents, which has been a challenging topic in the PBI industry, and also better proton conductivity and fuel cell performance. Chapter 3 described the

synthesis and characterization of a new fluorine-containing PBI for high-temperature polymer electrolyte membrane fuel cells. In this chapter, a new synthetic route of a fluorine-containing monomer (2,2'-bis(trifluoromethyl)-4,4'-biphenyldicarboxylic acid) was introduced. The PBI based on this new fluorine-containing monomer exhibited better organo-solubility and also better oxidative stability. These two new PBIs broadened our knowledge in PBI chemistry and provided new potential candidates for fuel cell related applications.

The second part of the dissertation is the understanding the structure-property relationships in PBI films for high temperature gas separation (Chapter 4 and Chapter 5). In Chapter 4, the influence of PBI main chain structures on H_2/CO_2 separation at elevated temperatures was studied and discussed. Four PBI derivatives with different main chain structures were designed to exhibit highly localized mobility at high temperatures, contain rigid and bent configurations that frustrated close chain packing, or possess bulky side groups. These PBIs were found to exhibit much improved H_2 permeability (up to 997.2 barrer) compared with base m-PBI (76.81 barrer) at 250 °C and 50 psia. Chapter 5 introduced random PBI based copolymers containing hexafluoroisopropylidene functional groups for gas separations at elevated temperatures. It was found that by using a random copolymerization method, a relative control can be realized on the free volume cavity size and concentration within the polymers and also on materials corresponding H_2/CO_2 separation performance (gas permeability & selectivity).

TABLE OF CONTENTS

LIST OF TABLES

LIST OF FIGURES

List of Abbreviations

AFC ..... Alkaline Fuel Cell

DMAc ..... N,N-dimethylacetamide

DMF ..... N,N-dimethylformamide

DMSO ..... Dimethyl Sulfoxide

DPIP ..... Diphenylisophthalate

FFV ..... Fractional Free Volume

FTM ..... Facilitated Transport Membrane

GDE ..... Gas Diffusion Electrode

HT-PEMFC ..... High Temperature Proton Exchange Membrane

IGCC ..... Integrated Gasification Combined Cycle

IPA ..... Isophthalic Acid

MCFC ..... Molten Carbonate Fuel Cell

MEA ..... Membrane Electrode Assembly

MMM ..... Mixed Matrix Membrane

NGL ..... Natural Gas Liquid

NMP N-methyl-2-pyrrolidinone

OCV ..... Open Circuit Voltage

PA ..... Phosphoric Acid

PAFC ..... Phosphoric Acid Fuel Cell

PA/RU ..... Phosphoric Acid per Polymer Repeat Unit

PBI ..... Polybenzimidazole

PDMS.....Polydimethylsiloxane

PEEK.....Polyetheretherketone

PEEKK.....Polyetheretherketoneketone

PEM .....Proton Exchange Membrane

PEMFC .....Proton Exchange Membrane Fuel Cell

PES..... Polyethersulfone

PFSA .....Perfluorosulfonic Acid

PI.....Polyimide

PPA .....Poly(phosphoric acid)

PSA .....Pressure Swing Adsorption

PSF..... Polysulfone

PTA..... Phosphotungstic Acid

PTFE .....Polytetrafluoroethylene

Syngas .....Synthesis Gas

SOFC.....Solid Oxide Fuel Cell

TAB.....Tertraaminobiphenyl

WXRD .....Wide Angle X-ray Diffraction

CHAPTER 1

INTRODUCTION

1.1 Fuel Cells

1.1.1 Fuel Cell Fundamentals

A fuel cell is an electrochemical device that converts chemical energy from fuel into electrical energy or electricity through an electrochemical reaction with oxidant (e.g., oxygen) [1]. Compared with other energy conversion devices such as internal combustion engine and batteries, it possesses several advantages such as broad fuel choices (e.g., hydrogen, methane and methanol), high energy conversion efficiency (up to 80%, not thermodynamically restricted by the Carnot efficiency), no need for recharging, and environmentally friendly (no pollutant emissions, the only chemical byproduct is water) [2-4]. Therefore, fuel cells represent a clean and promising alternative to conventional technologies for utilizing hydrocarbon fuel resources in various applications.

The concept of a fuel cell was demonstrated by Humphry Davy in 1801 and the first fuel cell (called the gas voltaic battery then) was invented by lawyer and scientist William Grove in 1839 [5]. As shown in Figure 1.1 (1), it is known that water can be split into its constituents – hydrogen and oxygen – due to an electric current being passed through it. On the contrary, when replacing the power supply with an ammeter (shown in Figure 1.1 (b)), this electrolysis procedure can be reversed and a small current is generated [3]. From then until early 1900s, many people tried to invent a fuel cell which could directly convert a hydrocarbon or coal into electricity. However, these attempts failed due to the lack of knowledge in materials chemistry and electricity. During the late 1950s, the large interest in fuel cell technology came from NASA's space program that developed fuel cell generators for manned space missions. During that period, the first proton exchange membrane fuel cell (PEMFC) was invented by General Electric (GE).

Although the fuel cell technology development continued in the 1970s and 1980s and a bright future for this technology was widely predicted around that time, only limited fuel cell devices actually appeared due to the poor cell performance, high cost and other technical limitations. Due to the growing concern in energy production, economic growth and environmental sustainability, attention was again turned to fuel cell technology in the 1990s. Fuel cells began to become commercial in several applications in 2007 and growth in shipments of fuel cell has accelerated rapidly since more applications have become commercial (Figure 1.2). The detailed descriptions and discussions about the history and the development of fuel cells can be found elsewhere [6-9].

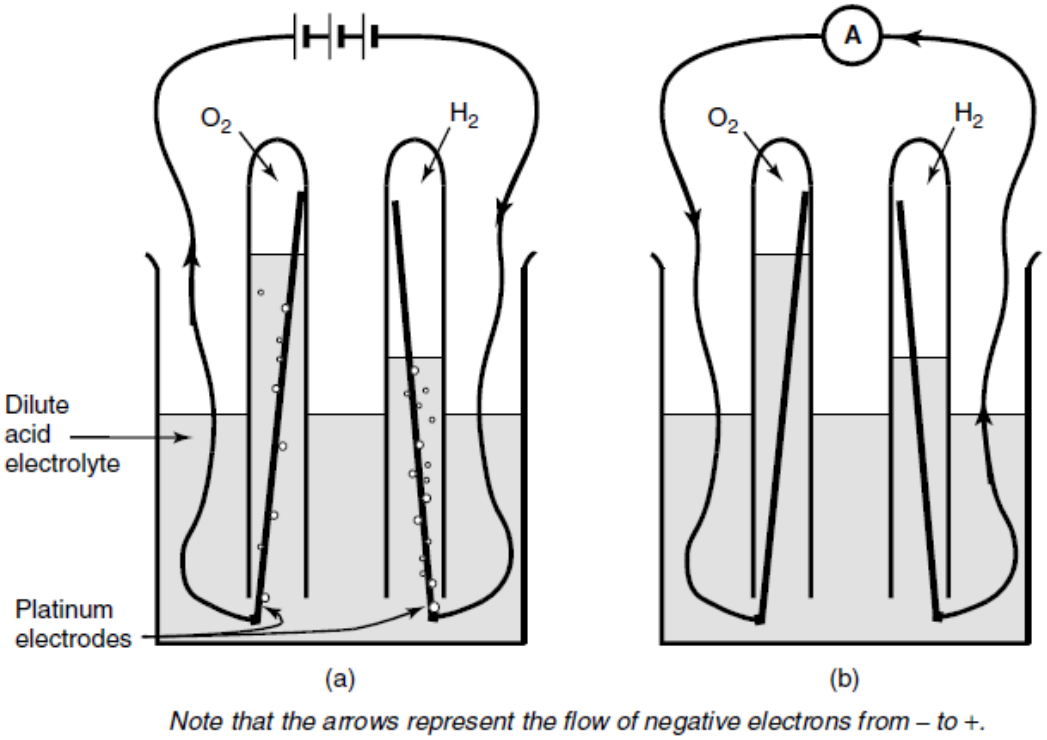

Figure 1.1 (a) The electrolysis of water. The water is separated into hydrogen and oxygen by the passage of an electric current; (b) A small current flows. The oxygen and hydrogen are recombining [3].

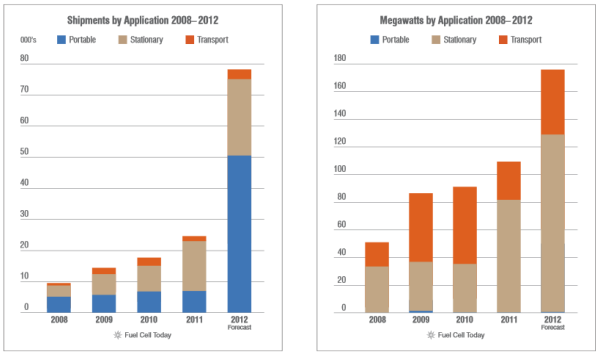

Figure 1.2 Growth in shipments and megawatts of fuel cells by applications in 2008 – 2012 [10].

Although fuel cell technology has evolved for over 170 years, its basic working principle still follows the original model demonstrated by Grove. A typical hydrogen fuel cell consists of an electrolyte layer which is sandwiched by an anode electrode and a cathode electrode [3]. As shown in Figure 1.3, hydrogen gas is split into electrons and protons at the anode side of an acid electrolyte fuel cell and energy is released during this reaction. The electrons will transfer from anode side to cathode side through external circuit while the protons will transfer though the electrolyte layer. At the cathode side, the oxygen gas reacts with electrons and protons to generate water. The reactions are shown below:

Anode: $2H_2 \rightarrow 4H^+ + 4e^-$

Cathode: $O_2 + 4e^- + 4H^+ \rightarrow 2H_2O$

Overall: $2H_2 + O_2 \rightarrow 2H_2O$

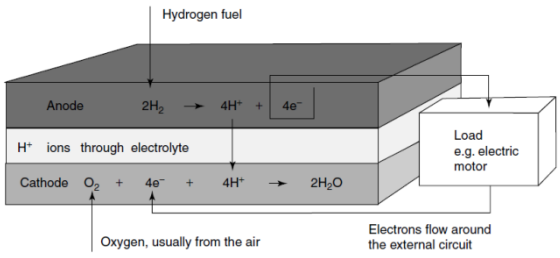

Figure 1.3 The basic configuration and reactions of an acid electrolyte fuel cell [3].

In an alkaline electrolyte fuel cell the overall reaction is the same. However, at the anode side, the hydrogen gas reacts with hydroxyl ion (OH^-) to generate electrons, water and release energy. At the cathode side the oxygen gas will be combined with electrons transferred from external circuit and water in the electrolyte to produce more OH^- ions. In order for the reactions to proceed, the electrolyte must be able to transfer OH^- ions from cathode side to anode side. The reactions are also shown below:

Anode: $2H_2 + 4OH^- \rightarrow 4H_2O + 4e^-$

Cathode: $O_2 + 4e^- + 4H_2O \rightarrow 4OH^-$

Overall: $2H_2 + O_2 \rightarrow 2H_2O$

So far, many different types of fuel cell have been developed based on various factors such as different electrolyte materials, side reactions, operating temperatures, and target applications, etc. Based on the different electrolyte materials, fuel cells can be categorized as follows:

1. Proton exchange membrane fuel cell (PEMFC)

2. Alkaline fuel cell (AFC)

3. Phosphoric acid fuel cell (PAFC)

4. Molten carbonate fuel cell (MCFC)

5. Solid oxide fuel cell (SOFC)

A brief overview and comparison of different fuel cell types are shown in Table 1.1 [11].

Table 1.1 Typical characteristics of fuel cell types [11].

Fuel Cell Type	Common Electrolyte	Operating Temperature	Typical Stack Size	Efficiency	Applications	Advantages	Disadvantages
Polymer Electrolyte Membrane (PEM)	Perfluoro sulfonic acid	50-100°C 122-212° typically 80°C	< 1kW–100kW	60% transportation 35% stationary	• Backup power • Portable power • Distributed generation • Transporation • Specialty vehicles	• Solid electrolyte reduces corrosion & electrolyte management problems • Low temperature • Quick start-up	• Expensive catalysts • Sensitive to fuel impurities • Low temperature waste heat
Alkaline (AFC)	Aqueous solution of potassium hydroxide soaked in a matrix	90-100°C 194-212°F	10–100 kW	60%	• Military • Space	• Cathode reaction faster in alkaline electrolyte, leads to high performance • Low cost components	• Sensitive to CO_2 in fuel and air • Electrolyte management
Phosphoric Acid (PAFC)	Phosphoric acid soaked in a matrix	150-200°C 302-392°F	400 kW 100 kW module	40%	• Distributed generation	• Higher temperature enables CHP • Increased tolerance to fuel impurities	• Pt catalyst • Long start up time • Low current and power
Molten Carbonate (MCFC)	Solution of lithium, sodium, and/or potassium carbonates, soaked in a matrix	600-700°C 1112-1292°F	300 kW-3 MW 300 kW module	45-50%	• Electric utility • Distributed generation	• High efficiency • Fuel flexibility • Can use a variety of catalysts • Suitable for CHP	• High temperature corrosion and breakdown of cell components • Long start up time • Low power density
Solid Oxide (SOFC)	Yttria stabilized zirconia	700-1000°C 1202-1832°F	1 kW–2 MW	60%	• Auxiliary power • Electric utility • Distributed generation	• High efficiency • Fuel flexibility • Can use a variety of catalysts • Solid electrolyte • Suitable for CHP & CHHP • Hybrid/GT cycle	• High temperature corrosion and breakdown of cell components • High temperature operation requires long start up time and limits

1.1.2 Proton Exchange Membrane Fuel Cell (PEMFC)

Among various types of fuel cell devices, proton exchange membrane fuel cells (PEMFCs), also known as polymer electrolyte membrane fuel cells, have attracted much attention and been considered as the most promising candidates in transportation, portable power, and residential power generator applications [12-14]. The first PEMFC unit was invented in the late 1950s by Willard Thomas Grubb at General Electric (GE) and the device was refined by another GE researcher, Leonard Niedrach, by using platinum as a catalyst on the membranes [6].

In general, the PEMFC utilizes a solid acidic polymer membrane (mostly water based) as its electrolyte layer, with platinum or a platinum-based catalyst on both anode and cathode electrodes. One advantage of the PEMFC compared with other fuel cell types especially the AFC and PAFC is the utilization of a solid electrolyte. The polymer-based electrolyte layer provides advantages such as suppressed corrosion effect, excellent proton conductivity, and prevention of the crossing-over of reactant gases as compared to liquid electrolytes. When comparing with high temperature fuel cells such as MCFC and SOFC, the operation temperature (<100 ºC) of a PEMFC provides a fast cell startup time, which is suitable for applications such as automobiles and portable devices [3].

The general operation scheme of a PEMFC is illustrated in Figure 1.4 (a) [15]. Similar to acid electrolyte fuel cells illustrated in section 1.1.1, a stream of fuel gases (e.g., pure H_2) is delivered to the anode side of the electrolyte membrane and split into H^+ ions and electrons with the aid of platinum catalyst. The porous and electronically conductive electrode layers are usually used to aid transportation of reactant gas and increase the active reaction areas. The electrons flow through external circuit to generate

electricity and the H^+ ions transport from anode to cathode directly through the electrolyte membrane. At the cathode side, the oxidant gases (e.g., oxygen, air) react with electrons and H^+ ions to generate the water as the only byproduct. An assembled stack of proton exchange membrane (PEM), anode electrode, and cathode electrode is called membrane electrode assembly (MEA), which represents the core part of a PEMFC device. As shown in Figure 1.4 (b) [16], the MEA is then assembled with other components such as gas diffusion layers, graphite plates and end plates to form a single PEMFC unit.

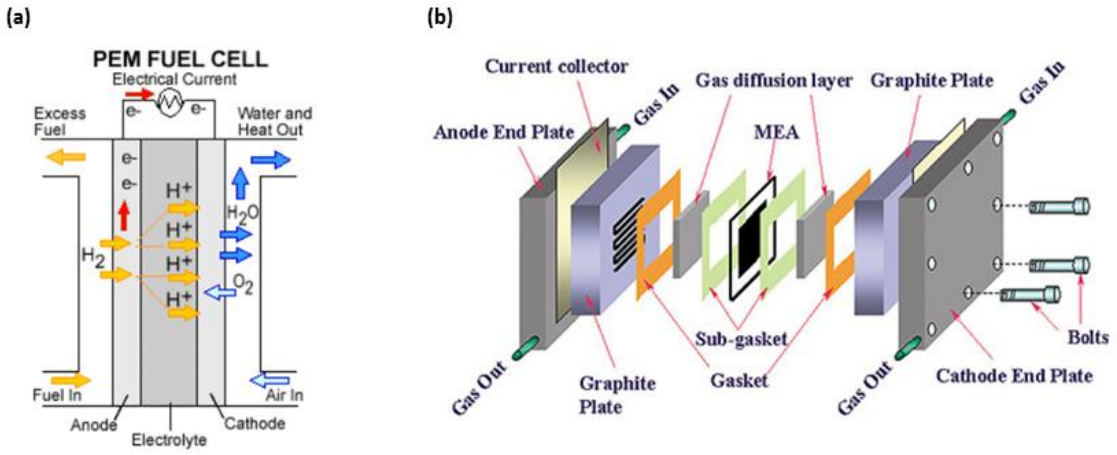

Figure 1.4 Schematic diagrams of (a) PEMFC operation principle [15] and (b) PEMFC single cell structure [16].

At the heart of an MEA, the proton exchange membrane (PEM), or polymer electrolyte membrane, plays a critical role in deciding the fuel cell's final performance and reliability. As a successful PEM material, the polymer must meet certain requirements as follows:

1. Low cost;

2. High proton conductivity;

3. Barrier to gas crossover;

4. Low electrical conductivity;

5. Excellent thermal, chemical, and mechanical stability.

Perfluorosulfonic acid (PFSA) polymers, such as Nafion® (commercial trademark of DuPont), Dow® (commercial trademark of Dow), and 3M PFSA polymer, are currently the state-of-the-art PEM materials commercially available due to their excellent proton conductivity (up to 0.10 S cm^{-1}, under fully hydrated conditions), good chemical stability, and excellent mechanical properties [17]. As shown in Figure 1.5, these materials possess a hydrophobic, perfluoronated (PTFE-like) polymer backbone, a ether-like side chain (also perfluoronated), and a hydrophilic sulfonic acid group which is attached at the end of the side chain. Due to the difference in hydrophobicity/hydrophilicity of the polymer structure, the polymer chains are segregated into different regions as shown in Figure 1.6. When these polymers (or membrane) are hydrated with water, the ionized regions are likely to form interconnected channels, giving the material excellent proton conductivity. Also, the PTFE-like polymer backbone gives the materials excellent thermal, chemical, and mechanical stabilities.

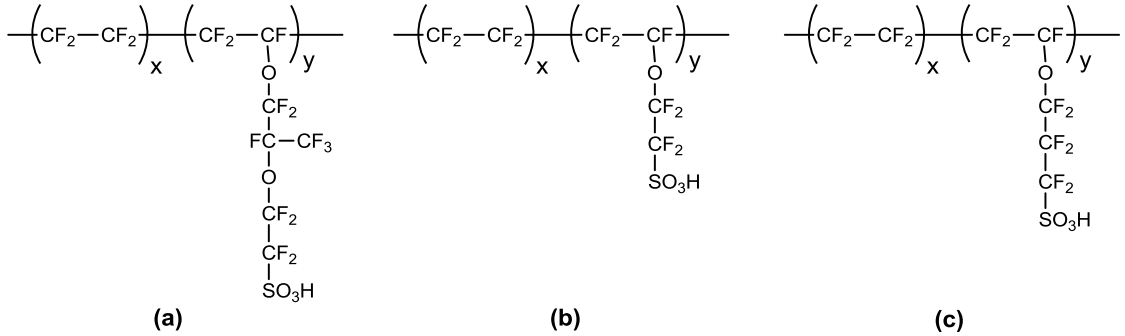

Figure 1.5 Chemical structures of PFSA membranes (a. DuPont's Nafion®; b. Dow's Dow®; c. 3M's PFSA polymer).

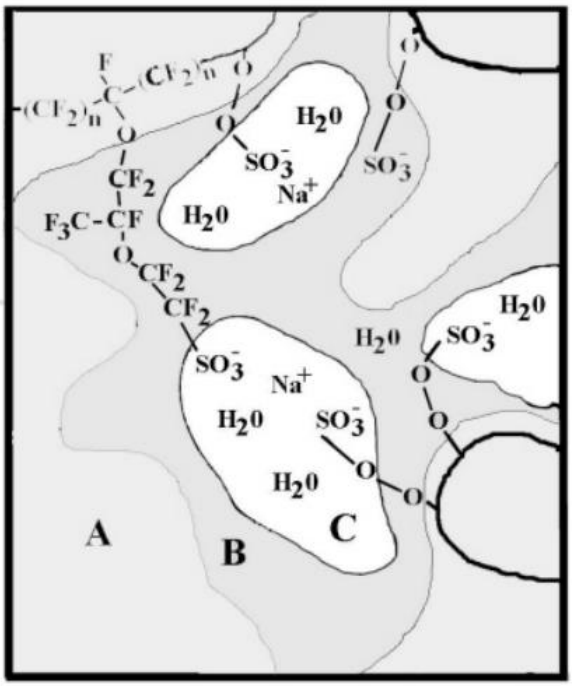

Figure 1.6 Morphology of PFSA membranes for PEMFC [18].

As the most widely studied PEM materials, the PFSA-based polymers exhibit several attractive properties for fuel cell applications. However, there are still some severe disadvantages that largely hinder the materials' large scale commercialization. A major issue of the PFSA-based materials (or PEMFC) is the difficulty and complexity of water management. Due to the relatively low fuel cell operating temperature (usually 50-80 ºC), water is generated in a liquid form and if it is not removed efficiently, flooding of the fuel cell will occur and cause the performance failure. Also, since water is acting as proton conductor, an appropriate humidity control is also critical to prevent the membrane dehydration and maintain reliable fuel cell performance. Another disadvantage of this type of fuel cell is its relatively low tolerance to fuel impurities (e.g., CO and SO_2). At low temperatures, even a very small amount of fuel impurities (ppm level) are able to bind to the platinum-based catalyst non-reversibly and cause a catalyst poisoning.

Another critical issue of PFSA-based materials is their high cost, which is up to approximately 700 US dollars per square meter (or up to 200 US dollars per kW). The expensive fluorination process is the main reason for the high cost of this type of material. Besides these, they also have disadvantages such as high methanol crossing-over and low mechanical property at high temperatures (>100 ºC).

1.1.3 High Temperature Proton Exchange Membrane Fuel Cell (HT-PEMFC)

As discussed above, most of the shortcomings associated with regular PEMFC technology based on PFSA membranes are attributed to low fuel cell operation temperatures. Therefore, a variant of the PEMFC which operates at elevated temperatures (> 100 ºC), known as the high temperature PEMFCs (HT-PEMFCs), has attracted much attention in recent years in order to overcome these shortcomings and achieve an improved performance.

Compared with low-temperature PEMFC, the HT-PEMFC provides a series of advantages including [19-20]:

1. Enhanced kinetics for both electrodes;

2. Simplified water/heat management;

3. Enhanced tolerance to fuel impurities (e.g., CO. from 10-200 ppm of CO at 80 ºC to 30000 ppm at 200 ºC);

4. Enhanced efficiency for the co-utilization of heat and electricity;

5. Simpler system design.

In recent years, tremendous research has been focused on investigating novel membrane materials/systems which are suitable for HT-PEMFC applications. These newly developed membranes could be divided into three main groups [20]: (1) modified

PFSA membranes; (2) alternative sulfonated polymers and their composite membranes; and (3) acid-base complex membrane systems.

Considerable work has been done in the past few decades on modification of PFSA-based membrane systems in order to improve the cell operating temperatures (>100 ºC). The most straight-forward approach that has been carried out is to improve water management system. An enhanced water management could give better controls on factors such as fuel humidification conditions, water drag from anode to cathode, and water back diffusion from cathode to anode [20]. However, this method also increases the system complexity. Another major approach that has been applied is to replace water with non-aqueous, low volatile solvents. These liquid proton conductors exhibit much lower vapor pressure compared with water therefore can be used at higher temperatures (up to 200 ºC). Typical solvents that have been studied include phosphoric acid, phosphotungstic acid (PTA), heterocycles (e.g., imidazole, pyrazole) and ionic liquids [21-23]. Besides those, solid inorganic particles or additives have also been used to improve the PEMFC performance at high temperatures [20].

Although much work has been done on the modification of PFSA-based membrane systems, the progress that has been made is not remarkable. Also, another big issue is that the perfluoronated PFSA materials are very expensive. Therefore, extensive effort has also been spent on investigating alternative sulfonated polymeric material including partially fluorinated polymers, polysiloxane polymers, and aromatic hydrocarbons. Among them, aromatic hydrocarbons possess advantages such as low-cost, thermal and chemical stability, and ease of functionalization with sulfonic acid groups, and are considered as ideal candidates for HT-PEMFC uses. Typical aromatic

hydrocarbon polymers which are being studied include polysulfone (PSF), polyethersulfone (PES), polyetheretherketone (PEEK), polyetheretherketoneketone (PEEKK), polybenzimidazole (PBI), polyimide (PI), and so on. All of these polymers can be sulfonated *via* either monomer modification or post-functionalization and they exhibit comparable or even improved proton conductivity compared with PFSA-based membranes. Also, in order to use these polymers at elevated cell operation temperatures, solid inorganic particles (or proton conductors) are also added to the polymer matrix to form organic-inorganic complex membranes and some progress has already been made. Detailed reviews on these topics can be found elsewhere [20].

The third approach to prepare HT-PEMFC is to investigate acid-base complex membranes. Some polymers with basic functional groups or basic backbones could be stably doped with inorganic low volatile acids (proton conductors) such as phosphoric acid and sulfuric acid. The acid-base complex membrane system that has been most widely studied is the phosphoric acid-polybenzimidazole complex membranes. Further introduction and discussion of this type of material will be discussed in a later section.

1.2 Membrane Gas Separation

1.2.1 Introduction

Membrane separation technologies have been recognized as powerful tools and promising solutions in solving some important global energy problems, reducing the environmental impact, and developing new industrial processes needed for a sustainable industrial growth [24]. They also represent a fast-growing industry; according to a new technical market research report, *Membrane Technologies for Liquid and Gas Separations (MST041F)*, the US market for membrane modules used in liquid and gas

separations was valued at $2.1 billion in 2012 and expected to reach $3.3 billion in 2017 at a five-year compound annual growth rate (CAGR) of 8.9%.

Membrane gas separation, as a very important branch of separation technologies, has been applied in several application areas such as gas processing and purification, energy production, chemical production, and environmental protection. Compared with well-established industrial gas separation processes such as cryogenic distillation, absorption, and pressure swing adsorption (PSA), it is considered as being more reliable, efficient, and cost-effective [25]. The use of membranes in separation processes is growing at a slow but steady rate. Baker in 2002 estimated the market scale of membrane gas separation technology in year 2020 will be five times of that of year 2000 [26]. Also, the rapid growth of new markets, for instance, the discovery and exploration of shale gas in recent years, provides even more opportunities to increase the market for membrane gas separation.

The original potential of using membranes to transport and separate important gas mixtures was demonstrated by Graham over a century ago [27]. He found that natural rubber polymeric membranes could be used for oxygen enrichment from atmospheric air (O_2/N_2 separation) and then proposed a three-step solution-diffusion gas transport mechanism, which is currently still used to explain how a small penetrant molecule permeates through a dense polymeric membrane [28]. Although more progress has been made since then, the commercialization of membranes for gas separation was hampered over a very long period of time due to the lack of materials with an optimized performance combination of gas permeability and selectivity and also to the technical barrier to fabricate high quality membrane modules (e.g., thin, defect-free films with high

surface areas) [29]. In the early 1970s, high-flux anisotropic membranes and large-surface-area membrane modules were successfully developed for reverse osmosis applications. Then in the early 1980s, Permea became the pioneer who adapted this technology in the gas separation area and successfully fabricated the first polysulfone (PSf) hollow-fiber membrane. Their membrane products were immediately successful in several applications, especially for the separation and recovery of hydrogen from purge gas streams of ammonia plants (H_2/N_2 separation). Following Permea's success, several companies started designing and fabricating their own membrane separation systems. For instance, Separex (now part of UOP), Cynara (now part of Natco), and GMS (now part of Kvaerner) successfully commercialized cellulose acetate membranes to separate carbon dioxide from natural gas (CO_2/NH_4 separation) in the mid-1980s; at the same time, UBE, Medal (now part of Air Liquide), and Generon (now part of MG) also fabricated advanced membrane systems for several applications (e.g., O_2/N_2; H_2/N_2; H_2/CH_4 separation) [26]. Since then, more and more companies have become involved into the membrane gas separation business and several novel membrane materials and applications areas have been developed so far. A milestone chart on the development history of membrane gas separations is shown in Figure 1.7 [26].

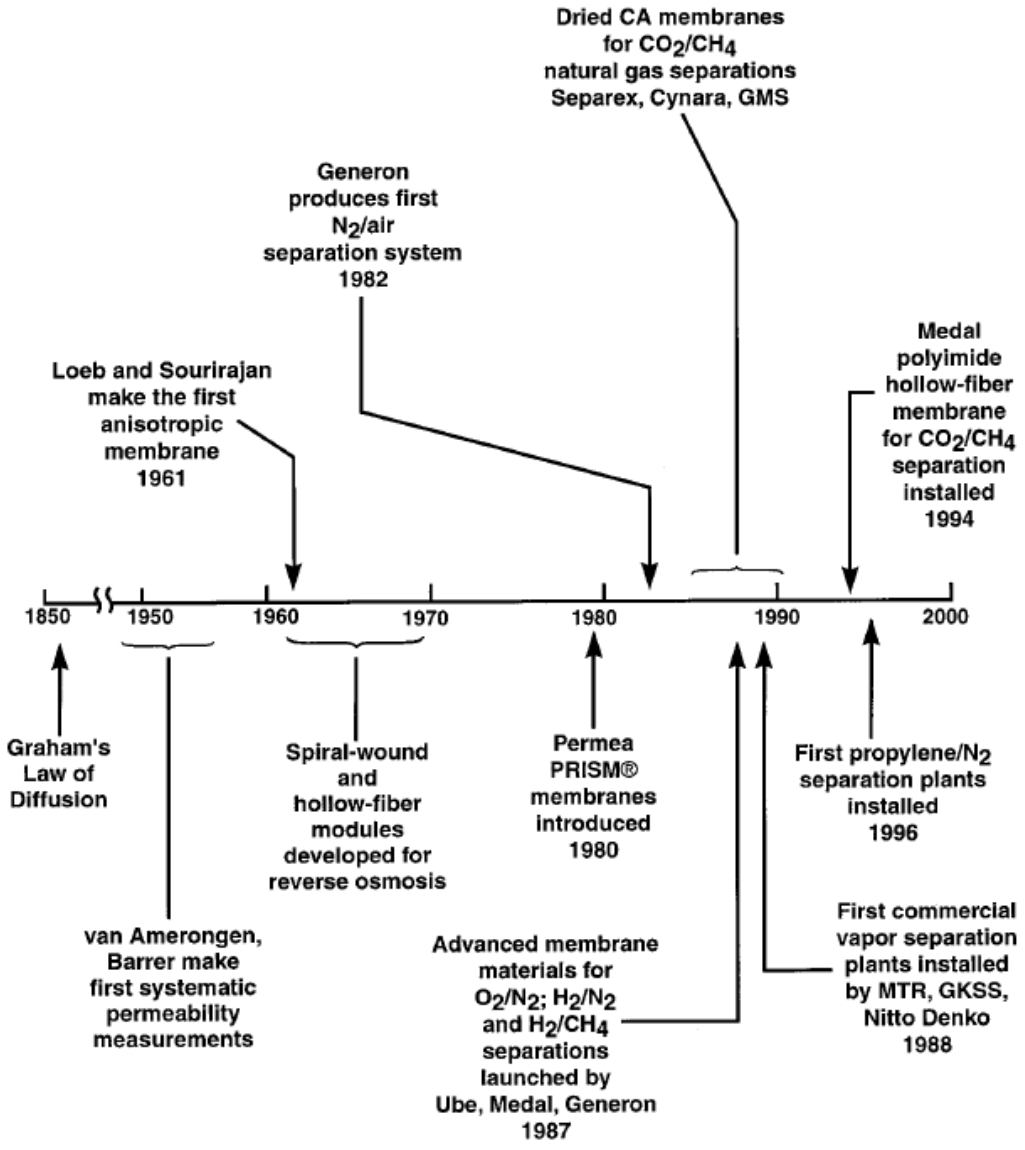

Figure 1.7 Milestones in the development of membrane gas separations [26].

1.2.2 Membrane Gas Separation Fundamentals

Except for the classical polymeric membranes, several other types of membranes (e.g., metal membranes, carbon-based membranes, zeolite membranes, Mixed-Matrix Membranes (MMMs), and Facilitated Transport Membranes (FTMs), etc.) have also been developed and extensively studied in the past few decades. These membranes are based

on different materials and different gas transport mechanisms and detailed reviews on them can be found elsewhere [24, 30].

As for dense polymeric membranes, a three-step "solution-diffusion" mechanism was proposed by Graham to explain the gas permeation over a century ago and is still widely used and accepted now by most membrane researchers. Figure 1.8 shows a schematic of a gas transport across a polymeric membrane [29]. In this model, penetrant molecules first dissolve into the upstream (high pressure) face of the membrane, diffuse across the membrane to the downstream (low pressure) side, and then desorb (or evaporate) from this face. The driving force of a gas penetrant to transport across a membrane is understood to be the differences in penetrant chemical potential (or the differences in penetrant partial pressure) across the membrane.

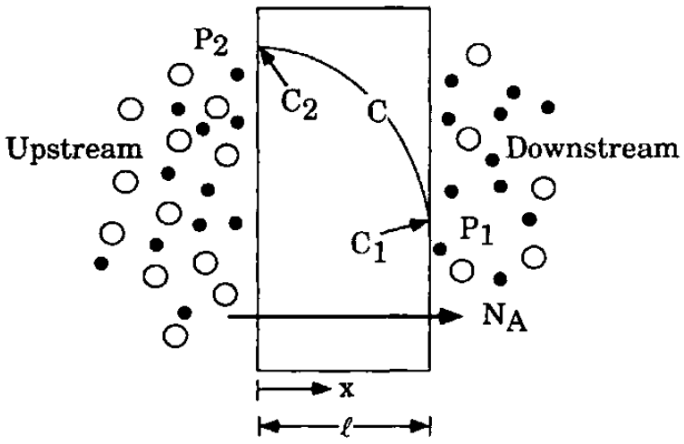

Figure 1.8 Schematic of penetrant transport across a membrane [29].

One important parameter to evaluate the gas separation performance of a polymeric membrane is the gas permeability. The permeability (P_A) of a penetrant gas A across a polymeric membrane of thickness l can be expressed as

$$P_A = \frac{N_A}{(p_2 - p_1)/l} = \frac{N_A}{-\Delta p/l} \quad (1)$$

In Eq. (1) and Figure 1.8, N_A is the steady state gas flux across the membrane; p_2 and p_1 are the partial pressures of gas A at upstream (feed side) and downstream (permeate side) sides of the membrane, respectively; Δp is defined as p_2-p_1. The unit of P in the SI system is mol $s^{-1}m^{-1}Pa^{-1}$. However, P is commonly and widely accepted and expressed in barrers as shown in Eq. (2)

$$1\ Barrer = 1 \times 10^{-10}\ \frac{cm^3\ (STP)\ cm}{cm^2\ sec\ cm\ Hg} \quad (2)$$

The P of various gases in polymeric membranes varies in wide range from 10^{-4} to 10^4 Barrer. Also, according to the "solution-diffusion" model, when the downstream pressure is maintained so low that $p_2 \gg p_1$ and $C_2 \gg C_1$, the permeability P can also be expressed as

$$P = D \times S \quad (3)$$

where D is the diffusion coefficient and S is the solubility coefficient.

Another key parameter for a polymeric membrane separation system is the gas selectivity. In a binary gas mixture system which is composed of gas component A and gas component B, the separation factor of gas A relative to gas B, α_{AB}, can be expressed as

$$\alpha_{AB} = \frac{y_A/y_B}{x_A/x_B} \quad (4)$$

where y_i and x_i refer to the mole fraction of gas component i in the gas phase at the downstream and upstream faces of the membrane, respectively. When the downstream pressure is negligible relative to the upstream pressure, the separation factor α_{AB} can be written as the ratio of permeabilities as follows:

$$\alpha_{AB} = \frac{P_A}{P_B} \quad (5)$$

where α_{AB} is called the ideal selectivity or ideal permselectivity. According to Eqs. (3) and (5), the ideal selectivity can be partitioned into diffusion selectivity (α_{AB}^{D}) and solubility selectivity (α_{AB}^{S}) as follows:

$$\alpha_{AB} = \left(\frac{D_A}{D_B}\right)\left(\frac{S_A}{S_B}\right) = \alpha_{AB}^{D}\alpha_{AB}^{S} \quad (6)$$

Therefore, to compete with other traditional industrial separation techniques and be valuable in practical gas separation uses, polymeric membranes must exhibit both high gas permeability and gas selectivity. Both of these two parameters largely depend on the gas solubility and gas diffusivity of a membrane. In general, gas solubility depends on factors such as operating conditions (e.g., temperature, pressure, and composition), penetrant condensability (solubility increases as condensability increases), polymer-penetrant interactions, polymer morphology, etc. Gas diffusivity depends on operating conditions as well but also on the penetrant size and shape, polymer free volume size and shape, polymer chain mobility, polymer morphology, etc.

In rubbery polymers, penetrant diffusivities can be orders of magnitude higher than in glassy polymers, which are mainly attributed to large-scale polymer segmental dynamics and large amount of free volume associated with the rubbery state [29]. However, the effect of penetrant size on penetrant diffusion coefficient is typically weaker in rubbery polymers than in glassy polymers. Therefore, rubbery polymers are much less effective than glassy polymers at separating gas molecules on the basis of small differences in molecular size. Typically, the selectivity of rubbery polymers is mainly influenced by differences in the condensability of the gas species (or the solubility of gas species in polymers). Therefore, one major application of rubbery polymer membranes is the removal of organic vapor (high condensability) from permanent gases

(low condensability). The most widely studied rubbery polymers are silicone rubber (e.g., polydimethylsiloxane (PDMS)), which exhibit high permeability and adequate vapor/permanent gas selectivities for some applications.

Much of the research related to the development of high performance polymers for gas separation applications has focused on glassy polymers due to their higher gas selectivity and better mechanical properties than rubbery polymers. When below Tg, the motion of individual chain segments becomes frozen with only small scale molecular motion remaining, the glassy polymers are then characterized by a small amount of free volume (usually < 10%). These small free volume characteristics give glassy polymers the ability to act as "molecular sieves" (high diffusion selectivity) to separate penetrant gases based on the differences in their sizes. More importantly, the gas permeation properties of glassy polymers are much more sensitive to the chemical structure of repeat units than rubbery polymers. For instance, the $P(CO_2)$ for polyacrylonitrile is 0.0003 Barrer while for poly(trimethylsilylpropyne) is 27000 Barrer, which is approximately 10^8-fold difference [31]. As a result, the proper design of polymer primary chemical structures becomes the key to the success in practical gas separation applications. Table 1.2 shows the most important rubbery and glassy polymers used in industrial gas separation applications [24].

Table 1.2 Most important rubbery and glassy polymers used in industrial gas separation applications [24].

Rubbery polymers	Glassy polymers
poly(dimethylsiloxane)	cellulose acetate
ethylene oxide/propylene oxide -amide copolymers	polyperfluorodioxoles
	polycarbonates
	polyimides
	poly(phenylene oxide)
	polysulfone

1.2.3 Industrial Applications of membrane Gas Separation

Membrane gas separation has been applied to a few industrial applications and is considered to be potentially useful in other industrial processes. Detailed discussions on this topic can be found in several review articles [24, 26, 31]. In the following paragraphs some industrial applications of membrane gas separation are briefly summarized.

Hydrogen Separation. Hydrogen recovery from ammonia purge gases (mainly H_2/N_2 separation) was among the first large-scale commercial applications in the membrane gas separation industry in the 1970s. High pressurized gas mixtures are produced directly from the ammonia reactor, which eliminates the complexity of post-pressurizing as the driving force for separation. Also, the large differences in sizes provide a decent H_2/N_2 selectivity. Later on, this technique was transferred to other situations for the recovery of hydrogen from gas mixtures, for instance, the H_2/CO separation to adjust the gas ratios in syngas production. In recent years, hydrogen recovery from refining streams in the petrochemical industry has been considered as a newly emerging field for membrane separation [24].

Air Separation. Air separation can be applied to both nitrogen and oxygen production. Nitrogen production by membrane systems is currently the largest gas separation process in use. It was reported that by using membranes with O_2/N_2 selectivity of ca. 8, a 99% pure nitrogen product can be successfully obtained [24]. However, for oxygen production, the practicality of membrane-based technique is still limited and will strongly depend on improvements in membrane separation performance, especially the O_2/N_2 selectivity, which is mainly due to the fact that oxygen is the minor component in air and high purity oxygen (>90%) is usually needed for industrial uses. The small size

difference between nitrogen (kinetic diameter=3.64 Å) and oxygen (kinetic diameter=3.45 Å) makes it difficult to separate oxygen with high efficiency by a simple size effect. Other solutions such as utilizing stabilizing liquid membranes to chemically bind the oxygen carrier to a polymer backbone to achieve better performance are currently under investigation [32].

Natural Gas Separation. Carbon dioxide removal from natural gas (natural gas sweetening, mainly CO_2/CH_4 separation) represents another huge market for membrane separation, which is due to the strict pipeline specifications in US (e.g., down to 2% vol. CO_2 for natural gas transportation). Tremendous effort has been spent by companies in realizing this process using membrane separation techniques (e.g., cellulose acetate based membrane designed by UOP). Except for carbon dioxide removal, membrane separation systems are found to be useful in other natural gas related separation processes, such as natural gas liquids (NGL) removal and natural gas dehydration. It is worthy to note that the shale gas boom in US in recent years will make membrane separation play a more important role in the natural gas processing industry.

CO_2 Capture and Sequestration. Carbon capture and sequestration has become a hot topic in recent decades due to the growing concern in global warming and more stringent environmental requirements. One big worldwide carbon generating source is the coal-based power plants, which produce much CO_2 during the fuel combustion. Three main solutions have been proposed to capture the carbon and alleviate the problem, which includes: *pre-combustion carbon capture, post-combustion carbon capture, and oxygen enrichment*. The details for pre-combustion carbon capture (mainly H_2/CO_2 separation) will be discussed in a later section. The post-combustion carbon capture

(mainly CO_2/N_2 separation) has been studied for a long time. However, since the gas mixtures are at ambient pressure after combustion and post-pressurization is needed as the driving force for separation, this procedure is not considered to be commercially feasible so far. In an oxygen enrichment process, pure oxygen (ca. 95%) is proposed to be used instead of air in fuel combustion, which could largely decrease the amount of flue gas and makes it easier to separate (due to high CO_2 concentration in gas mixtures). However, so far an oxy-fuel power plant is not considered to be cost-effective.

Vapor/Vapor Separation. Vapor/vapor separation such as ethylene/ethane separation and propane/propylene separation is believed to be a likely major application field for membranes in the future. Since these mixtures have similar boiling points, traditional separation techniques, especially large towers and high reflux ratios, are required to achieve good separations. The facilitated-transport membranes (FTMs) have been considered as promising candidates to replace conventional separation techniques if high separation performance and good reliability could be realized in the future [33].

1.3 Polybenzimidazole (PBI)

1.3.1 Introduction to PBI

Polybenzimidazoles (PBI) represent a class of heterocyclic polymers containing the benzimidazole moiety as part of the polymer repeat unit. The general structure of PBI is shown in Figure 1.9, where R_1 can be a direct bond, ether, sulfone, or other linking groups and R_2 can be either aryl or alkyl group; R_3 is usually hydrogen but can also be substituted by other functional groups *via* N-substitution reaction; R_4 can be sulfonic acid or nitro group through post-polymerization ring substitution.

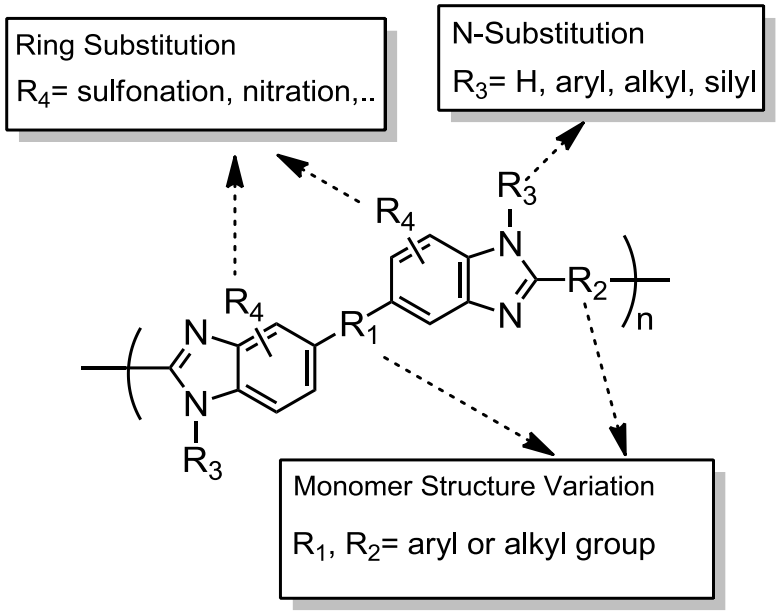

Figure 1.9 General chemical structure of polybenzimidazole.

The aliphatic PBI (where R_2 is an aliphatic group) was firstly developed by Brinker and Robinson in 1959 [34] and then the first aromatic PBI (where R_2 is an aromatic group) was development by Marvel and Vogel at University of Illinois in 1961 and later at DuPont [35]. In 1983, Celanese Corp. commercialized a *meta* analogue of an aromatic PBI (m-PBI, poly(2,2'-m-phenylene-5,5'-bibenzimidazole), commercial trademark Celazole®), as shown in Figure 1.10, to produce fibers and textiles for thermal protective clothing and fire blocking applications [36-37]. Currently the m-PBI is produced by PBI Performance Products, Inc.

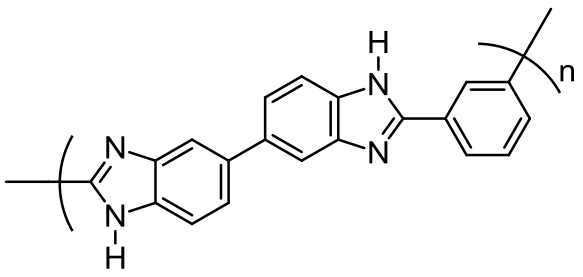

Figure 1.10 Structure of m-PBI (poly(2,2'-m-phenylene-5,5'-bibenzimidazole)).

PBI represents a class of high performance engineering thermoplastics which exhibit excellent thermal, chemical, and mechanical stability. It does not burn, melt or contribute fuel to flames. The glass transition temperature (Tg) of m-PBI is approximately 425 ºC and the decomposition temperature is higher than 700 ºC. It also possesses advantages such as excellent chemical resistance, low heat transfer, low tenacity, etc. Detailed property descriptions of PBI-based commercial products can be found elsewhere [37-38].

PBI can be synthesized *via* polycondensation reaction of tetraamines and dicarboxylate derivatives by either melt/solid polymerization or solution polymerization techniques (as shown in Figure 1.11). A two stage melt/solid polycondensation reaction of tertraaminobiphenyl (TAB) and diphenylisophthalate (DPIP) has been used for the commercial production of m-PBI. In the first stage, the low molecular weight PBI pre-polymers are produced in the form of foam due to generation of large amount of phenol and water moisture. Then the pre-polymers are crushed and reheated at ca. 360 ºC as the second stage to produce high molecular weight m-PBI products. This method is suitable for PBI commercial production since it does not require solvent and postprocessing after polymerization is relatively easy. However, the molecular weight of PBI is restricted due to the heterogeneous reaction characteristics [39].

An alternative method to synthesis PBI is by solution polymerization. Some high polarity organic solvents such as N,N-dimethylacetamide (DMAc) and N-methyl-2-pyrrolidinone (NMP) were reported for PBI synthesis [40-42]. However, the most commonly used solvent is poly(phosphoric acid) (PPA) [43-44]. PPA possesses several advantages [43] over other solvents: *(1) it is a good solvent for both monomers and*

polymers, and can also react with monomers to form mixed anhydride to activate the reaction; (2) it can work as a condensation reagent to move the reaction equilibrium forward; (3) much cheaper diacid monomers can be used directly instead of diesters; (4) the reaction temperature (<220 ºC) is lower to prevent polymer cross-linking; (5) it can produce high molecular weight linear PBI polymers. Therefore, PPA is more suitable for laboratory-level synthesis and study of PBI polymers.

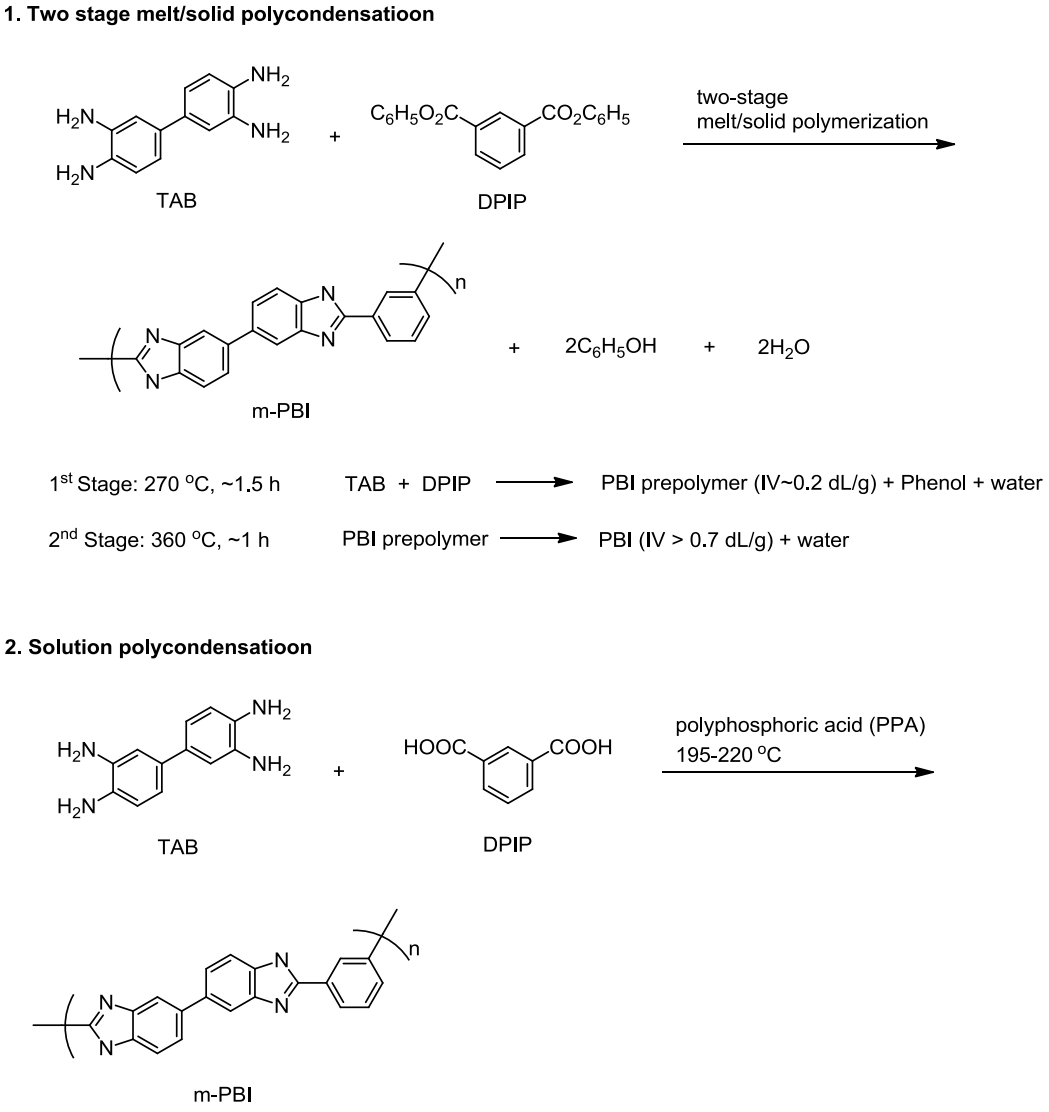

Figure 1.11 Synthesis of m-PBI by 1) two stage melt/solid polymerization and 2) solution polymerization.

1.3.2 Applications of PBI in HT-PEMFC.

As stated in the previous section, the HT-PEMFC (120-200 °C) possesses several advantages compared with traditional low-temperature fuel cells (< 100 ºC). Among various membrane materials that have been studied for HT-PEMFC uses, phosphoric acid (PA) doped polybenzimidazole (PBI) has been considered as the most promising candidate due to its outstanding fuel cell performance and long term reliability.

As a class of basic polymers with slight basicity (pKa=5.5 as protonated), PBIs are able to be doped with high boiling point inorganic acids such as phosphoric acid and sulfuric acid and then form a stable acid-base complex membrane system [20, 45]. PA doped PBI membranes were first proposed and investigated by Litt and Wainright et al. at Case Western Reserve University (CWRU) as a low-cost and high performance membrane material candidate for HT-PEMFC application in the mid-1990s [21, 46-47]. They found that m-PBI was able to be stably doped with up to ca. 10 moles PA per repeat unit (PA/RU) and exhibit decent proton conductivity at 180 ºC (up to 0.1 S/cm). The membrane also exhibited appreciable mechanical strength and could be fabricated into a membrane electrode assembly (MEA) for long term fuel cell testing. Since then, tremendous effort has been put on understanding and exploring the PA-PBI based fuel cell systems *via* different approaches, such as novel PBI chemistry, new membrane processing techniques, etc. [45].

It was reported that slight changes in the chemical structure of PBI polymers will result in big property differences (e.g., polymer solubility, oxidative stability, mechanical strength, polymer morphology, proton conducting mechanism, and the corresponding fuel cell performance, etc.) [48-50]. Therefore, a large amount of PBI analogues (as shown in

Figure 1.12) have been developed and studied in the past two decades. The m-PBI is the one that has been widely studied which is probably due to its commercial availability. *para*-PBI membrane prepared *via* a "PPA process" was found to exhibit higher PA doping level, better proton conductivity, and better long-term performance than m-PBI [51]. As a result, it has been commercialized by BASF Fuel Cell, Inc. for the HT-PEMFC applications.

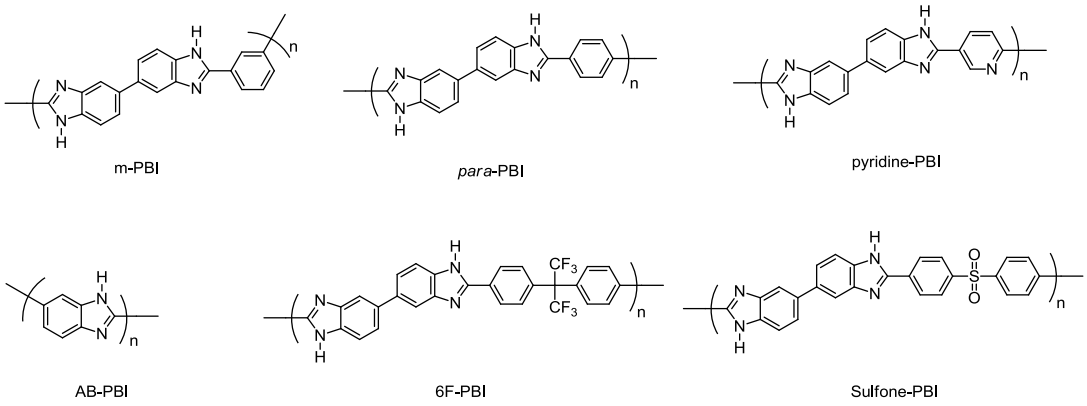

Figure 1.12 Chemical structures of PBI derivatives that have been investigated in HT-PEMFCs [48-52].

Another key parameter which is found to largely affect the final fuel cell performance is the membrane processing technique. As shown in Figure 1.13, two main PA doped PBI membrane preparation methods (1. acid imbibing process; 2. PPA process) have been reported and extensively studied. In the conventional acid imbibing process, PBI powders are first dissolved in organic solvents (e.g., DMAc), cast into PBI dense films, and then dipped into PA bath to obtain final PA doped PBI membranes [46]. In general, PBI has a poor solubility in most organic solvents due to its rigid polymer chains and strong pi-pi stacking interactions; it can only be dissolved in a few high polar, aprotic solvents such as DMAc, NMP, DMF, etc. Lithium salt (e.g. LiCl) is sometimes added as a phase stabilizer to increase the stability of the PBI solution. Different PA doping levels

can be obtained by varying PA bath concentrations, membrane soaking time, and acid bath temperatures. In general, PBI membranes with PA doping levels of ca. 5-6 PA/RU are considered to be suitable for fuel cell use. Another membrane processing method is called the "PPA process", which was invented by Benicewicz et al. at Rensselaer Polytechnic Institute (RPI) and published in 2005 [44], and is used for the commercial production of PA-doped *para*-PBI membranes by BASF Fuel Cell. In this process, a high temperature PBI/PPA solution was used for film casting directly at the end of the polymerization to form a PBI/PPA wet film. As the temperature cools down and at controlled relative humidity (RH), PPA is hydrolyzed into PA and a robust PBI gel membrane is formed. This method is much less tedious and the corresponding PBI membrane exhibits much higher acid doping levels and proton conductivities compared to conventional imbibing method. However, this PPA process also shows disadvantages such as relatively low mechanical strength for the final membrane.

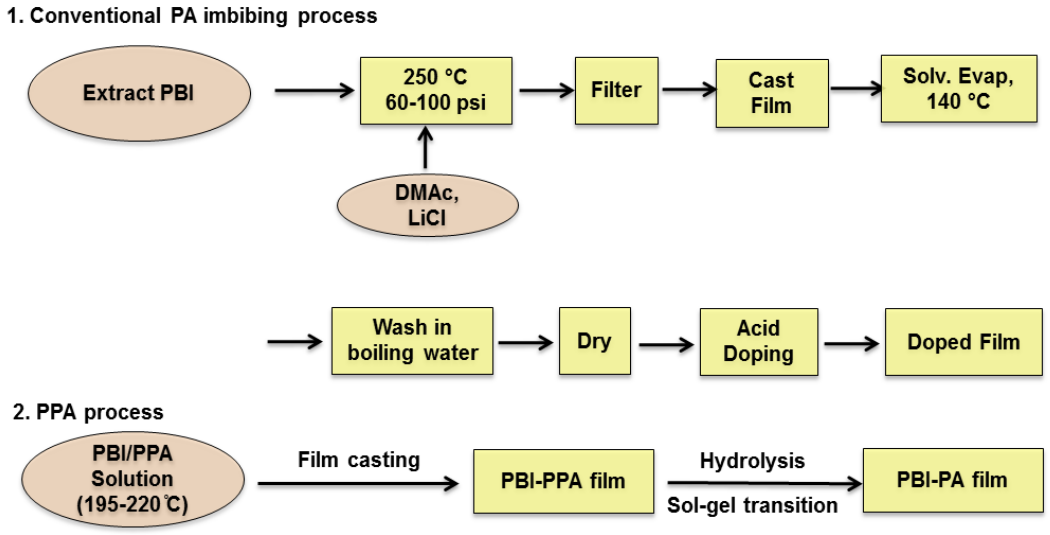

Figure 1.13 PA doped PBI membrane processing methods (1. Conventional acid imbibing process; 2. PPA process).

1.3.3 Applications of PBI in high temperature H_2/CO_2 separation.

Compared to PBI based fuel cells, the history of utilizing PBI polymers as potential membrane materials for gas separation applications is much shorter. In general, PBI is known as a class of rigid-rod polymers with tightly packed chain structures. This nature is attributed to PBI's strong hydrogen bonding (both *inter*- and *intra*-molecular) and *pi-pi* interactions within polymer chains. Therefore, PBI possesses very small sizes and distribution of free volume within the polymers, and is considered as poor gas separation materials at ambient temperatures due to extremely low gas diffusivity or gas permeability. However, in recent studies people found the situation might be different when the gas processing temperature is raised to higher than 150 °C. Encouragingly, PBI's rigidity and excellent thermal and chemical stability makes it a very promising candidate for high temperature gas separation, especially in pre-combustion carbon capture applications (or H_2/CO_2 separation) [53-55].

As mentioned in the former section, carbon capture and sequestration has gained much attention in recent years due to growing concerns on environmental protections. One of the largest carbon emission sources around the world is the traditional pulverized coal (PC) power plant. In order to achieve a more efficient and cleaner utilization of these carbon heavy fuel sources (e.g. coal), an integrated gasification combined cycle (IGCC) power plant was developed a few years ago. Figure 1.14 shows the simplified scheme for an IGCC procedure [56]. Firstly, the coal or biomass fuel sources will be gasified by reacting with oxygen and water at high temperature and high pressure to generate a raw synthesis gas (syngas) mixture (mainly composed of H_2 and CO). Then if CO_2 capture is to be applied at the IGCC plant, the raw syngas will be reacted with steam in a shift

reactor to produce more H_2 by the water-gas-shift reaction ($CO+H_2O \rightarrow H_2+CO_2$). The gas leaving the shift reactor usually consists of about 56% H_2, 40% CO_2, and 4% other gases. The separation of this warm (150-450 ºC) and pressurized (ca. 700 psia) gas mixture, is called pre-combustion carbon capture. It would produce clean H_2 fuels for various energy related uses and is much more cost-effective than post-combustion carbon capture (CO_2/N_2 separation) found at traditional coal fired power plants.

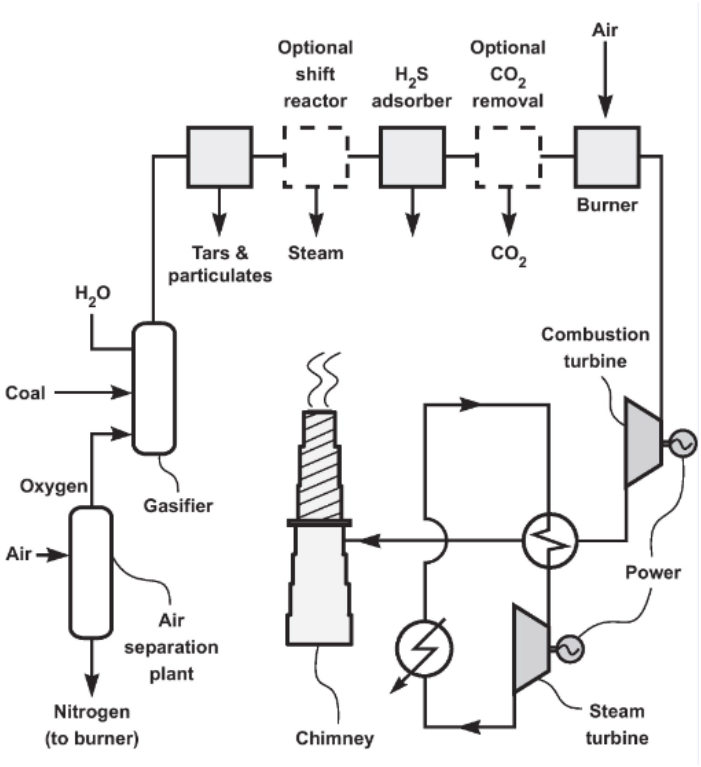

Figure 1.14 Simplified flow diagram for integrated gasification combined cycle (IGCC) power plants [56].

Many studies are being conducted on investigating novel barrier materials, including polymer materials, for the pre-combustion carbon capture application. However, most commercial polymers exhibit poor capability to discriminate between these two penetrant molecules at high temperatures due to factors such as largely increased chain segmental motions and CO_2 plasticization effects. As a special case, PBI

was found to exhibit much more attractive gas separation property at high temperatures due to its extremely rigid structure and excellent thermal resilience compared with other candidates. Pesiri et al. at Los Alamos National Laboratory (LANL) did the preliminary study on gas separation performance of m-PBI in 2003 [53]. They found that although PBI is a poor material for ambient temperature gas separation, it shows industry attractive H_2/CO_2 selectivity (up to about 25) when the temperature reached 250 ºC. Figure 1.15 shows the H_2/CO_2 separation performance of a meniscus m-PBI membrane. Another team (Singh et al.) at LANL also used m-PBI to successfully fabricate PBI/ZrO_2/Stainless Steel composite membranes and found the corresponding membrane module exhibited excellent long term stability in simulated dry syngas operation conditions at high temperature (up to 250 ºC) [54]. Also, Kumbharkar et al. at Imperial College London utilized m-PBI to prepare PBI based asymmetric hollow fiber membranes, which provides the technical feasibility for commercialization of PBI based membranes for practical industrial uses [55].

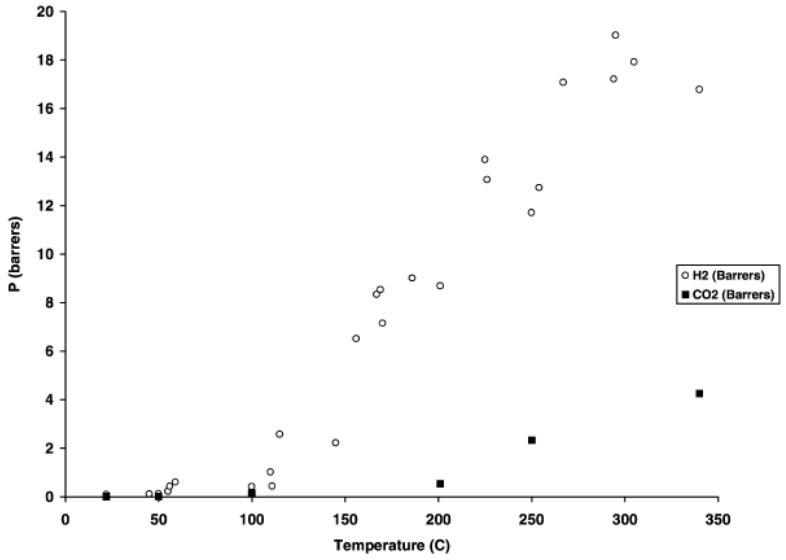

Figure 1.15 Permeance of m-PBI meniscus membrane as a function of temperature for single gases H_2 and CO_2 [53].

So far, almost all the research has focused on utilizing m-PBI as gas-selective membrane materials for H_2/CO_2 separation study, which could be caused by the commercial availability of m-PBI. However, although m-PBI exhibits industrial attractive gas selectivity, its gas permeability is very low even at elevated temperatures. It was reported that the H_2 permeability of m-PBI at 250 ºC is only ca. 75 Barrer, indicating that extremely thin PBI layers (<100 nm) are required to achieve enough H_2 flux in real industry use, which is very difficult to realize with current membrane module fabrication techniques [55]. Therefore, it is believed that the key to develop PBI membrane materials with more industrially attractive gas separation performance is to improve its gas permeability while still maintaining appreciable gas selectivity.

1.4 Research Proposals

1.4.1 Exploring Novel PBI Chemistry for HT-PEMFC Applications

The main goal of this research was to explore novel PBI chemistry and membrane processing methods in order to achieve better performances (e.g., processability, oxidative stability, mechanical property, acid doping ability, etc.) to be used in HT-PEMFCs. As discussed in the previous section, these membrane properties are believed to be closely related to PBI chemical structures and membrane fabrication procedures. Hence, this work will be beneficial for us to achieve better understanding of PBI structure-process-performance relationships and to design the next generation of PBI fuel cell membranes.

A major target of this work was to improve PBI's processability (or organo-solubility). PBI is known for its very poor solubility in most organic solvents due to its nature of rigid structure and tightly chain packing characteristics, which largely limits its

uses in commercial applications. Only a few high polar solvents (e.g. DMAc, NMP) are able to dissolve low molecular weight PBI at low polymer weight percentage with the aid of lithium salt as phase stabilizer. Thus, we propose that the introduction of bulky, twisted or bent functional groups into the PBI main chain could potentially suppress the polymer chain packing and then increase its solubility. In this work, two novel PBI variants containing either phenylindane or fluorine functional groups were synthesized and found to exhibit much improved solubility than commercial m-PBI. Also, the synthesis of monomer and polymers, as well as the characterization of thermal, chemical, mechanical, and electrochemical properties was carefully studied to understand their structure-property relationships.

Another challenge of this work was to fabricate acid doped polymer membranes from these novel structure PBI polymers and to understand the effect of membrane morphologies on their corresponding fuel cell properties. As mentioned in the former section, the "PPA process" was reported as an effective way to fabricate PBI fuel cell membranes with high acid loading and excellent proton conductivity. However, this method does not apply to all the PBI polymers and the mechanical properties of membranes made by the "PPA process" are relatively low. Thus, it is necessary to explore other possible PBI membrane fabrication methods and to achieve improved reliability for long term fuel cell uses. In this work, the preparation of acid doped PBI membranes was attempted by both the "PPA process" and traditional acid imbibing methods and mechanically strong PBI membranes were successfully fabricated. Several influencing factors, including membrane fabrication conditions and acid loading levels,

of these PBIs were carefully studied and optimized to obtain high quality PBI fuel cell membranes.

Finally, the novel PBI membranes were fabricated into the Membrane Electrode Assembly (MEA) by an optimized "acid dipping" hot press procedure. Their corresponding fuel cell performance were carefully investigated under different operation conditions (e.g., different oxidants, different operation temperatures) and compared with previously reported PBI fuel cell membrane systems.

1.4.2 Understanding the Structure-Property Relationships in PBI Films for High Temperature H_2/CO_2 Separation

The primary objectives of this research were to investigate the fundamental polymer chemistry and polymer physics of novel PBI films for use in H_2/CO_2 separation and to develop an understanding of the fundamental structural characteristics which influence the gas transport properties of the films. We investigated and defined the interactions of primary chemical structure and morphology (free volume) that enable these films to perform industrially important gas separations at high temperatures. We also focused on addressing the basic questions of chemical structure-morphology-transport in PBI films for gas separation applications.

A major responsibility of this research was the synthesis of PBI polymer variants at high molecular weight through a variety of approaches. The successful "PPA Process" was applied to a variety of monomers and was useful for a majority of PBI polymer syntheses. Synthetic conditions based on Eaton's Reagent has been developed as well which was successful when the PPA process was unable to yield high molecular weight polymers [57]. Overall, a full complement of synthetic skills was applied to prepare PBI

polymers of varying structures and assist in the transfer of down-selected candidates into a commercially viable production process.

As shown in Figure 1.16, three main approaches were used to prepare PBI polymers that may have enhanced diffusivity, with the understanding that diffusivity affects the transport properties more than solubility effects. The *first approach was to utilize bulky groups* on PBI backbone structures to "open up" the molecular packing of the polymer chains. Although this is not easily predicted because of conflicting effects of polymer crystallization, this was the most straightforward approach. In spite of the long history of PBI polymers, very little work has been done on understanding the effects of structure on free volume in PBI polymers, and then relating this fundamental property on gas transport properties. Initially, we prepared PBI's with simple substituents (e.g., bromo, nitro, hydroxyl, etc.) on both the *meta*- and *para*-PBI backbones. Thermal stability requirements limit many possible substituents, although these were not eliminated for our initial studies. With an appropriate structure formed by initial film processing, a secondary elimination/crosslinking step may still yield a membrane with desirable properties. A *second approach was one of creating frustrated chain packing* to prevent close chain packing. In this approach, we used some of the design approaches that have been used successfully in areas such as processable polyimides and wholly aromatic polyesters for liquid crystalline applications. Bent, crankshaft and rotations are motifs that can be incorporated into polymer structures, and have all been used to affect packing of chains in the solid state. As an example of the effectiveness of these tools, wholly aromatic polyesters were known for several decades as unprocessable polymers that would neither melt nor dissolve in any solvents. Crankshaft-type monomers,

sometimes used in combination with other motifs were found to drop the melting points from >500˚C (theoretical) to lower than 300˚C. This was fundamentally a result of decreasing the effectiveness of chain packing. We explored these motifs and combinations of motifs to enhance the free volume in PBI polymers. Our *third general approach was to use large, high mobility groups* in the polymer backbone. Typical examples of this structure are the bisphenol A and hexafluoroisopropylidene structures. At higher temperatures, an unusually large amount of rotation of such large groups can create larger distances between chains and will certainly change the transport properties of polymers containing these groups. We also investigated the effects of copolymer architecture control (random, block, etc.) in each of the previous approaches. Overall, the combination of primary chemical structure and polymer architecture provides a broad platform for us to understand the structure-property relationships and to tailor transport properties in PBI polymers.

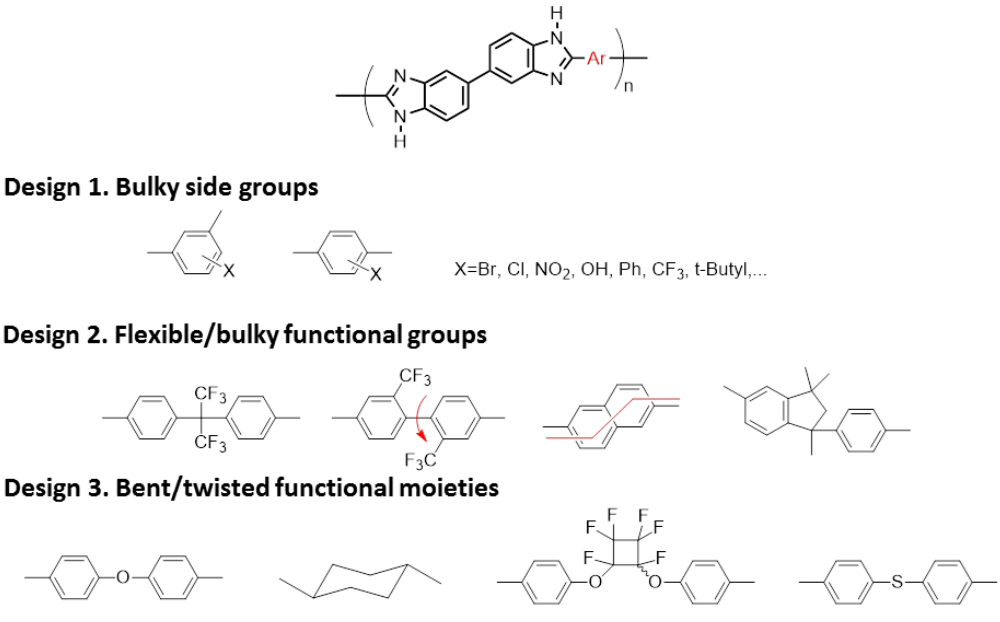

Figure 1.16 Three main approaches for PBI structures variation.

1.5 References

[1] *Fuel Cell Handbook*. Seventh ed.; EG&G Technical Services, Inc.: November 2004.

[2] E. Yeager, *Science* **1961,** 134, 1178.

[3] J. Larminie; A. Dicks; M. S. McDonald, *Fuel cell systems explained*. Wiley Chichester: 2003; Vol. 2.

[4] S. Srinivasan, *Fuel cells: from fundamentals to applications*. Springer: 2006.

[5] W. R. Grove, *London and Edinburgh Philosophical Magazine and Journal of Science* **1839,** 14, 127.

[6] History of Fuel Cell. http://www.fuelcelltoday.com/about-fuel-cells/history (accessed September 4, 2013).

[7] A. J. Appleby, *J Power Sources* **1990,** 29, 3.

[8] F. T. Bacon, *Electrochim Acta* **1969,** 14, 569.

[9] M. L. Perry; T. F. Fuller, *J Electochem Soc* **2002,** 149, S59.

[10] The Fuel Cell Industry Review. http://www.fuelcelltoday.com/media/1713685/fct_review_2012.pdf (accessed September 4, 2013).

[11] Comparison of Fuel Cell Technologies. http://www1.eere.energy.gov/hydrogenandfuelcells/fuelcells/pdfs/fc_comparison_chart.pdf (accessed September 4, 2013).

[12] K. W. Boddeker; K. V. Peinemann; S. P. Nunes, *J Memb Sci* **2001,** 185, 1.

[13] P. Costamagna; S. Srinivasan, *J Power Sources* **2001,** 102, 253.

[14] P. Costamagna; S. Srinivasan, *J Power Sources* **2001,** 102, 242.

[15] Types of Fuel Cells. http://www1.eere.energy.gov/hydrogenandfuelcells/fuelcells/fc_types.html (accessed September 4, 2013).

[16] Fuel for Thoughts on Cars of the Future. http://www.scientific-computing.com/features/feature.php?feature_id=126 (accessed September 4, 2013).

[17] K. A. Mauritz; R. B. Moore, *Chem Rev* **2004,** 104, 4535.

[18] Nafion - Perfluorosulfonate Ionomer. http://www.sfu.ca/~brodovit/files/chem367/nafion_info.pdf (accessed September 4, 2013).

[19] C. Yang; P. Costamagna; S. Srinivasan; J. Benziger; A. B. Bocarsly, *J Power Sources* **2001,** 103, 1.

[20] Q. Li; R. He; J. O. Jensen; N. J. Bjerrum, *Chem Mater* **2003,** 15, 4896.

[21] R. Savinell; E. Yeager; D. Tryk; U. Landau; J. Wainright; D. Weng; K. Lux; M. Litt; C. Rogers, *J Electrochem Soc* **1994,** 141, L46.

[22] S. Malhotra; R. Datta, *J Electrochem Soc* **1997,** 144, L23.

[23] J. Z. Sun; L. R. Jordan; M. Forsyth; D. R. MacFarlane, *Electrochim Acta* **2001,** 46, 1703.

[24] P. Bernardo; E. Drioli; G. Golemme, *Ind Eng Chem Res* **2009,** 48, 4638.

[25] S. A. Stern, *J Membr Sci* **1994,** 94, 1.

[26] R. W. Baker, *Ind Eng Chem Res* **2002,** 41, 1393.

[27] T. Graham, *Phil Mag J Sci* **1866,** 401.

[28] W. J. Koros; G. K. Fleming, *J Membr Sci* **1993,** 83, 1.

[29] K. F. Ghosal; B. D. Freeman, *Polym Adv Technol* **1993,** 5, 673.

[30] N. W. Ockwig; T. M. Nenoff, *Chem Rev* **2007,** 107, 4078.

[31] Y. Yampolskii, *Macromolecules* **2012,** 45, 3298.

[32] T. Suzuki; H. Yasuda; H. Nishide; X. S. Chen; E. Tsuchida, *J Membr Sci* **1996,** 112, 155.

[33] R. D. Noble; C. A. Koval, Review of Facilitated Transport Membranes. In *Materials Science of Membranes for Gas and Vapor Separation*, John Wiley & Sons, Ltd: 2006; pp 411.

[34] K. C. Blinker, US Patent, US 2, 904, 537 A, 1959.

[35] H. Vogel; C. S. Marvel, *J Polym Sci* **1961,** 50, 511.

[36] E. J. Powers; G. A. Serad, *Abstr Pap Am Chem S* **1986,** 191, 75.

[37] D. R. Coffin; G. A. Serad; H. L. Hicks; R. T. Montgomery, *Text Res J* **1982,** 52, 466.

[38] A. S. Buckley; D. E. Stuetz; Serad, G. A., *Encycl Polym Sci Eng* **1987,** 11, 572.

[39] T. S. Chung, *J Macromol Sci R M C* **1997,** C37, 277.

[40] F. L. Hedberg; C. S. Marvel, *Nuova Chimica* **1974,** 3, 51.

[41] F. L. Hedberg; C. S. Marvel, *J Polym Sci, Part A: Polym Chem* **1974,** 12, 1823.

[42] J. Higgins; C. S. Marvel, *J Polym Sci* **1970,** A1, 8, 171.

[43] Y. Iwakura; Y. Imai; K. Uno, *J Polym Sci Part A: Polym Chem* **1964,** 2, 2605.

[44] L. Xiao; H. Zhang; E. Scanlon; L. S. Ramanathan; E.-W. Choe; D. Rogers; T. Apple; B. C. Benicewicz, *Chem Mater* **2005,** 17, 5328.

[45] Q. Li; R. He; J. O. Jensen; N. J. Bjerrum, *Fuel Cells* **2004,** 4, 147.

[46] J. S. Wainright; J. T. Wang; R. F. Savinell; M. Litt; H. Moaddel; C. Rogers, *Proc - Electrochem Soc* **1994,** 255.

[47] J. S. Wainright; J. T. Wang; D. Weng; R. F. Savinell; M. Litt, *J Electrochem Soc* **1995,** 142, L121.

[48] A. L. Gulledge; B. Gu; B. C. Benicewicz, *J Polym Sci Part A: Polym Chem* **2012,** 50, 306.

[49] G. Qian; B. C. Benicewicz, *J Polym Sci Part A: Polym Chem* **2009,** 47, 4064.

[50] S. Yu; B. C. Benicewicz, *Macromolecules* **2009,** 42, 8640.

[51] S. Yu; H. Zhang; L. Xiao; E. W. Choe; B. C. Benicewicz, *Fuel Cells* **2009,** 9, 318.

[52] E. W. Neuse, *Adv Polym Sci* **1982,** 47, 1.

[53] D. R. Pesiri; B. Jorgensen; R. C. Dye, *J Membr Sci* **2003,** 218, 11.

[54] K. A. Berchtold; R. P. Singh; J. S. Young; K. W. Dudeck, *J Membr Sci* **2012,** 415, 265.

[55] S. C. Kumbharkar; Y. Liu; K. Li, *J Membr Sci* **2011,** 375, 231.

[56] T. C. Merkel; M. Zhou; R. W. Baker, *J Membr Sci* **2012,** 389, 441.

[57] G. Qian; D. W. Smith Jr; B. C. Benicewicz, *Polymer* **2009,** 50, 3911.

CHAPTER 2

SYNTHESIS AND CHARACTERIZATION OF PHENYLINDANE-CONTAINING POLYBENZIMIDAZOLE FOR HIGH-TEMPERATURE POLYMER ELECTROLYTE MEMBRANE FUEL CELL[1]

[1] X. Li, X. Chen and B.C. Benicewicz, *J Power Sources* **2013**, 243, 796.
Reprinted here with permission of publisher.

2.1 Introduction

In recent years, high-temperature proton exchange membrane fuel cells (PEMFCs) operating at 120-200 °C have been considered as very promising candidates for both transportation and stationary applications. Compared with traditional low temperature PEMFC systems (operated < 100 °C), they may provide several benefits such as improved catalyst kinetics, higher tolerance to fuel impurities (e.g. CO), simplified reformation schemes, and increased efficiency for the cogeneration of heat and electricity [1-5]. As the key part of the PEMFC, the polymer electrolyte membrane (PEM) plays an important role in deciding the device's final performance and reliability. Among various types of novel PEM materials that have been developed so far, the polybenzimidazole (PBI)-phosphoric acid (PA) complex membrane system is considered as the most effective one to meet requirements such as high proton conductivity and good chemical and thermal stability for high-temperature operations.

Although PBI represents a large family of heterocyclic polymers containing the benzimidazole moiety as part of the polymer repeat unit, many people use the acronym for one specific PBI variant – poly[2,2'-(m-phenylene)-5,5'-bibenzimidazole] (m-PBI), since it is the only commercialized PBI product originally produced by Celanese Corp. (now by PBI Performance Products). In 1995, Wainright et al. first described the idea that PBI could be doped with low vapor pressure inorganic proton conductors such as PA to use in high-temperature fuel cells[6]. Since then, tremendous work has been done on modifying the PEM systems based on m-PBI via different approaches. The typical strategies include optimization of membrane fabrication techniques [7-10], polymer cross-linking [11-14], polymer blend membranes [15-18], polymer composite membranes

[19-20], etc. However, the improvements have been relatively limited and the PBI systems still suffer from drawbacks such as weak mechanical strength at high acid loading and poor long-term stability. Another issue with m-PBI is its poor processability. The polymer chains of m-PBI are closely correlated due to the intermolecular hydrogen bonding and π-π stacking, thus the polymer has a high Tg (~425 °C) and can only dissolve in a few polar aprotic solvents such as *N*,*N*-dimethylacetamide (DMAc) and *N*-methylpyrrolidone (NMP) at relatively low concentrations.

Instead of relying solely on the chemical and physical modifications of m-PBI, investigations of new PBI chemical structures at the molecular level provides us a much broader window to study and design this class of materials to potentially achieve better combinations of properties. One advantage of PBI synthesis is that the chemistry is relatively straightforward. To synthesize PBIs at the laboratory-scale usually only requires a single-step solution polycondensation reaction from tetraamines and dicarboxylic acids or their simple derivatives. By varying the structure of the monomers, especially the structure of dicarboxylic acid, it is easy to alter the PBI backbone, morphology and several other corresponding properties, which would enhance our understanding of the structure-property relationships within these materials. Surprisingly, there is only limited research on new PBI structures with the detailed study of their corresponding fuel cell properties. These include PBIs containing partially fluorinated groups [21-22], sulfone linkages [18, 23], and ether linkages[24]. By using a novel sol-gel process, our lab has successfully synthesized a series of novel PBIs with higher acid doping levels and improved properties [10, 25-27]. These results also confirmed that the

chemical structure of PBIs affects the final fuel cell performance, thus supporting the view that efforts are needed to fully understand structure-property relationships.

Among numerous potential functional moieties that could be examined to improve the processability of PBI polymers, the phenylindane group has not been previously considered. First, there are very limited reports about PBIs containing aliphatic groups, especially with a full study of their physicochemical properties as potential PEM materials [28-29]. Bhavsar et al. synthesized a series of PBIs containing linear aliphatic moieties with increasing number of -CH_2- groups and found the membranes prepared by the sol-gel process showed high acid loading (up to 32 PA/RU) and several other comparable properties as those of fully aromatic PBIs [29]. Therefore, it would be interesting to introduce an aliphatic ring moiety into the PBI backbone that could help further understand the structure-property relationship of PBIs. Second, the phenylindane group possesses a rigid and bent structure, which could potentially disrupt the chain packing and improve the polymer solubility when introduced into the PBI backbone [30-32]. As an example, Ding et al. synthesized a series of novel polyamides containing the phenylindane moieties which exhibited good solubility in polar organic solvents and several other improved properties [30]. Another example is the commercially available polyimide, Matrimid®, which is highly soluble in common organic solvents such as methylene chloride and tetrahydrofuran, exhibits a high Tg (dry film, 265 °C) and good gas transport properties. Also, the PBI morphology changes caused by the introduction of the phenylindane functionality are expected to affect several corresponding polymer properties as PEM materials, such as water uptake, acid swelling ability, proton conductivity, and mechanical strength.

In this work, a PBI variant containing the phenylindane moiety (phenylindane-PBI) was prepared as well as the highly studied m-PBI by solution polymerization in polyphosphoric acid (PPA) for detailed comparisons. The polymerization conditions of phenylindane-PBI were carefully studied to obtain high molecular weight polymers. The introduction of the new functional group improved the polymer's solubility while still maintaining good thermal stability as compared to m-PBI. Both PBIs were fabricated into membranes using both of the major membrane fabrication processes and their corresponding properties such as acid doping behavior, mechanical stability and proton conductivity were compared. The phenylindane-PBI exhibited some improved properties as compared to m-PBI, indicating it is promising candidate for novel PEM materials.

2.2 Experimental

2.2.1 Materials

3,3',4,4'-Tetraaminobiphenyl (TAB, polymer grade, ~97.5%) was donated by BASF Fuel Cell. 1,1,3-Trimethyl-3-phenylindan-4',5-dicarboxylic acid (phenylindane diacid) and isophthalic acid (IPA) were purchased from Amoco Chemicals. Polyphosphoric acid (PPA, 115%) was purchased from Aldrich Chemical. Phosphoric acid (PA, 85%) was purchased from Fisher Scientific. All the other common solvents such as N,N-dimethylacetamide (DMAc), N-methylpyrrolidone (NMP), and N,N-dimethylformamide (DMF) were purchased from Fisher Scientific. Unless otherwise specified, all chemicals were used as received.

2.2.2 Polymer Synthesis

In a typical synthetic procedure for phenylindane-PBI, TAB (2.143 g, 10 mmol), phenylindane diacid (3.243 g, 10 mmol), and PPA (60-100 g) were added to a 100 ml

round-bottomed flask equipped with an overhead mechanical stirrer and nitrogen inlet/outlet. The reaction solution was mechanically stirred at 50 rpm and purged with slow nitrogen flow during the entire reaction. A programmable temperature controller with ramp and soak features was used to control the reaction temperatures. The following general temperature profile was used: stir at 50 °C for 1 hour, ramp to 140 °C over 2 hours, stir at 140 °C for 4 hours, ramp to 175 °C over 3 hours, stir at 175 °C for 6 hours, ramp to 195 °C over 2 hours, stir at 195°C for 35 hours. As the polymerization proceeded, the solution developed a dark brown color and became more viscous. Then the polymer solution was poured into water to quench the reaction, pulverized, neutralized with ammonium hydroxide, and dried in oven at 110 °C overnight to obtain the products. The synthetic procedure of m-PBI was similar and the detailed reaction conditions (e.g. monomer charge, temperature, time) were described previously [33].

2.2.3 PBI Membrane Preparation

2.2.3.1 PPA Process

At the end of polymerization, the hot phenylindane-PBI/PPA solution (approximately 60-80 g) was poured onto a clean flat glass substrate (size: 35 cm × 25 cm; preheated in oven at 130℃) and then cast in air using a film applicator with gate thicknesses varying from 15 mils (0.381 mm) to 25 mils (0.635 mm). The whole plate was then transferred to a humidity chamber with relative humidity of 55% for 24 hours to obtain the PA-doped PBI membrane. Further preparation details can also be found in previously published work [10, 27].

2.2.3.2 Conventional PA Imbibing Process

The general membrane preparation procedure for both phenylindane-PBI and m-PBI was described herein: 1.000 g PBI powder was mixed with approximately 30 ml DMAc in a 100 ml round-bottom flask and then refluxed for 3-4 hours until most polymers were dissolved. After the solution was cooled to r.t., centrifugation at 6000 rpm for 30 minutes was applied to remove the undissolved or swollen parts. PBI dense membrane was then cast in a glove bag under dry nitrogen atmosphere. The PBI solution was poured onto a clean glass plate which was taped with glass slides on each side to restrain the movement of the solution. After casting, the membrane was pre-dried inside the glove bag with a hotplate temperature of 40-50℃ overnight to remove most solvent. Then the film was transferred to the vacuum oven and dried at 110℃ overnight to obtain the PBI dense membrane. The acid-doped membrane was prepared by soaking the PBI dense membrane into different concentration PA solutions for more than 48 hours.

2.2.4 Characterization

2.2.4.1 Polymer Characterization

^{1}H NMR spectra were recorded on a Varian Mercury 400 spectrometer. FTIR spectra were recorded on a PerkinElmer Spectrum 100 FT-IR spectrometer with a three reflection diamond/ZnSe crystal. The inherent viscosities (IV's) of the polymers were measured with a Cannon Ubbelohde viscometer at a polymer concentration of 0.2 g dL^{-1} in concentrated sulfuric acid (96 wt%) at 30℃. Thermogravimetric analysis (TGA) thermograms were obtained using TA Q5000 IR Thermogravimetric Analyzer at a heating rate of 10℃ min^{-1} under nitrogen flow (20 ml/min). The densities of polymers were measured with a Kimble* Kimax* specific gravity bottle using cyclohexane as solvent at

30℃. The solubility of PBIs was evaluated by mixing PBIs with respective solvents and shaking on a wrist action shaker at r.t. for approximately 48 hours.

2.2.4.2 Membrane Characterization

The tensile properties of the PBI membranes were measured by TA RSA III Solid Analyzer at a constant Hencky strain rate of 0.001 second^{-1} at ambient condition without environment control. PBI specimens were cut according to ASTM D882 standard. The PA doping level, expressed as moles of PA per mole of PBI repeat unit (PA/RU), was measured using a Metrohm 716 DMS Titrino Automated Titrater with 0.01 M NaOH solution and calculated according to Eq. (1). The V_{NaOH} and C_{NaOH} are the volume and concentration of the NaOH required for the neutralization to reach the first equivalent point (EP1). The M_w is the molecular weight of the PBI repeat unit. The W_{dry} is the dry weight of the polymer obtaining by heating the sample in oven at 110℃ overnight after titration. Through-plane proton conductivities (σ) of PBI membranes were measured by a four-probe AC impedance method using a Zahner IM6e electrochemical station with a frequency range from 1Hz to 100 kHz and amplitude of 5 mV. According to Eq. (2), the D is the distance between two inner electrodes. The W and T are the width and thickness of the membrane. R is the experimental value of membrane impedance. During the testing, a programmable oven was used to control the testing temperatures following an initial heating cycle from r.t. to 180 °C to remove the water from the membrane. The detailed measurement method and fitting model was described previously [10].

$$X = (V_{NaOH} \times C_{NaOH} \times M_w)/W_{dry} \quad (1)$$

$$\sigma = D/(W \times T \times R) \quad (2)$$

2.2.4.3 Membrane Electrode Assembly (MEA) Fabrication and Fuel Cell Testing

Single cells with active area of 10.15 cm^2 were used to measure the fuel cell performance of the PBI membranes. The gas diffusion electrodes (GDE) were acquired from BASF Fuel Cell and the catalyst loading on anode and cathode sides were 1.0 mg cm^{-2} Pt and 1.0 mg cm^{-2} Pt alloy, respectively. To fabricate the MEA, the membrane was quickly dipped into 85% PA solution for 10-20 seconds, placed between the anode and cathode electrodes, and then hot-pressed at 140℃ and 6 N cm^{-2} for 600 seconds. The MEA was then assembled into a single cell fuel cell testing hardware. The fuel cell fabrication consisted of following components (from anode side to the MEA): stainless steel end plate with attached heater, anode current collector, gas flow field plate, and MEA. After assembly, the bolts of the cell were tightened evenly with 45 in-lbs torque. Fuel cell performance testing was conducted using a commercial fuel cell testing station from Fuel Cell Technology. All the gases (fuel and oxidant gases) were used without humidification and fed to the anode and cathode at a stoichiometric ratio of 1.2 and 2.0, respectively, in flow tracking mode.

2.3 Results and Discussion

2.3.1 Polymer Synthesis and Characterization

2.3.1.1 Polymer Synthesis

Synthetic approaches for PBI polymers have been studied for several decades and two common methods are the melt/solid polymerization and solution polymerization. A two-stage melt/solid polymerization has been applied to the production of commercial m-PBI and has some advantages for industrial production such as solvent-less conditions and easy processing after the reaction. However, the IV's of the m-PBI are relatively

limited due to the characteristics of the heterogeneous reaction conditions. A few patents reported the synthesis of phenylindane-PBI by the two-stage melt/solid polymerization and polymers with IV's as high as 0.63 dL g^{-1} (measured at a concentration of 0.4 wt% in concentrated sulfuric acid (97 wt%)) were produced[34-36]. However, the solution polymerization of PBIs in PPA is more convenient for laboratory study since it uses milder reaction temperatures and homogeneous reaction conditions, and can easily produce high molecular weight polymers. Therefore, the synthesis of phenylindane-PBI from TAB and phenylindane diacid by solution polymerization in PPA was investigated in this study (Figure 2.1). Polymerization conditions for the phenylindane-PBI were experimentally determined and Figure 2.2 shows the results for polymerization conducted at 195℃ with varying monomer concentrations. Under these conditions, a maximum IV (IV=1.00 dL g^{-1}) was observed for monomer concentrations of approximately 6.5 wt%. The step growth reaction was inhibited when the monomer concentration was too low and only low IV polymers were obtained (dilution effect). When the monomer concentration was higher than 6.5 wt%, the polymer solution became too viscous for efficient stirring, which also resulted in lower polymer molecular weight. For comparison, m-PBI was also prepared in PPA (Figure 2.1) following literature protocols and relatively high molecular weight polymers (IV=1.18-1.39 dL g^{-1}) were produced [33].

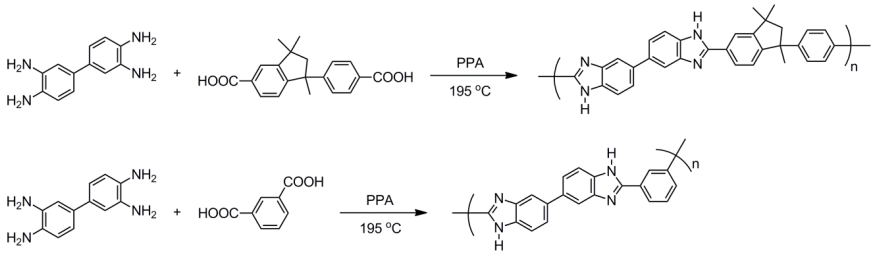

Figure 2.1 Synthesis of phenylindane-PBI (upper) and m-PBI (lower) in PPA.

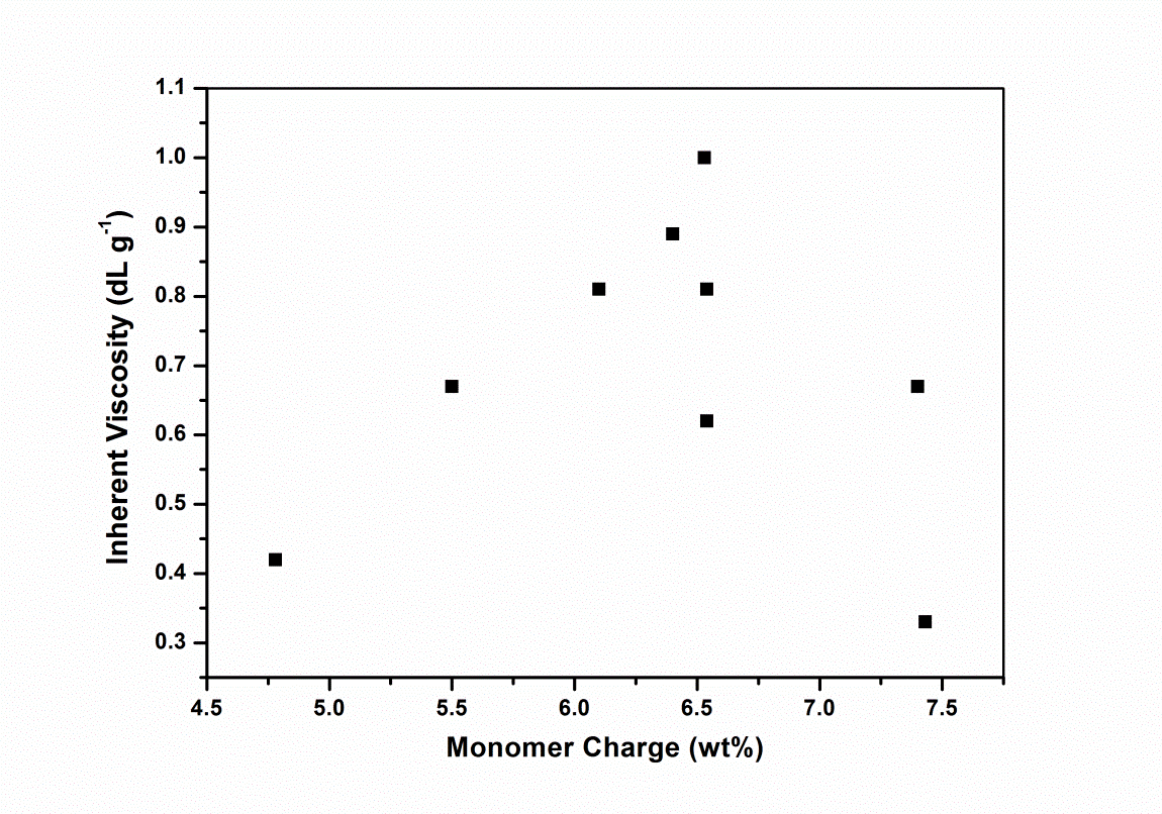

Figure 2.2 Effect of monomer concentration on IV for phenylindane-PBI at a polymerization temperature of 195℃.

2.3.1.2 Spectral characterization

The FTIR spectra of both phenylindane-PBI and m-PBI are shown in Figure 2.3 and exhibited common absorptions at 3150 cm^{-1}, 1600 cm^{-1}, 1430 cm^{-1} and 1410 cm^{-1}. The band at 3150 cm^{-1} corresponds to the stretching vibration of the hydrogen bonded N-H group. The region 1650-1400 cm^{-1} is characteristic of the benzimidazole ring and these bands were mostly attributed to the C=C and C=N stretching and the benzimidazole ring vibration. For phenylindane-PBI, absorption peaks at 2859-2960 cm^{-1} were observed, which were attributed to the aliphatic C-H bonds in the aliphatic ring of the phenylindane moiety. Both PBIs were also characterized by ^{1}H NMR using DMSO-d_6 solvent as shown in Figures 2.4 and 2.5. The characteristic proton signals of benzimidazole unit were

observed, such as the imidazole protons (H_4; 12.7-13.5 ppm) and biphenyl protons (H_1, H_2, and H_3; 7.5-8.2 ppm). These characterizations confirmed the successful preparation of desired phenylindane-PBI and m-PBI.

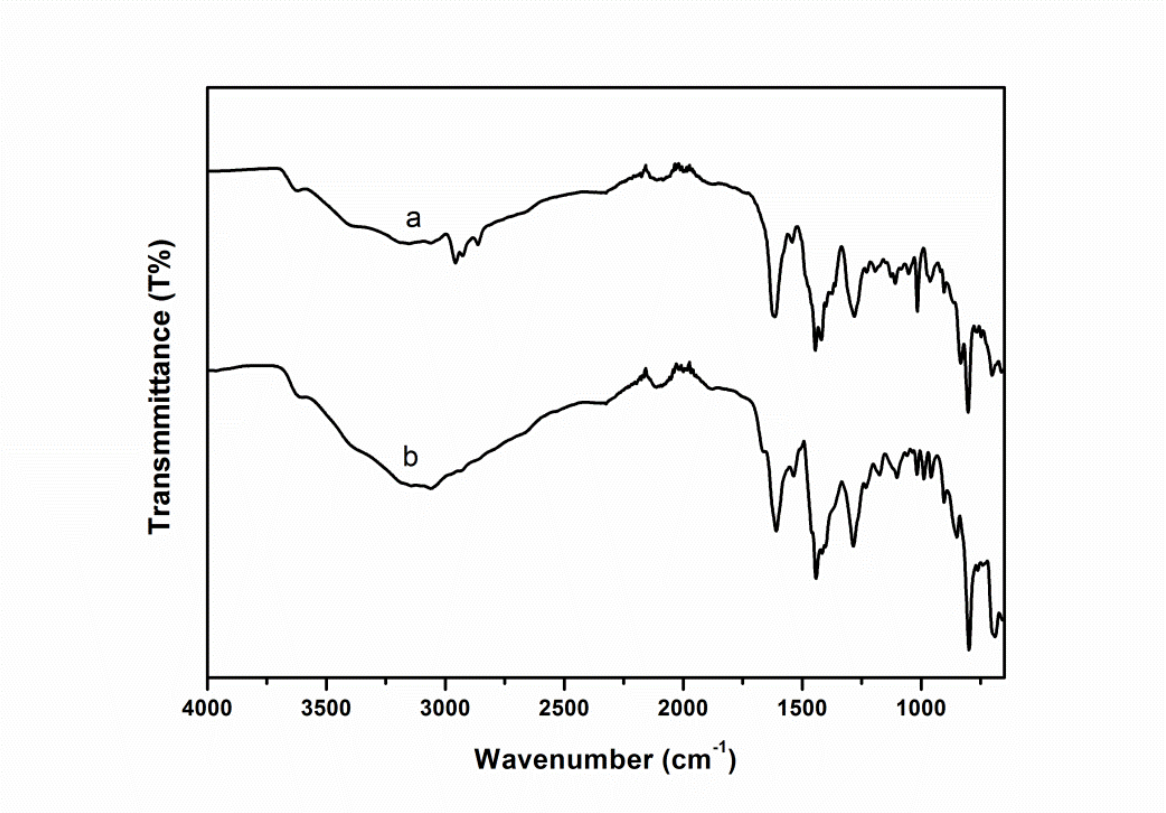

Figure 2.3 FTIR spectra of phenylindane-PBI (a) and m-PBI (b).

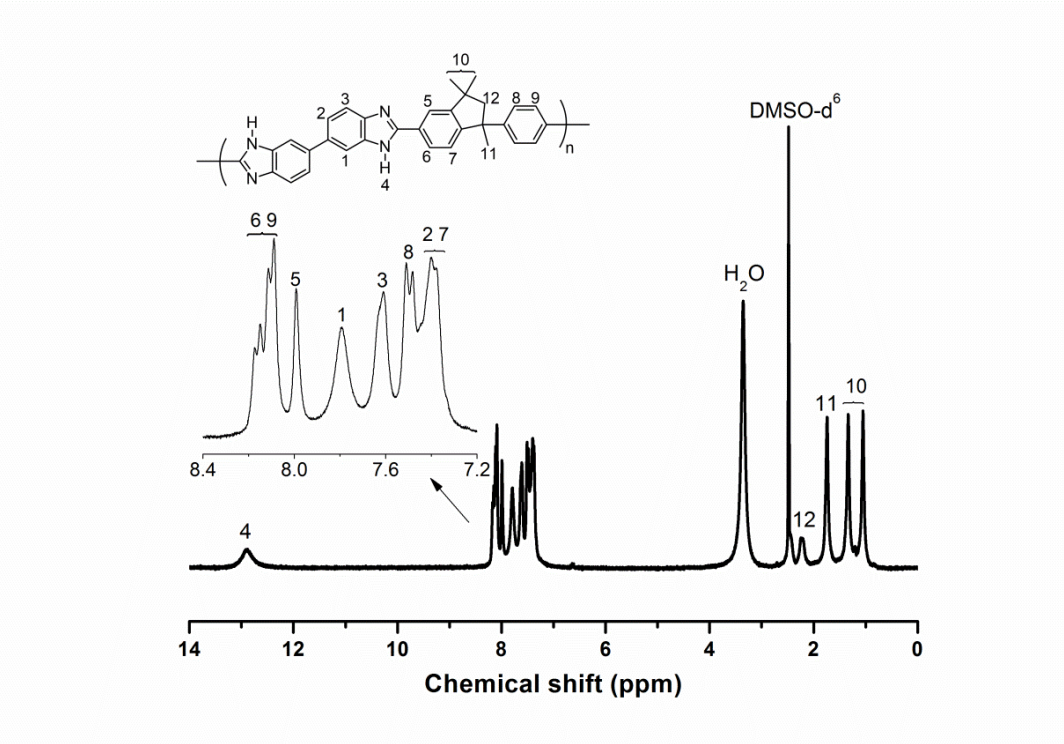

Figure 2.4 ^{1}H NMR spectrum of phenylindane-PBI.

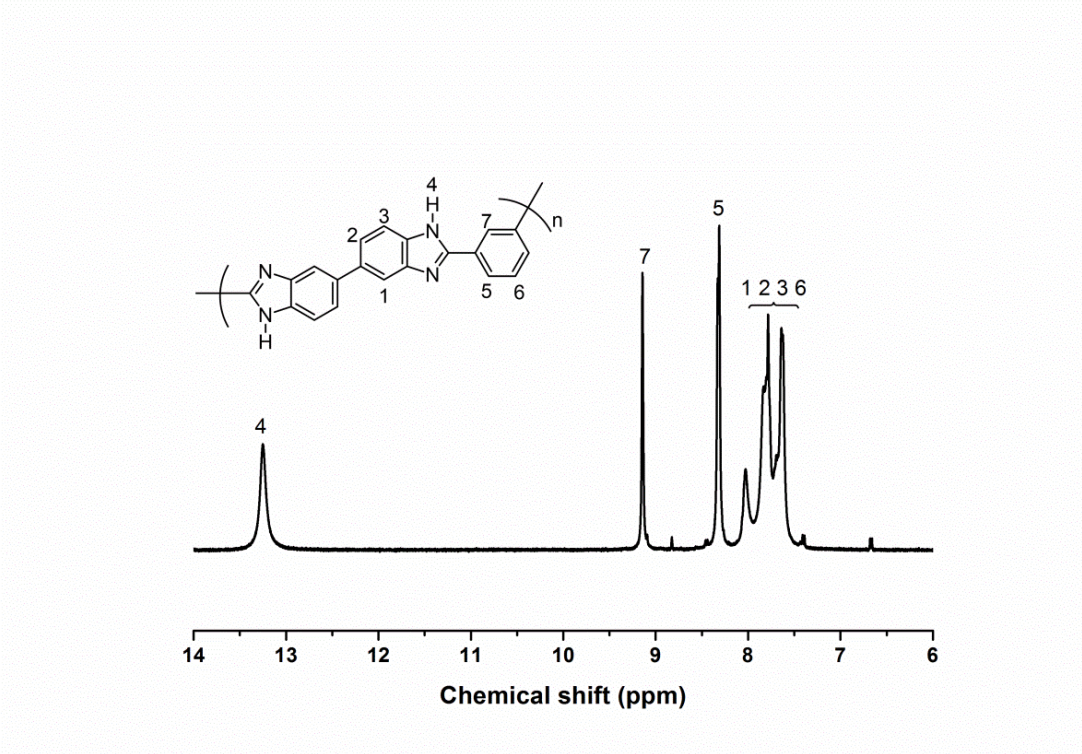

Figure 2.5 ^{1}H NMR spectrum of m-PBI.

2.3.1.3 Thermal Properties

The thermal stabilities of both phenylindane-PBI and m-PBI were studied using TGA under nitrogen flow (Figure 2.6) and all of the weight loss calculations were based on the dry weight of polymers after water removal. The initial water loss of m-PBI between room temperature and ca. 300℃ was 16.73 wt%, which is consistent with previous results (for reference, the moisture content of m-PBI is 15-18 wt% [37]). In contrast, phenylindane-PBI showed much lower moisture content of 5.56 wt%, which was attributed to the hydrophobic characteristic of the aliphatic five-member ring within the phenylindane moiety. Decomposition temperatures at different weight losses (0.02 wt%, 5 wt%, and 10 wt%) and weight retained at 900℃ of both PBIs are given in Table 2.1. The data illustrate that both polymers exhibit excellent thermal stability (less than 5 wt% loss at 500℃), which is characteristic of the rigid aromatic polymer backbones. The thermal stability of phenylindane-PBI was slightly lower than that of m-PBI due to the introduction of phenylindane linkages into the polymer main chain but it is still sufficient for realistic fuel cell applications.

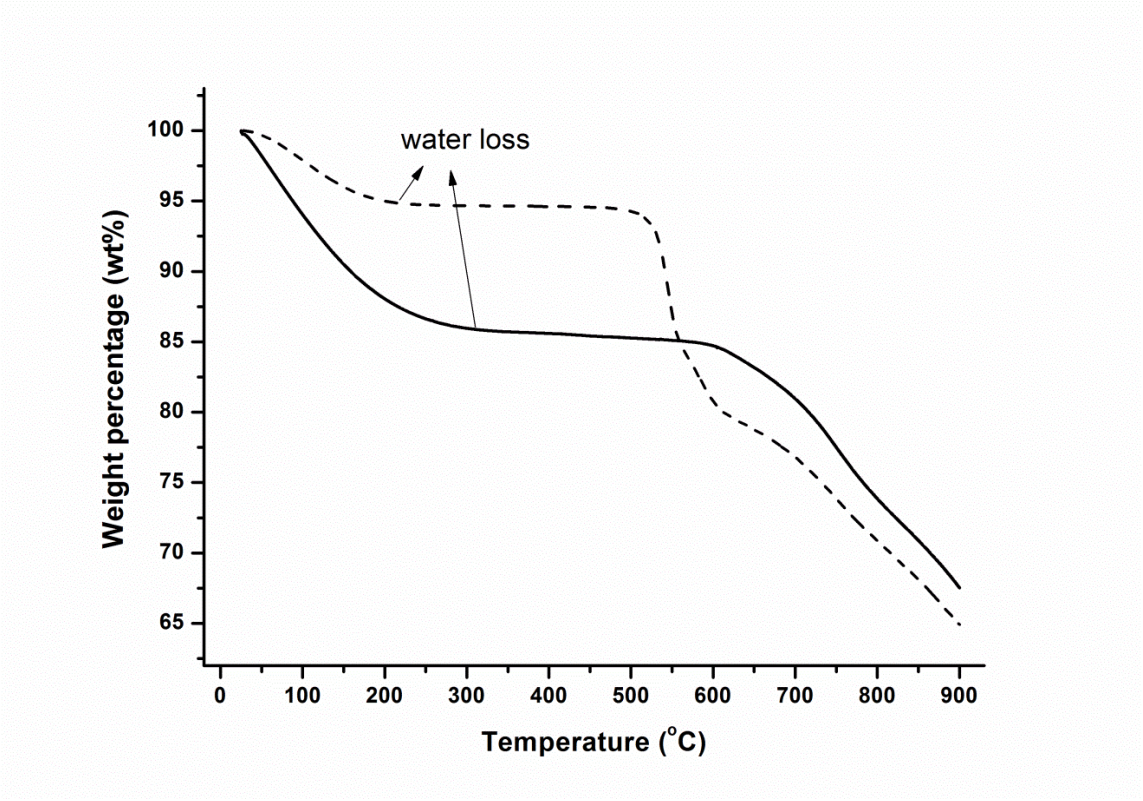

Figure 2.6 TGA thermograms of phenylindane (dash) and m-PBI (solid) under nitrogen atmosphere.

2.3.1.4 Density and Estimated Fractional Free Volume (FFV)

The densities of phenylindane-PBI and m-PBI were measured using approximately 100 mg pre-dried PBI powders in a gravity bottle at 30℃. Water was employed as a solvent for initial measurements but the results were found to be unreliable due to the strong water absorption of PBIs as discussed in section 2.3.1.3. Therefore, cyclohexane was chosen as a suitable solvent since it is not absorbed by PBIs and has a relatively low density (0.76919 g cm^{-3}, 30℃). The densities of phenylindane-PBI and m-PBI were found to be 1.16 g cm^{-3} and 1.33 g cm^{-3}, respectively. The m-PBI density measured in this work was similar to previous results (1.3 g cm^{-3} and 1.269 g cm^{-3}) [38-39]. The fractional free volume (FFV) was calculated using Bondi's group contribution approach [40] and the results are shown in Table 1. Phenylindane-PBI exhibited a larger

FFV (FFV=0.162) than m-PBI (FFV=0.136), indicating a less efficient polymer chain packing which was attributed to the introduction of the rigid bent phenylindane linkages.

Table 2.1 Physical properties of PBI variants.

			TGA				
Polymer	Density (g cm^{-3})	Estimated FFV[a]	Water loss (wt%)[b]	$TD_{0.02}$ (℃)[c]	TD_5 (℃)[c]	TD_{10} (℃)[c]	T900 (wt%)[d]
phenylindane-PBI	1.16	0.162	5.56	315.9	541.9	558.0	68.54
m-PBI	1.33	0.136	16.73	379.4	691.2	753.7	78.8

a. Fractional free volume (FFV) was calculated from Bondi's group contribution approach [40].
b. Water content from the initial weight loss.
c. Temperature at which 0.02%, 5%, and 10% weight loss occurred, respectively.
d. Retained weight% at 900℃.

2.3.1.5 Solubility

The solubility characteristics of PBIs shown in Table 2.2 were evaluated at ambient temperature. Although the dissolution properties of m-PBI have been widely reported, the results are somewhat controversial. The reported dissolution properties of m-PBI have varied due to factors such as preparative methods, polymer molecular weight (IV), and dissolution conditions. Therefore, a m-PBI with IV of 1.39 dL g^{-1} was used in this study for comparison with phenylindane-PBI. Under these conditions, m-PBI was only partially soluble in selected polar aprotic solvents such as DMAc, DMAc/LiCl (4 wt%), and NMP at a relatively low concentration (3.0 wt%). The solubility of phenylindane-PBI was much better than m-PBI and at ambient temperature the polymer was mostly dissolved in these polar aprotic solvents with concentrations up to 10.0 wt%. These results demonstrated that the introduction of the bulky bent phenylindane structure into the polymer backbone was effective in improving the polymer's solubility. However, both PBIs were insoluble in common organic solvents such as acetone, THF, or methanol.

Table 2.2 Solubility characteristics of phenylindane-PBI and m-PBI.

Polymer	IV (dL g^{-1})	DMAc	LiCl/DMAc	NMP	DMF	Acetone	THF	MeOH
phenylindane-PBI	1	++	++	++	++	—	—	—
m-PBI	1.39	+	+	+	+	—	—	—

DMAc: N, N-dimethylacetamide; LiCl/DMAc: 4 wt% LiCl in DMAc; NMP: N-methyl-2-pyrrolidinone; DMF: dimethylformamide; THF: tetrahydrofuran; MeOH: methanol.
++: mostly soluble with 10.0 wt% PBI solution; +: partially soluble with polymer swelling with 3.0 wt% PBI solution; -: insoluble.

2.3.2 Membrane Preparation and Characterization

2.3.2.1 Membrane Preparation

As shown in Figure 2.7, two different processes (PPA process and conventional PA imbibing process) were applied to the preparation of PA-doped phenylindane-PBI membranes. The novel PPA process, developed by Benicewicz et al., offers advantages such as an easier processing procedure and higher membrane acid doping levels as compared to the conventional imbibing process [10, 27]. Therefore, our initial work focused on the preparation of acid-doped membranes via the PPA process. However, the PA-doped phenylindane-PBI membranes (Figure 2.8 (left)) obtained were opaque and mechanically weak, indicating strong phase separation instead of gel formation. The film was not suitable for proton conductivity and fuel cell performance studies. The conventional PA imbibing method was also investigated and the initial films that were cast and dried in the open air were opaque and mechanically weak which was attributed to the strong water absorption and phase separation. In contrast, films obtained in a dry nitrogen environment were transparent and much stronger, as shown in Figure 2.8 (right). For comparison, PA-doped m-PBI membranes were also prepared by the conventional imbibing process.

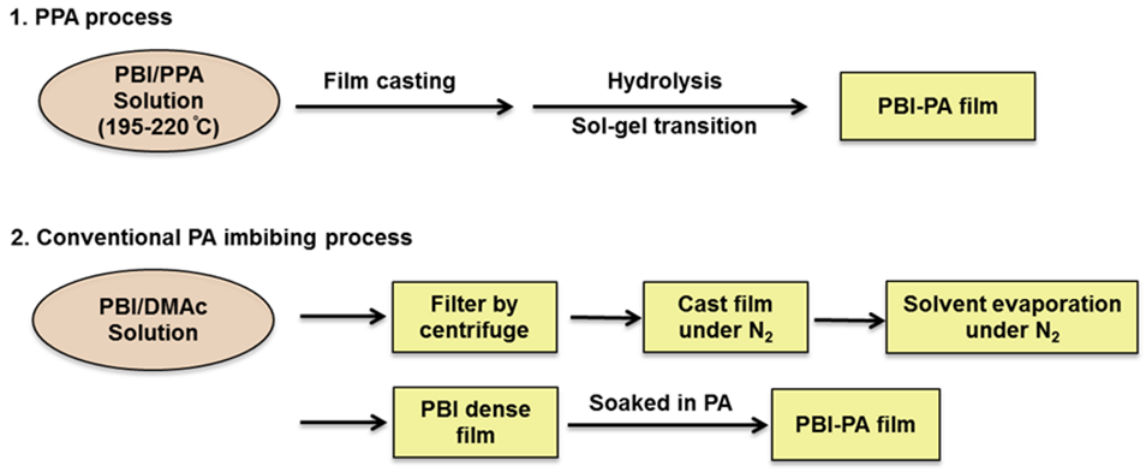

Figure 2.7 PA-doped phenylindane-PBI membranes prepared by two different preparation methods (left: PPA process; right: conventional PA imbibing process).

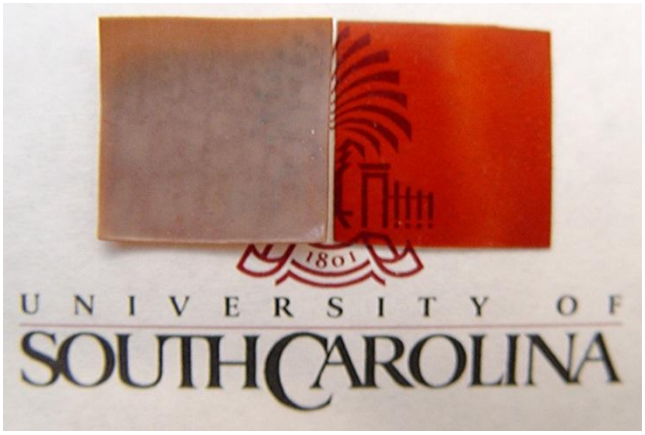

Figure 2.8 PA-doped PBI membrane preparation methods.

2.3.2.2 Acid Absorption

The acid absorption behaviors of PBIs have been studied previously and it was reported that m-PBI could be doped as high as 16 PA/RU although the loss of mechanical integrity was noted at higher doping levels [41-42]. In this work, phenylindane-PBI and m-PBI dense membranes were doped by immersion into PA solutions with different concentrations (70 %-90 %) for more than 48 hours to study and compare their absorption and stability behaviors in PA. As shown in Figure 2.9, both phenylindane-PBI and m-PBI showed similar trends of increasing PA doping levels with increasing PA

concentrations. The phenylindane-PBI exhibited good stability in 90 % PA solution with a doping level of approximately 22 PA/RU but produced a soft membrane. The PA doping levels of phenylindane-PBI in 70 %, 80 %, and 85 % PA solutions were 5.7, 7.3, and 10.0 PA/RU, respectively. For comparison, m-PBI was stable in 85% PA and became partially dissolved in 90 % PA after a few hours. The PA doping levels of m-PBI in 70-85% PA solution (3.8-10.3 PA/RU) were slightly lower than those of phenylindane-PBI. However, it is important to note the differences in the formula weight of the different repeat units. Therefore, the phosphoric acid weight percentages (without the water) were also calculated for the two PBIs at different acid doping levels (Figure 2.10). For similar acid doping levels, m-PBI membranes possessed a higher acid weight percentage than phenylindane-PBI membranes.

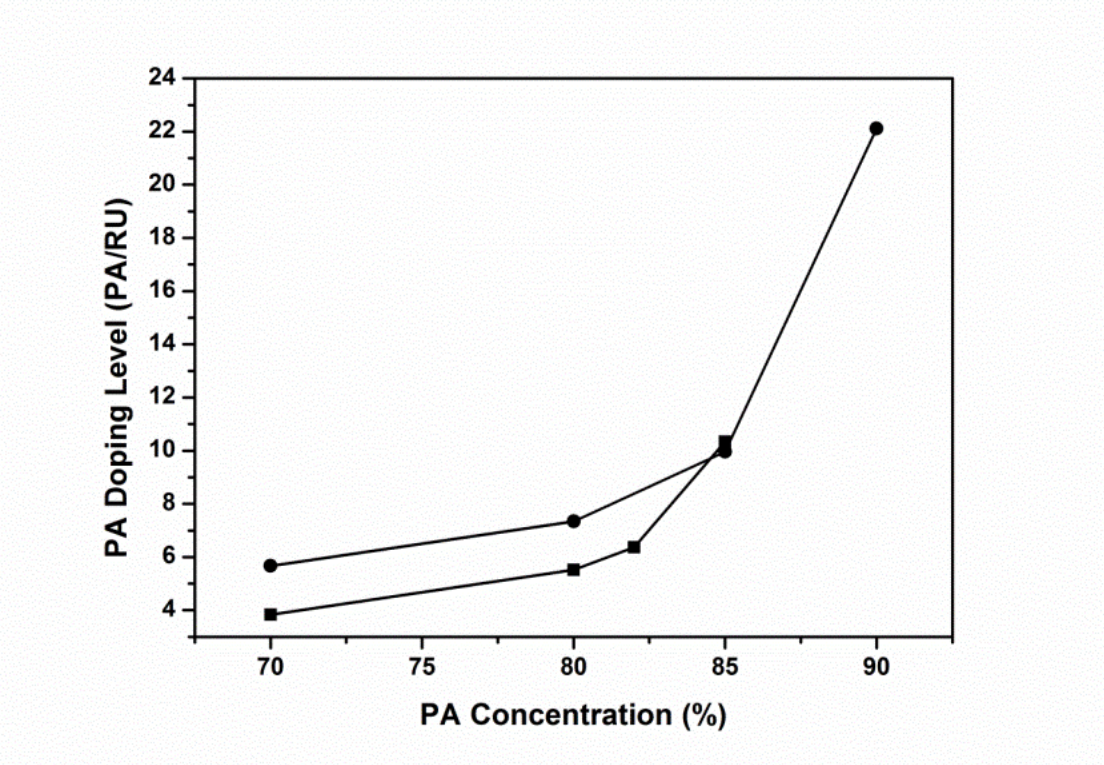

Figure 2.9 PA doping level of phenylindane-PBI (circle) and m-PBI (square) treated with different PA concentrations.

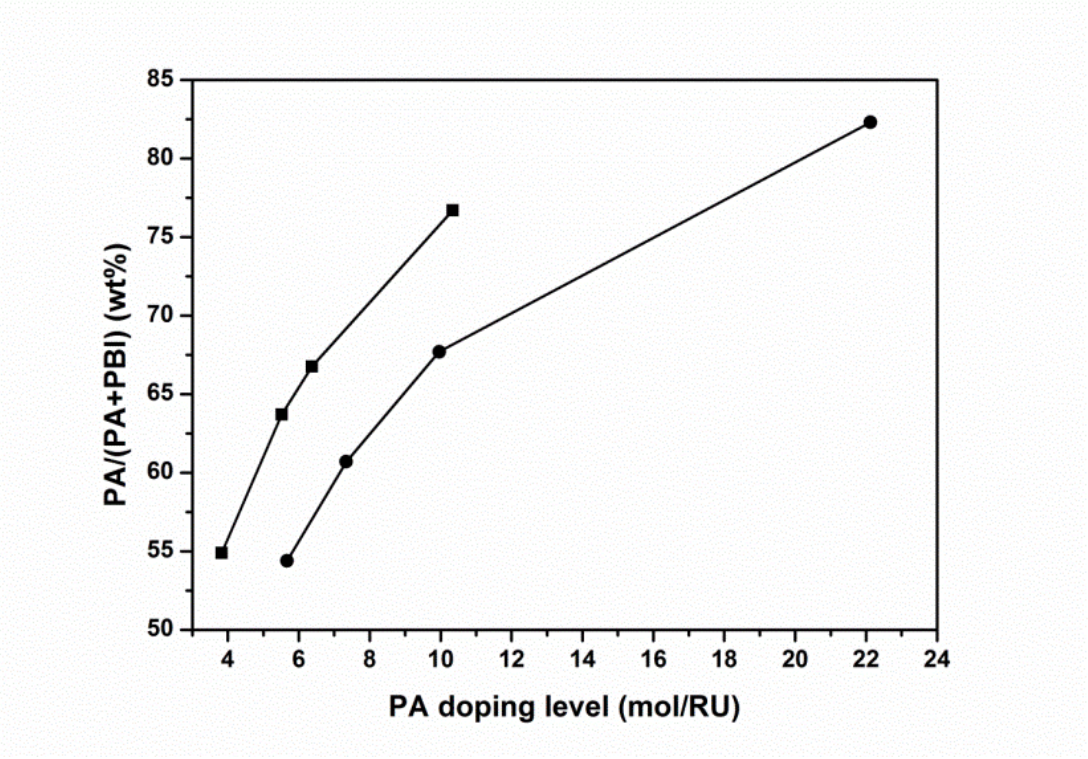

Figure 2.10 PA weight percentages of phenylindane-PBI (circle) and m-PBI (square) at different acid doping levels.

2.3.2.3 Mechanical properties

As noted previously for PA-doped PBI membranes, there is often a tradeoff between acid doping level and mechanical properties [9]. Higher acid doping levels usually provide higher membrane ionic conductivity but can result in drawbacks such as loss of mechanical strength and leaching out of "free" acid during the fuel cell operation [43]. The mechanical properties of phenylindane-PBI (IV=1.00 dL g^{-1}) and m-PBI with similar IV's (IV=1.18 dL g^{-1}) were studied as a function of PA doping level at ambient conditions (Figure 2.11 and Figure 2.12). It was found that both the tensile strength and modulus of these membranes were reduced drastically when doped with PA due to the plasticization effect but generally showed similar properties at high doping levels.

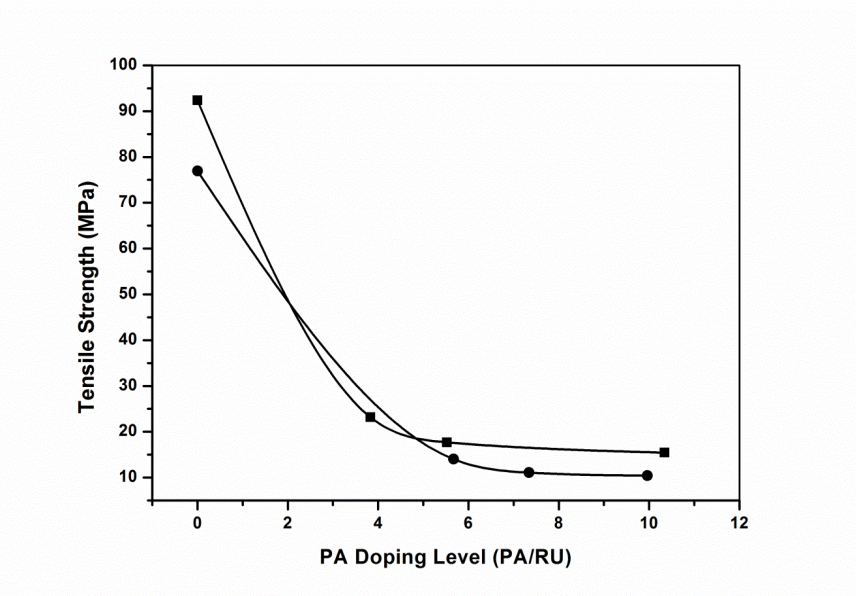

Figure 2.11 Tensile strength of PBI membranes (circle: phenylindane-PBI; square: m-PBI) as a function of PA doping level at ambient temperature.

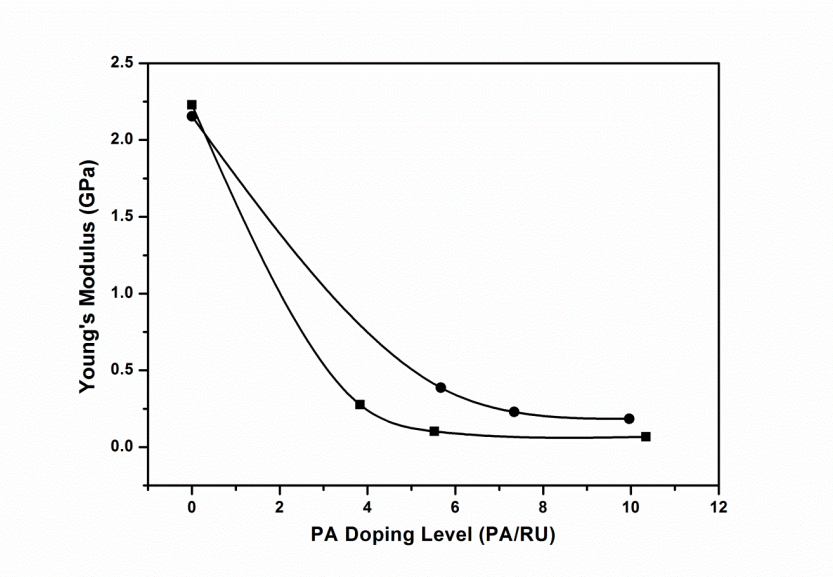

Figure 2.12 Young's modulus of PBI membranes (circle: phenylindane-PBI; square: m-PBI) as a function of PA doping level at ambient temperature.

2.3.2.4 Proton conductivity

Proton conductivities of phenylindane-PBI membranes with different acid doping levels were measured from room temperature to 180℃ without humidification and are

shown in Figure 2.13. As expected, the proton conductivities increased with both temperature and PA doping levels. At relatively low temperatures (< 80℃), the membrane conductivities were all below 0.01 S cm^{-1} and the differences between them were relatively small. As the temperature increased from 80℃ to 180℃, the conductivities increased and the differences also became larger. For a phenylindane-PBI membrane with a doping level of 10.0 PA/RU, the maximum proton conductivity was 0.061 S cm^{-1} at 180℃. For comparison, the PA-doped m-PBI membrane showed a similar conductivity of 0.062 S/cm but with a lower acid loading (6.4 PA/RU). However, when comparisons are made based on the PA weight percentage in the membrane, both membranes contained approximately 67 wt% PA, and exhibited nearly identical proton conductivities.

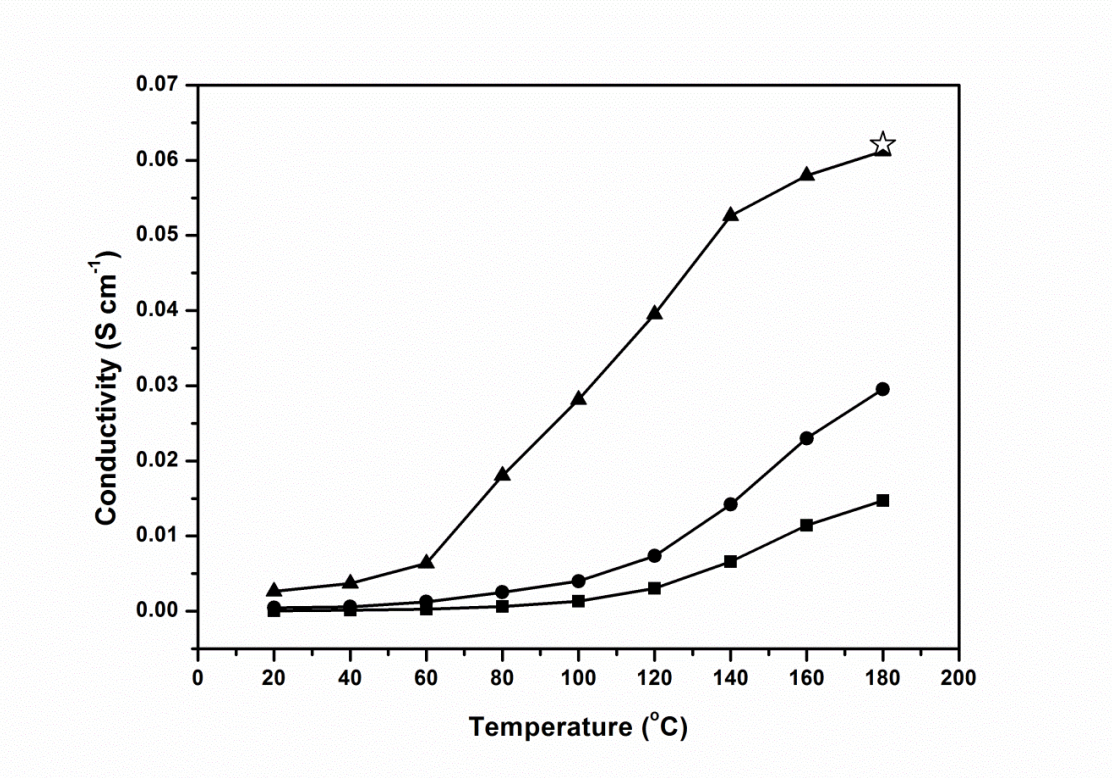

Figure 2.13 Proton conductivities of PA-doped phenylindane-PBI membranes (square: 5.7 mol PA/RU; circle: 7.4 mol PA/RU; triangle: PA/RU) and PA-doped m-PBI membranes (unfilled star: 6.4 PA/RU).

2.3.2.5 Fuel cell testing

Phenylindane-PBI membranes with a PA doping level of 10.0 PA/RU were chosen for the initial MEA fabrications. However, the fuel cell results showed that the membrane mechanical properties were not sufficient for cell operation and pinholes were created during the hot-pressing procedure. As evidence, low open circuit voltages (OCV) (<0.8 V) were observed during the initial fuel cell testing which were attributed to gas cross-over. Therefore, the phenylindane-PBI membrane with a lower PA loading (7.4 PA/RU) and higher mechanical properties was used for subsequent fuel cell studies. The membranes were dipped in 85% PA for a few seconds (10-20 sec) prior to MEA fabrication to decrease the interfacial resistance between the membrane and electrodes.

Fuel cell performance studies were conducted on single 10 cm^2 cells. Figure 2.14 and Figure 2.15 show the polarization curves of phenylindane-PBI membranes obtained under H_2/air (**a**) and H_2/O_2 (**b**) (supplied at 1.2 and 2.0 stoichiometric flows) over a range of temperatures (120 - 180℃). With both oxidants, the fuel cell performance of phenylindane-PBI membranes gradually increased with temperature. At 180℃ and a current density of 0.2 A cm^{-2}, the cell voltage of phenylindane-PBI in H_2/air was approximately 0.66 V and increased to approximately 0.72 V when the gases were switched to H_2/O_2, which was attributed to the increased oxygen partial pressure (from 0.21 atm to 1 atm). For comparison, m-PBI membranes with similar PA doping levels (PA=7.7 PA/RU) were also tested using the same MEA preparation and fuel cell testing conditions (1 atm, 180℃, H_2/air (1.2 and 2.0 stoichiometric flows) (Figure 2.16). The m-PBI showed similar fuel cell performance at low current densities but a higher rate of voltage loss as the current density was increased into the gas transport loss region when

compared with phenylindane-PBI. The maximum power density using H_2/air of phenylindane-PBI was approximately 0.36 W cm^{-2}, which was higher than m-PBI (approximately 0.32 W cm^{-2}).

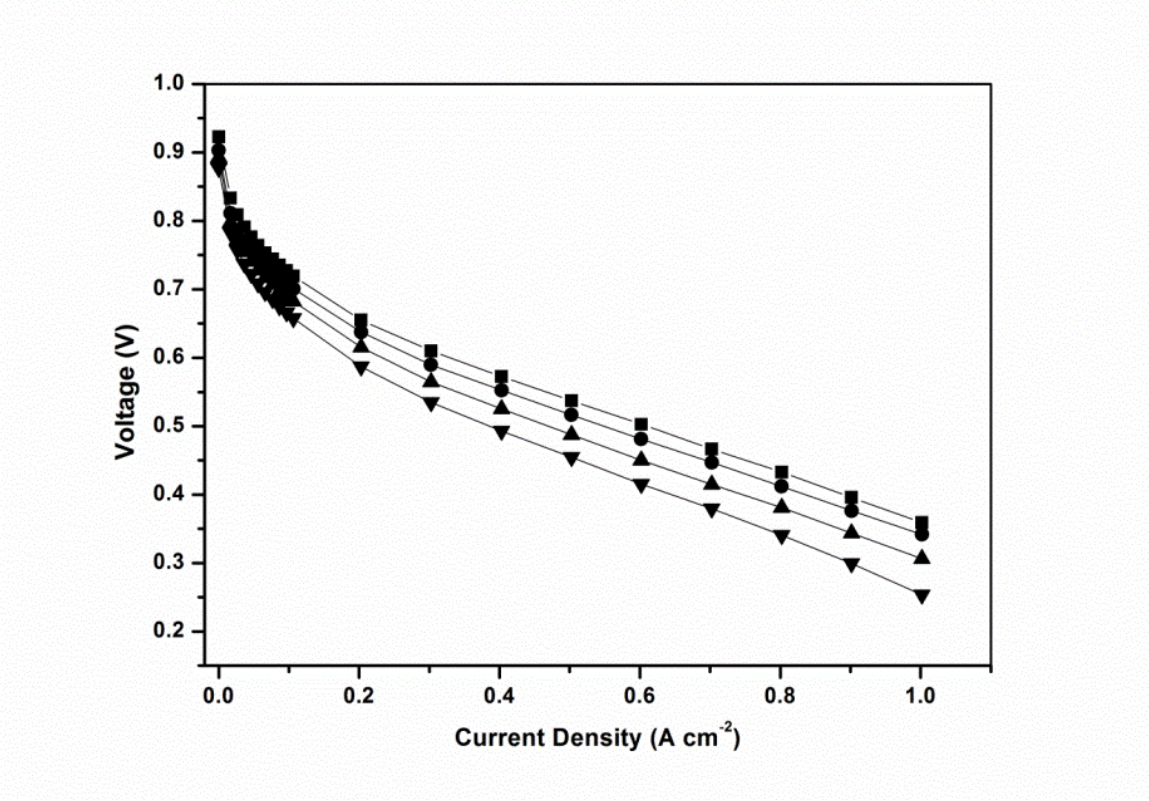

Figure 2.14 Polarization curves for MEAs using phenylindane-PBI membrane under H_2/air at various temperatures: squares - 180℃; circles - 160℃; uptriangles - 140℃; downtriangles - 120℃. (Fuel cell operation conditions: atmospheric pressure (1 atm), constant stoic H_2 (λ=1.2)/air (λ=2.0), no external humidification).

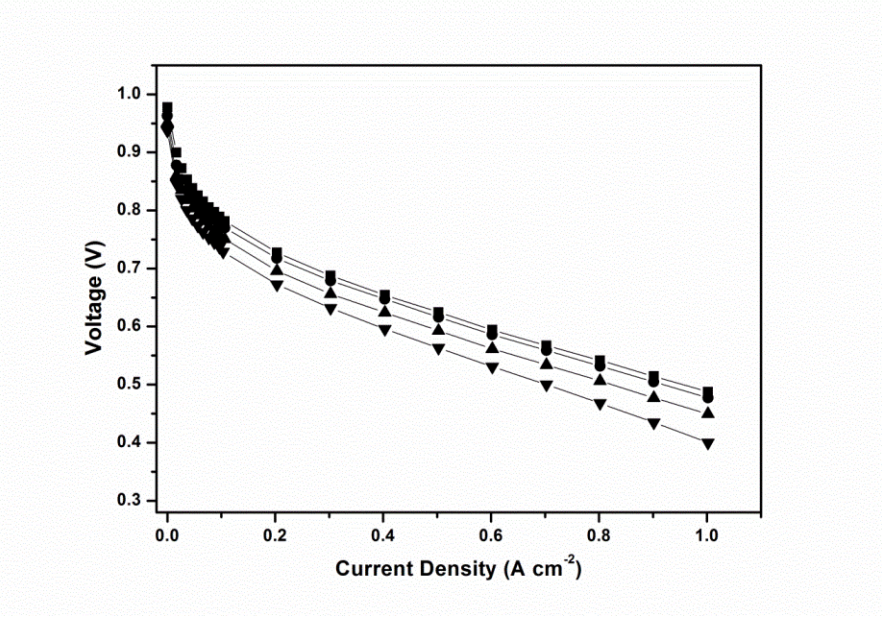

Figure 2.15 Polarization curves for MEAs using phenylindane-PBI membrane under H_2/O_2 at various temperatures: squares - 180℃; circles - 160℃; uptriangles - 140℃; downtriangles - 120℃. (Fuel cell operation conditions: atmospheric pressure (1 atm), constant stoic H_2 (λ=1.2)/O_2 (λ=2.0), no external humidification).

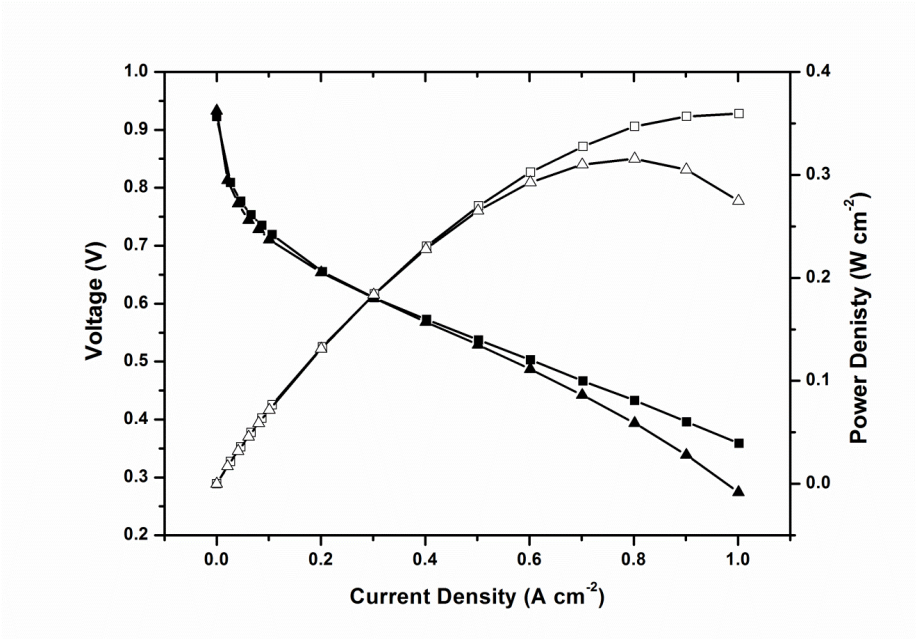

Figure 2.16 Polarization curves (filled symbols) and power density curves (unfilled symbols) for MEAs using phenylindane-PBI membranes (squares) and m-PBI membranes (uptriangles). (Fuel cell operation conditions: atmospheric pressure (1 atm), 180℃, constant stoic H_2 (λ=1.2)/air (λ=2.0), no external humidification).

2.4 Conclusions

A high molecular weight, thermally stable, and organo-soluble phenylindane-PBI was synthesized from 3,3',4,4'-tetraaminobiphenyl and 1,1,3-trimethyl-3-phenylindan-4',5-dicarboxylic acid in PPA. Investigation of polymerization conditions to achieve high molecular weight polymers was explored by varying the initial monomer concentrations. A m-PBI with similar IV was also prepared in PPA for detailed comparisons. The TGA curves showed that the thermal stability of phenylindane-PBI was slightly lower than that of m-PBI but still sufficient for practical fuel cell applications. The introduction of the rigid and bent phenylindane moiety into the PBI backbone disrupted the close polymer chain packing, as evidenced by the higher FFV and increased solubility of phenylindane-PBI compared with m-PBI. Acid-doped PBI membranes were prepared by both the PPA process and the conventional imbibing process, and the latter process produced membranes at intermediate doping levels with mechanical properties that could be tested in fuel cells. The relationships among PA concentrations, PA doping levels, and mechanical properties of the phenylindane-PBI membranes and m-PBI membranes were also evaluated and compared. Phenylindane-PBI membranes could be doped to approximately 10.0 PA/RU in 85% PA solution which exhibited a proton conductivity of 0.062 S cm^{-1} at 180 ℃. Fuel cells based on the PA-doped phenylindane-PBI membranes showed 0.65 V at 0.2 A cm^{-2} for hydrogen/air at 180℃ when operated at atmosphere pressure and dry gases. The fuel cell performance was slightly higher than the PA-doped m-PBI membrane prepared and tested under similar conditions.

2.5 References

[1] Q. Li; R. He; J. O. Jensen; N. J. Bjerrum, *Chem Mater* **2003,** 15, 4896.

[2] C. Yang; P. Costamagna; S. Srinivasan; J. Benziger; A. B. Bocarsly, *J Power Sources* **2001,** 103, 1.

[3] J. Zhang; Z. Xie; J. Zhang; Y. Tanga; C. Song; T. Navessin; Z. Shi; D. Song; H. Wang; D. P. Wilkinson; Z. -S. Liu; S. Holdcroft, *J Power Sources* **2006,** 160, 872.

[4] Y. -L. Ma; J. S. Wainright; M. H. Litt; R. F. Savinell, *J Electrochem Soc* **2004,** 151, A8.

[5] P. Jannasch, *Curr Opin Colloid Interface Sci* **2003,** 8, 96.

[6] J. S. Wainright; J. -T. Wang; D. Weng; R. F. Savinell; M. Litt, *J Electrochem Soc* **1995,** 142, L121.

[7] M. Litt, Ameri, R., Wang, Y., Savinell, R., Wainwright, J. S., *Mater Res Soc Symp Proc* **1999**.

[8] J. S. Wainright, Litt, M. H., Savinell, R. F. in: W. Vielstichm, A. Lamm, H. A. Gasteiger (Eds.), *Handbook of Fuel Cells*. John Wiley & Sons Ltd.: **2003**; Vol. 3.

[9] Q. Li; J. O. Jensen; R. F. Savinell; N. J. Bjerrum, *Prog Polym Sci* **2009,** 34, 449.

[10] L. Xiao; H. Zhang; E. Scanlon; L. S. Ramanathan; E.-W. Choe; D. Rogers; T. Apple; B. C. Benicewicz, *Chem Mater* **2005,** 17, 5328.

[11] Q. Li; C. Pan; J. O. Jensen; P. Noye; N. J. Bjerrum, *Chem Mater* **2007,** 19, 350.

[12] Y. Zhai; H. Zhang; Y. Zhang; D. Xing, *J Power Sources* **2007,** 169, 259.

[13] P. Noyé; Q. Li; C. Pan; N. J. Bjerrum, *Polym Adv Technol* **2008,** 19, 1270.

[14] N. Xu; X. Guo; J. Fang; H. Xu; J. Yin, *J Polym Sci Part A: Polym Chem* **2009,** 47, 6992.

[15] M. Hazarika; T. Jana, *ACS Appl Mater Interfaces* **2012,** 4, 5256.

[16] D. Arunbabu; A. Sannigrahi; T. Jana, *J Phys Chem B* **2008,** 112, 5305.

[17] V. Deimede; G. A. Voyiatzis; J. K. Kallitsis; Q. Li; N. J. Bjerrum, *Macromolecules* **2000,** 33, 7609.

[18] Q. Li; H. C. Rudbeck; A. Chromik; J. O. Jensen; C. Pan; T. Steenberg; M. Calverley; N. J. Bjerrum; J. Kerres, *J Membr Sci* **2010,** 347, 260.

[19] R. He; Q. Li; G. Xiao; N. J. Bjerrum, *J Membr Sci* **2003,** 226, 169.

[20] P. Staiti; M. Minutoli; S. Hocevar, *J Power Sources* **2000,** 90, 231.

[21] S. W. Chuang; S. L. C. Hsu, *J Polym Sci Part A: Polym Chem* **2006,** 44, 4508.

[22] H. Pu; L. Wang; H. Pan; D. Wan, *J Polym Sci Part A: Poylm Chem* **2010,** 48, 2115.

[23] J. Yang; Q. Li; L. N. Cleemann; C. Xu; J. O. Jensen; C. Pan; N. J. Bjerrum; R. He, *J Mater Chem* **2012,** 22, 11185.

[24] T. H. Kim; S. K. Kim; T. W. Lim; J. C. Lee, *J Membr Sci* **2008,** 323, 362.

[25] S. Yu; B. C. Benicewicz, *Macromolecules* **2009,** 42, 8640.

[26] A. L. Gulledge; B. Gu; B. C. Benicewicz, *J Polym Sci Part A: Polym Chem* **2012,** 50, 306.

[27] S. Yu; L. Xiao; B. C. Benicewicz, *Fuel Cells* **2008,** 8, 165.

[28] G. Qian; D. W. Smith Jr; B. C. Benicewicz, *Polymer* **2009,** 50, 3911.

[29] R. S. Bhavsar; S. B. Nahire; M. S. Kale; S. G. Patil; P. P. Aher; R. A. Bhavsar; U. K. Kharul, *J Appl Polym Sci* **2011,** 120, 1090.

[30] Y. Ding; B. Bikson, *Polymer* **2002,** 43, 4709.

[31] G. Maier; M. Wolf; M. Bleha; Z. Pientka, *J Membr Sci* **1998,** 143, 105.

[32] G. Maier; M. Wolf; M. Bleha; Z. Pientka, *J Membr Sci* **1998,** 143, 115.

[33] H. Zhang, Novel phosphoric acid doped polybenzimidazole membranes for fuel cells. Ph.D. Thesis, Rensselaer Polytechnic Institute, 2004.

[34] B. C. Ward, US Patent, US 4, 588, 808, 1986.

[35] B. C. Ward, US Patent, US 4, 672, 104, 1987.

[36] B. G. Dawkins; J. D. Baker; R. H. Joiner, US Patent, US 7, 060, 782, 2006.

[37] A. S. Buckley; D. E. Stuetz; G. A. Serad, *Encycl Polym Sci Eng* **1987,** 11, 572.

[38] E. Foldes; E. Fekete; F. E. Karasz; B. Pukanszky, *Polymer* **2000,** 41, 975.

[39] M. R. Tarasevich; Z. R. Karichev; V. A. Bogdanovskaya; L. N. Kuznetsova; B. N. Efremov; A. V. Kapustin, *Russ J Electrochem*+ **2004,** 40, 653.

[40] A. Bondi, *J Phys Chem-Us* **1964,** 68, 441.

[41] Q. Li; R. He; J. O. Jensen; N. J. Bjerrum, *Fuel Cells* **2004,** 4, 147.

[42] Q. Li; H. A. Hjuler; N. J. Bjerrum, *J Appl Electrochem* **2001,** 31, 773.

[43] J. W. Lee; S. B. Khan; K. Akhtar; K. I. Kim; Tae-WonYoo; K. W. Seo; H. Han; A. M. Asiri, *Int J Electrochem Sc* **2012,** 7, 6276.

CHAPTER 3

SYNTHESIS AND CHARACTERIZATION OF A NEW FLUORINE-CONTAINING POLYBENZIMIDAZOLE FOR HIGH-TEMPERATURE POLYMER ELECTROLYTE MEMBRANE FUEL CELL[2]

[2] X. Li, G. Qian, X. Chen, B.C. Benicewicz, *Fuel Cells* **2013**, 13, 832.
Reprinted here with permission of publisher.

3.1 Introduction

Polybenzimidazoles (PBI) are a class of heterocyclic polymers which have exceptional thermal, chemical, and mechanical stabilities at elevated temperatures. When fabricated into membranes and doped with low vapor pressure proton conductors such as phosphoric acid (PA), the corresponding acid-doped PBI membranes were reported as promising alternatives to traditional perfluorosulfonic acid type membranes (e.g. Nafion®). For the application of polymer electrolyte membrane fuel cells (PEMFCs) such membranes provide benefits such as high operational temperatures (120 °C – 200 °C), fast electrode kinetics, simplified water management, and high tolerance to fuel impurities (e.g. CO, H_2S) [1-5]. Among various PBI derivatives, m-PBI (poly(2,2'-(m-phenylene)-5,5'-bibenzimidazole) is the most studied due to its commercial availability, but it also has weaknesses such as weak mechanical properties at high acid loading and poor solubility in organic solvents. Another important PBI variant is *para*-PBI (poly(2,2'-(p-phenylene)-5,5'-bibenzimidazole). Its acid-doped membrane was prepared by a special sol-gel process and exhibited higher acid doping levels (> 30 mol PA per PBI repeat unit) and better proton conductivity (>0.2 S cm^{-1}) than m-PBI while still maintaining robust mechanical strength [3, 6]. However, the stiff chain characteristic of *para*-PBI caused by more rigid *para*-oriented moiety makes the polymer virtually insoluble in any organic solvents, which limits its processing window. Therefore, in recent years considerable research has been focused on investigating new PBI chemistry which could offer a better combination of desired properties for fuel cell applications.

One effective way to improve the performance of polymers is to introduce fluorine or fluorine-containing groups (e.g. trifluoromethyl group ($-CF_3$)) into the

polymer structure [7-8]. This strategy has been widely used in the structural modifications of high-performance polymers such as polyimides, polyamides and poly(arylene ether)s and the respective polymers show good solubility in organic solvents, low water uptake and dielectric properties, and high thermal and oxidative stability [9-13]. Some partially fluorinated PBIs such as 4F-PBI, 6F-PBI and PFCB-PBI have already been synthesized and exhibited better solubility, thermal and oxidative stability than non-fluorinated PBIs [14-16]. When assessing novel fluorine-containing structures, a special group that had not been previously investigated was the 2,2'-bistrifluoromethyl-4,4'-biphenylene moiety. It is well known that the steric repulsion of trifluoromethyl groups at the 2 and 2' position of the biphenyl group will force the nonplanarity of the two phenyl rings while simultaneously maintaining the rigid rod-like backbone [17]. This specific conformation was reported to be able to largely suppress the close chain packing of polymer backbones and improve the polymer's solubility and other properties [17-19]. In this work, a novel fluorine-containing PBI (BTBP-PBI) has been successfully synthesized from 3,3',4,4'-tetraaminobiphenyl and 2,2'-bis(trifluoromethyl)-4,4'-biphenyldicarboxylic acid by solution polymerization in Eaton's reagent [20]. Polymerization conditions were investigated to achieve high molecular weight polymers. Commercial m-PBI and partially fluorinated 6F-PBI containing similar functional groups (-CF_3) as BTBP-PBI were also synthesized in this work for detailed comparisons [14, 21]. All the polymers were fully characterized by FTIR, ^{1}H-NMR, ^{19}F-NMR, TGA, WAXS and other techniques. PA-doped PBI membranes were prepared via traditional PA imbibing procedures and the acid doping behavior, mechanical properties, and proton conductivity of the membranes were studied. The PBI membranes were also fabricated

into membrane electrode assemblies (MEA) and tested under various conditions to evaluate its fuel cell performance.

3.2 Experimental

3.2.1 Materials

2,2'-Bis(trifluoromethyl)benzidine (98.5%) was purchased from Akron Polymer Systems. 3,3',4,4'-Tetraaminobiphenyl (TAB, polymer grade, ~97.5%) was donated by Celanese Ventures, GmbH (now, BASF Fuel Cell). Polyphosphoric acid (PPA, 115%) was purchased from Aldrich Chemical Co. All other reagents (e.g. sodium cyanide, sodium nitrite, copper cyanide, etc.) and solvents (e.g. N,N-dimethylacetamide, 1-methyl-2-pyrrolidinone, ammonium hydroxide, etc.) were purchased from Fisher Scientific. Unless otherwise specified, all chemicals were used without further purification.

3.2.2 Monomer and Polymer Synthesis

3.2.2.1 Synthesis of 2,2'-Bis(trifluoromethyl)-4,4'-biphenyldicarbonitrile (2)

To a 500 ml round-bottom flask, 2,2'-bis(trifluoromethyl)benzidine (16.012 g, 50 mmol), hydrochloric acid (41.6 ml, 12.1 M), and water (100 ml) were added. The mixture was then heated at approximately 100 °C for 20-30 min until the solution became clear and developed a light orange color. The following operations were all conducted in an ice bath (0-5 °C) unless otherwise noted. A solution of sodium nitrite (8.624 g, 125 mmol) in 100 ml water was added dropwise to the above-mentioned ammonium salt solution to obtain an orange color solution. The reaction mixture was stirred for 1 h, and then neutralized by sodium bicarbonate solution until pH was 7. To a 500 ml beaker, copper cyanide (11.195 g, 125 mmol), sodium cyanide (18.378 g, 375 mmol), and water (100 ml) were added to obtain a clear solution. The diazonium salt solution was then gradually

added to the cyanating reagent solution with vigorous mechanical stirring. The light brown precipitate that formed was collected by filtration and sublimated under vacuum at 130 °C to obtain white crystals (4.901 g, yield 25.6 %). ^{1}H-NMR (400 Hz, DMSO-d_6): 7.684(d, J=8, 2H, Ar-**H**), 8.262 (dd, $J_{1,2}$=$J_{3,4}$=1.6, $J_{1,3}$=$J_{2,4}$=8, 2H, Ar-**H**), and 8.494 (d, J=1.2, 2H, Ar-**H**). ^{13}C-NMR (400 Hz, DMSO-d_6): 113.379, 117.590, 121.779, 124.504, 130.913, 132.912, 136.157, 140.192. Elemental Analysis for $C_{16}H_6N_2F_6$: C, 56.48; H, 1.78; N, 8.23; F, 33.50. Found: C, 56.49; H, 1.70; N, 8.23; F, 33.13.

3.2.2.2 Synthesis of 2,2'-Bis(trifluoromethyl)-4,4'-biphenyldicarboxylic Acid (3)

The dicarboxylic acid was synthesized following the procedures in the literature [22]. To a 100 ml round-bottom flask, 2,2'-bis(trifluoromethyl)-4,4'-biphenyldicarbonitrile (2.722 g, 8 mmol), potassium hydroxide (2.016 g, 36 mmol), ethylene glycol (18 ml) and water (1 ml) were added. The mixture was heated to reflux overnight. After refluxing, vacuum distillation was performed to the light yellow solution to remove some solvent (>10 ml). When the solution was cooled to room temperature, the white precipitate formed was collected by filtration and then dissolved in approximately 250 ml water. The solution was filtered again to remove undissolved byproduct and acidified by concentrated hydrochloric acid (12 M) until pH=1. The white precipitate was collected by filtration and dried at 110 °C overnight to obtain the final product in 82.7% yield. ^{1}H-NMR (400 Hz, DMSO-d_6): 7.566 (d, J=8, 2H, Ar-**H**), 8.240 (dd, $J_{1,2}$=$J_{3,4}$=1.6, $J_{1,3}$=$J_{2,4}$=8, 2H, Ar-**H**), 8.286 (d, J=1.2, 2H, Ar-**H**), and 13.663 (b, 2H, COO**H**). ^{13}C-NMR (400 Hz, DMSO-d_6): 122.378, 125.102, 126.894, 132.164, 132.525, 132.699, 140.411, 166.126. Elemental Analysis for $C_{16}H_8O_4F_6$: C, 50.81; H, 2.13; F, 30.14. Found: C, 50.71; H, 2.01; F, 29.86.

3.2.2.3 Synthesis of PBI Polymers

The general synthetic procedure of BTBP-PBI is described as follows. A 100 ml, three-necked, round-bottom flask was fitted with an overhead mechanical stirrer and nitrogen inlet and outlet. Eaton's reagent (PPMA, phosphorous pentoxide: methanesulfonic acid=1: 10, w: w) was prepared according to the literature [20]. 2,2'-Bis(trifluoromethyl)-4,4'-biphenyldicarboxylic acid (1.135 g, 3 mmol) and TAB (0.643 g, 3 mmol) were added to the reactor in a nitrogen glove box, followed by the addition of 12-20 ml of PPMA. The reaction mixture was then stirred by the mechanical stirrer at 55 rpm and purged with slow nitrogen flow. The reaction temperature was controlled by a programmable temperature controller with ramp and soak capabilities. The typical final polymerization temperatures were 140 °C for 30-40 hours. As the reaction proceeded, the solution became more viscous and developed a dark brown color. At the end of the polymerization, the polymer solution was poured into water, pulverized, neutralized with ammonium hydroxide, and vacuum dried at 110 ℃ overnight to obtain the polymer powders. The general synthetic procedure of m-PBI and 6F-PBI is similar as that of BTBP-PBI. The detailed polymerization conditions can be found in literature [14, 21].

3.2.3 PA-Doped PBI Membrane Preparation

To a 50 ml round bottom flask, BTBP-PBI powders (0.500 g) and N,N-dimethylacetamide (DMAc, 33 ml) were mixed and then refluxed (oil bath temperature 180 °C) for 2-3 hours until most polymers were dissolved. After refluxing, the undissolved or swollen polymers were removed by centrifugation at 5000 rpm for 0.5 hour to obtain a clear PBI solution. Dense PBI films were prepared by solution casting under dry nitrogen atmosphere. The PBI solution was slowly poured onto a clean glass

plate which was taped with glass slides on each side to restrain the movement of solution. After casting, the wet-film was dried slowly under nitrogen at approximately 40 °C (hot-plate temperature) to remove most solvent. Then the film was transferred to the vacuum oven and heated at 110 °C overnight to obtain the PBI dense membranes. The PA-doped BTBP-PBI membrane was obtained by immersing the PBI dense membrane into PA solutions with varying concentrations for more than 48 hours. The PA-doped m-PBI and 6F-PBI membranes were prepared following similar procedures.

3.2.4 Characterization

3.2.4.1 Monomer and Polymer Characterization

^{1}H NMR, ^{13}C NMR and ^{19}F NMR spectra were recorded on a Varian Mercury 400 spectrometer. FTIR spectra were recorded on a PerkinElmer Spectrum 100 FT-IR spectrometer with a three reflection diamond/ZnSe crystal. The inherent viscosities (IV's) of the polymer samples were measured with a Cannon Ubbelohde viscometer at a polymer concentration of 0.2 g/dL in concentrated sulfuric acid (96 wt%) at 30 °C. Thermogravimetric analysis (TGA) thermograms were obtained using TA Q5000 IR Thermogravimetric Analyzer at a heating rate of 10 °C /min under nitrogen flow (20 ml/min). The solubility of PBIs was evaluated at ambient temperature. The PBI powders were mixed with different solvents and shaken on a wrist action shaker for more than 48 hours. Oxidative stability was studied based on dry polymer powders by Fenton's test. Fenton's reagent (20 ppm Fe(II) in 3% H_2O_2) is a very effective method to generate hydroxyl/peroxyl radicals. The polymer powders were pre-dried in oven at 110 °C overnight and weighed. Then they were placed into Fenton's reagent at r.t. and 80 °C for

24 hours. After that, the samples were filtered, washed with water and dried in the oven at 110 °C for 24 hours to obtain the final weight.

3.2.4.2 Membrane Characterization

The wide angle X-ray diffraction (WXRD) was measured on a Rigaku MiniFlexll Desktop X-ray Diffractometer with the Cu-Kalpha (lamda=1.5419 anstrom) radiation. The data were recorded in the 2theta range from 3 to 45 degree at a rate of 2 degree per minute. The tensile properties of the BTBP-PBI membranes were measured by TA RSA III Solid Analyzer at a constant Hencky strain rate of 0.001/second at ambient temperature without external environment control. PBI specimens were cut according to ASTM D882 standard. The PA doping levels of PBI membranes were measured using a Metrohm 716 DMS Titrino Antomated Titrater with 0.01 M sodium hydroxide solution. The PA doping levels, X, were expressed as moles of PA per mole of PBI repeat unit (PA/RU) and calculated using Eq. (1). The V_{NaOH} and C_{NaOH} are the volume and concentration of sodium hydroxide required for the neutralization to reach the first equivalent point (EP1). The W_{dry} is the dry weight of polymer obtaining by drying the sample in oven at 110 °C overnight after titration. Mw is the molecular weight of the PBI repeat unit. Proton conductivities (σ) were measured through a four-probe AC impedance method using a Zahner IM6e electrochemical station with a frequency range from 1Hz to 100 kHz and amplitude of 5 mV. A rectangular sample was cut from the membrane and placed in a polysulfone cell with four platinum electrodes. Both two outer electrodes and two inner electrodes were placed on opposite sides of the membrane to obtain through-plane membrane proton conductivity. A programmable oven was used to measure the proton conductivity at different temperatures and two conductivity runs were performed.

In the first run, the temperature was raised to 180 °C to remove the water; in the second run, the data were collected for proton conductivity calculation according to the Eq. (2). The D is the distance between two inner electrodes. W and T stands for the width and thickness of the membrane, respectively. R is the impedance value measured.

$$X = (V_{NaOH} \times C_{NaOH} \times M_w)/W_{dry} \quad (1)$$

$$\sigma = D/(W \times T \times R) \quad (2)$$

3.2.4.3 Membrane Electrode Assembly (MEA) Fabrication and Fuel Cell Testing

The fuel cell gas diffusion electrodes with carbon cloth substrates and catalyst loading of 1.0 mg/cm^2 (Anode: Pt; Cathode: Pt alloy) were acquired from BASF Fuel Cell, Inc. The MEA with an active area of 10.15 cm^2 was fabricated by quickly dipping the respective PA-doped membranes (24 μm thickness) into 85% PA bath for 10-20 seconds, placing between an anode electrode and a cathode electrode, and then directly hot pressing without shim at 140 °C and 6N/cm^2 for approximately 10 minutes. The MEA was then assembled into a single cell fuel cell testing hardware and the compression ratio of the MEA was controlled by gaskets to reach approximately 80-85%. Fuel cell performance testing was conducted by a commercial fuel cell testing station from Fuel Cell Technologies, Inc. Polarization curves were obtained from 120 °C to 180 °C with H_2/Air and H_2/O_2 as fuel/oxidant gases at a stoichiometric ratio of 1.2 and 2.0, respectively, without external humidification or back pressure.

3.3 Results and Discussion

3.3.1 Synthesis of 2,2'-Bis(trifluoromethyl)-4,4'-biphenyldicarboxylic acid

The synthesis of 2,2'-bis(trifluoromethyl)-4,4'-biphenyldicarboxylic acid (**3**) was reported previously.[22-24] In the reported synthetic schemes, the key step is the

preparation of a dinitrile intermediate (**2**), namely 2,2'-bis(trifluoromethyl)-4,4'-biphenyldicarbonitrile, by a metal-catalyzed aromatic coupling reaction. However, the preparation of the dinitrile precursor required multiple-step procedures and the coupling reaction provided relatively low yields and a large amount of by-products such as m-aminobenzotrifluoride, which could be caused by the existence of two strong electron-withdrawing groups (-CN, -CF_3) on a single reactant [24]. In this work, the synthesis of the diacid monomer was achieved through a simplified two-step method by using 2,2'-bis(trifluoromethyl)benzidine (**1**) as the starting material (Figure 3.1). Copper(I) cyanide was employed initially as the Sandmeyer cyanating reagent to transform the diamine to dinitrile but only gave a very low yield (15.2%). Therefore, a tetrahedral copper-cyano complex ($Na_3[Cu(CN)_3]$) was introduced and moderately improved the yield to 25.6%.[25] The reason for the low reaction yield is not clear and under further investigation. Hydrolysis of dinitrile to the diacid was accomplished readily in a high yield (82.7%).

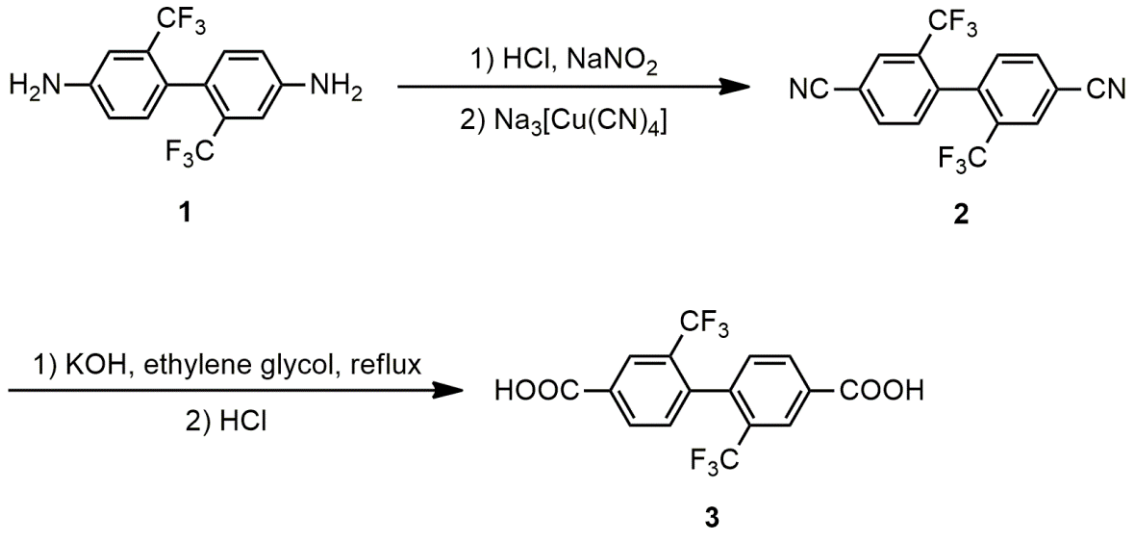

Figure 3.1 Synthesis of 2,2'-bis(trifluoromethyl)-4,4'-biphenyldicarboxylic acid.

3.3.2 Synthesis of PBI Polymers

There are several strategies for the synthesis of PBI polymers such as melt polymerization and solution polymerization. A two-stage melt-solid polymerization method is currently applied for the production of commercially available m-PBI. Another important synthetic approach is by solution polymerization in polyphosphoric acid (PPA). It is more favored for laboratory-scale study since it can be used as both solvent and condensation reagent and often produces high molecular weight polymers. Therefore, the solution polymerization of BTBP-PBI in PPA was also investigated early in this study. The diacid monomer exhibited good solubility in PPA at elevated temperatures. However, as the temperature rose to approximately 170℃, the polymer solution turned into a gel-like mass within a few minutes, which could be caused by cross-linking of polymer. As partial evidence, the product could not be fully dissolved in concentrated sulfuric acid to obtain IV's via our standard methods.

Eaton's reagent (PPMA, phosphorous pentoxide: methanesulfonic acid=1: 10, w: w) was reported to be a convenient alternative to PPA for carrying out alkylation and acylation reactions on aromatic systems [20]. It also provides advantages over PPA such as lower viscosity and moderate reaction temperatures. Qian et al. reported the utilization of PPMA on the polymerization of a novel fluorinated-PBI and high molecular weight products (IV=1.55 dL/g) were obtained [15]. Therefore, PPMA was also examined in this work and high molecular weight polymers were successfully produced (Figure 3.2). The following stepwise temperature control was used to ensure both monomers were fully dissolved before the polymerization: stir at 50 °C for 1 hour, ramp to 100 °C over 6 hours, stir at 100 °C for 18 hours, ramp to 140 °C over 6 hours, stir at 140 °C for 30-40

hours. Polymerization conditions were then experimentally optimized and Figure 3.4 shows the effect of the monomer charge on the IV of BTBP-PBI at a final polymerization temperature of 140℃. It was found that the IV of the polymer reached the maximum of 1.60 dL/g when the monomer concentration was approximately 1mmol: 5.5 ml (monomer: solvent). When the monomer concentration was too high, the solution was found to be too viscous for efficient stirring. In contrast, when the concentration was too low, step growth reaction was inhibited.

High molecular weight m-PBI (1.39 dL g^{-1}) and 6F-PBI (1.07 dL g^{-1}) were also prepared by solution polymerization in PPA according to the literature [14, 21]. The general synthetic scheme and the structures of PBIs are shown in Figure 3.3.

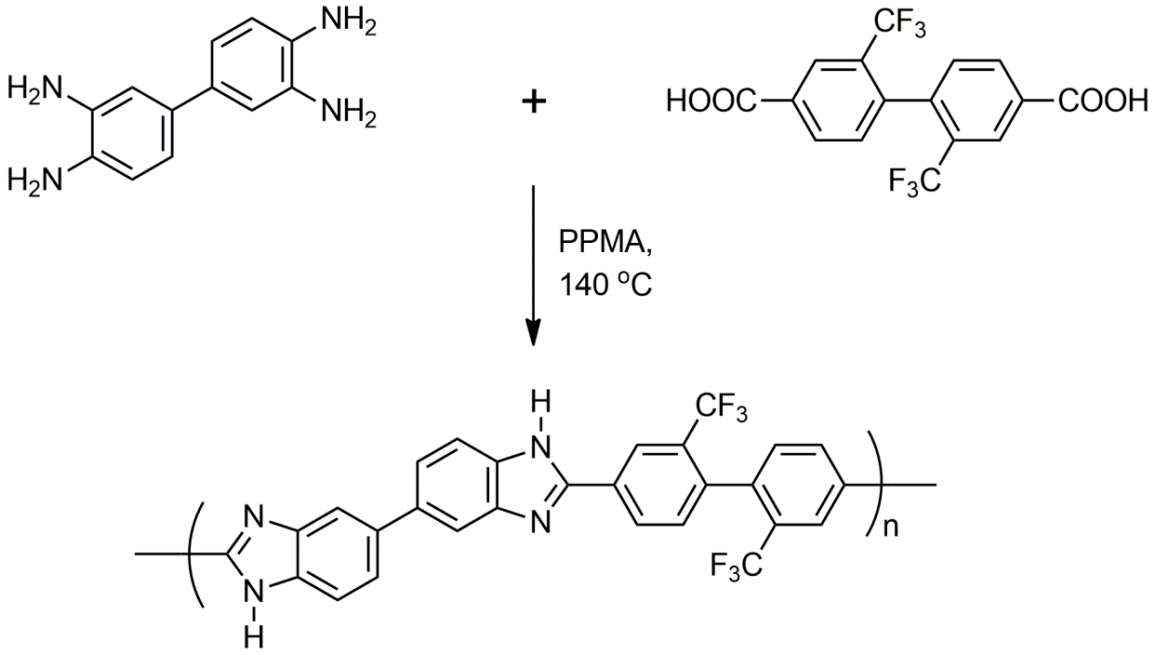

Figure 3.2 Synthesis of BTBP-PBI in Eaton's Reagent.

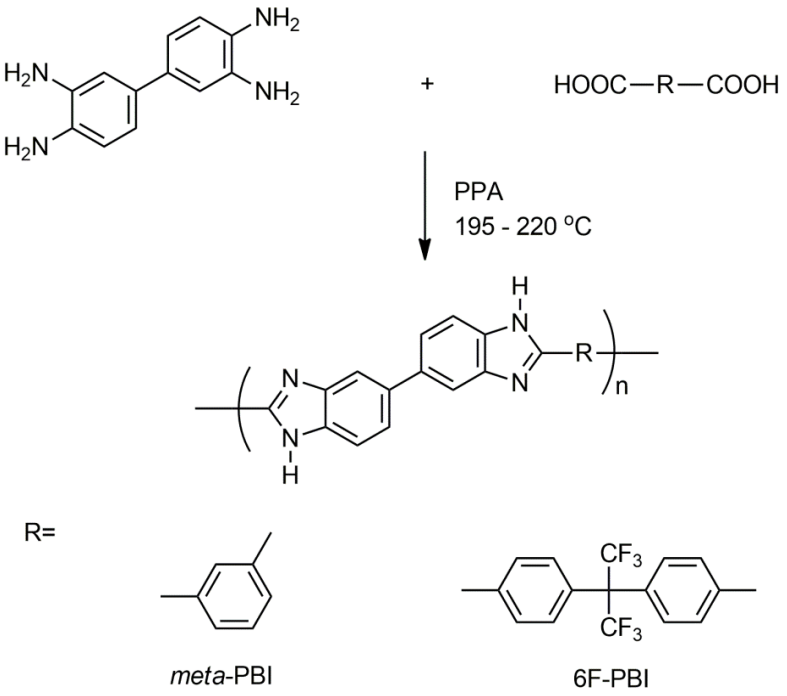

Figure 3.3 Synthesis of m-PBI and 6F-PBI in PPA.

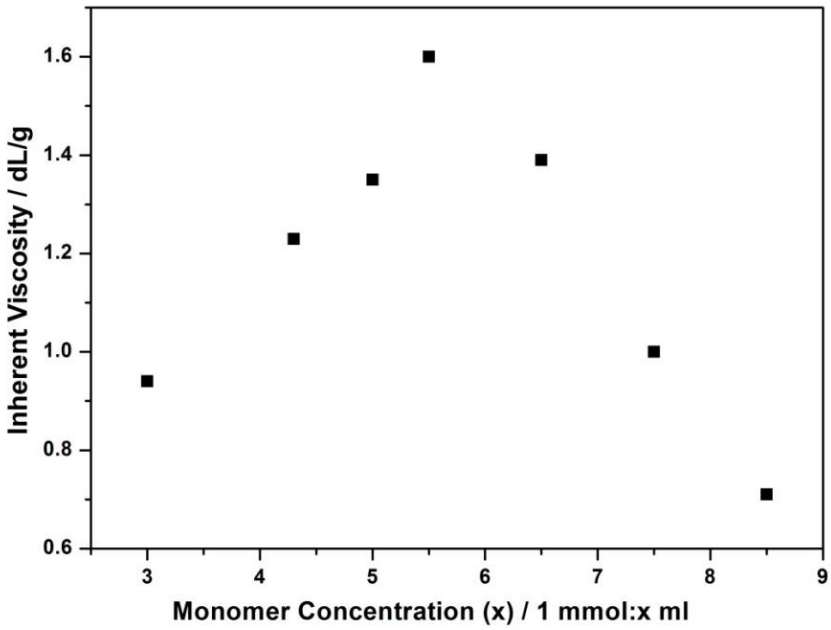

Figure 3.4 Effect of monomer concentration on IV for BTBP-PBI at a polymerization temperature of 140℃.

3.3.3 Polymer Characterization

3.3.3.1 Spectral Characterization

The BTBP-PBI as well as m-PBI and 6F-PBI were characterized by FTIR and the spectra are shown in Figure 3.5. All polymers exhibited characteristic absorption bands in the broad region of 3500-2800 cm^{-1} which are ascribed to the hydrogen bonded and non-hydrogen bonded N-H and aromatic C-H stretching of the benzimidazole rings. The region 1630-1380 cm^{-1} was attributed to the C=C and C=N stretching, in-plane ring vibration of benzimidazole as well as imidazole ring breathing mode. The broad peak at 1259-1313 cm^{-1} corresponded to the C-F stretching vibration of BTBP-PBI. The polymers were also characterized by ^{1}H NMR and ^{19}F NMR. In the ^{1}H-NMR spectra (Figures 3.6, Figure 3.7 and Figure 3.8), the benzimidazole characteristic proton signals were observed in all PBIs such as imidazole protons (e.g., for BTBP-PBI, H_4; 13.36 ppm) and biphenyl protons (e.g., for BTBP-PBI, H_1, H_2 and H_3; 7.68-8.07 ppm). In the ^{19}F-NMR spectra (Figures 3.9 and Figure 3.10), the fluorine signals of BTBP-PBI and 6F-PBI were observed at -57 ppm and -63 ppm, respectively. All the characterizations confirmed the successful preparation of the desired PBI polymers.

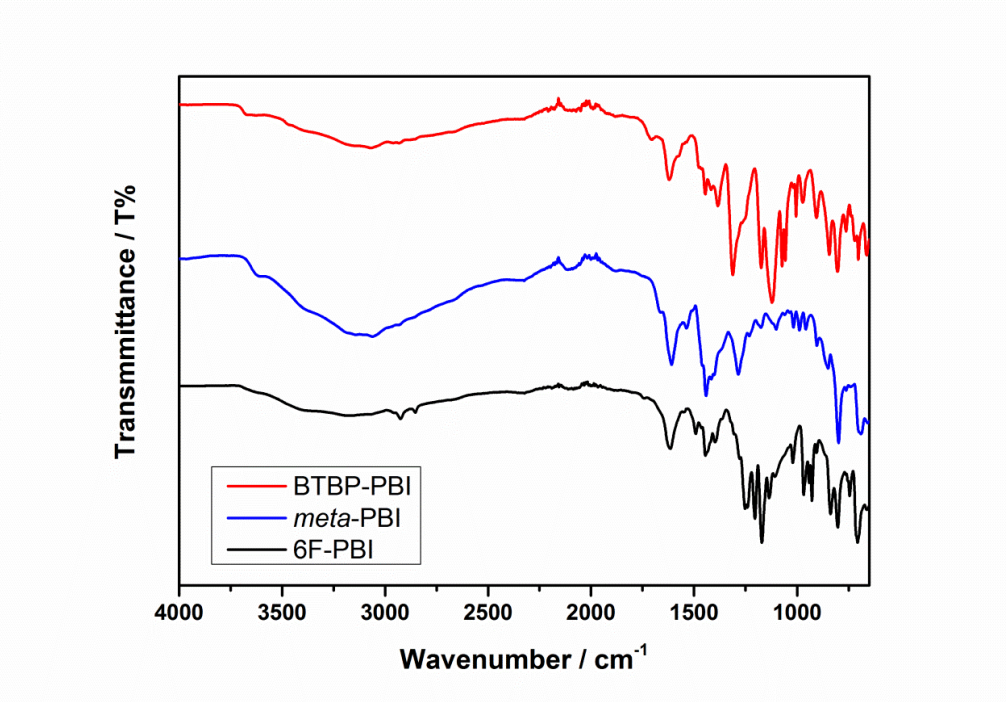

Figure 3.5 FTIR spectra of BTBP-PBI, m-PBI and 6F-PBI.

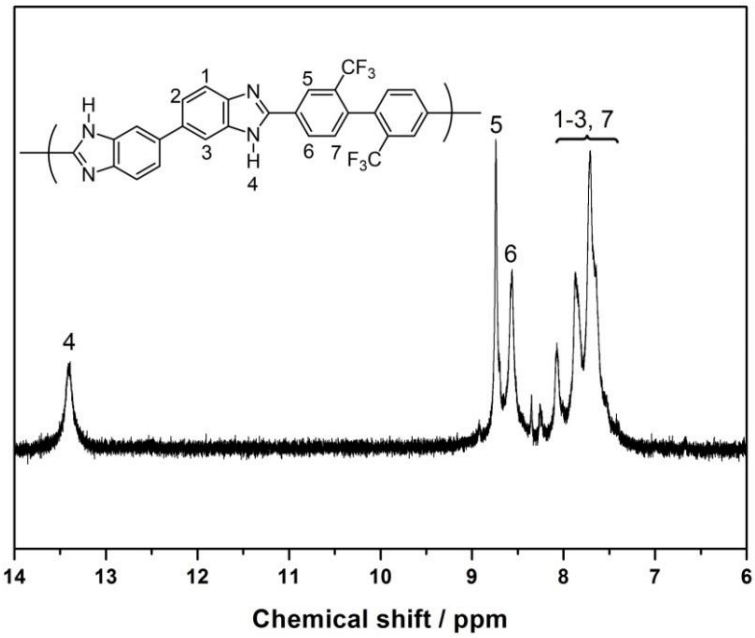

Figure 3.6 ^{1}H NMR spectrum of BTBP-PBI in DMSO-d^{6}.

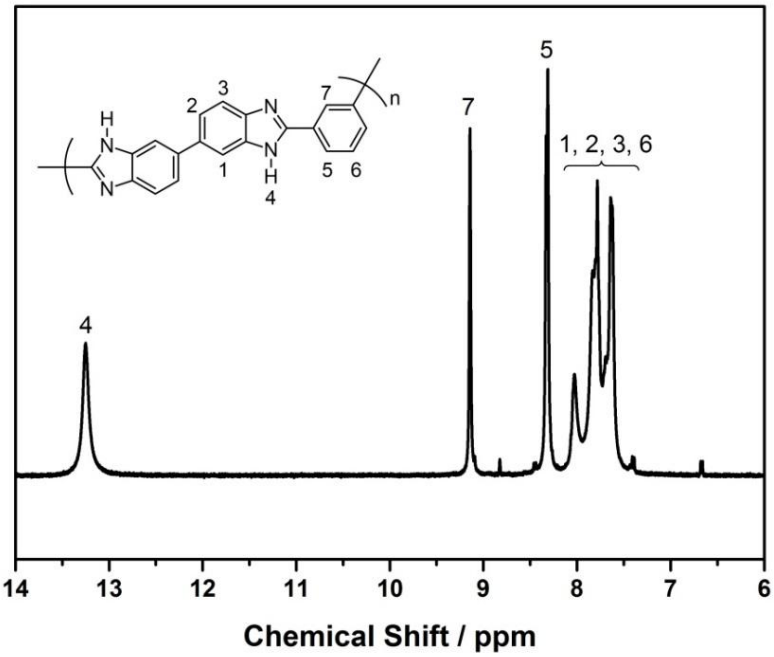

Figure 3.7 ^{1}H NMR spectrum of m-PBI in DMSO-d^{6}.

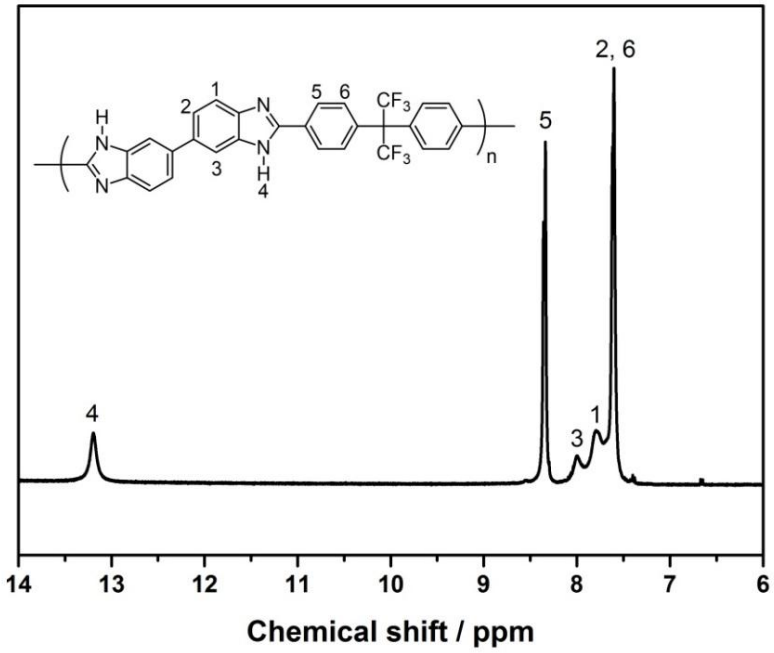

Figure 3.8 ^{1}H NMR spectrum of 6F-PBI in DMSO-d^{6}.

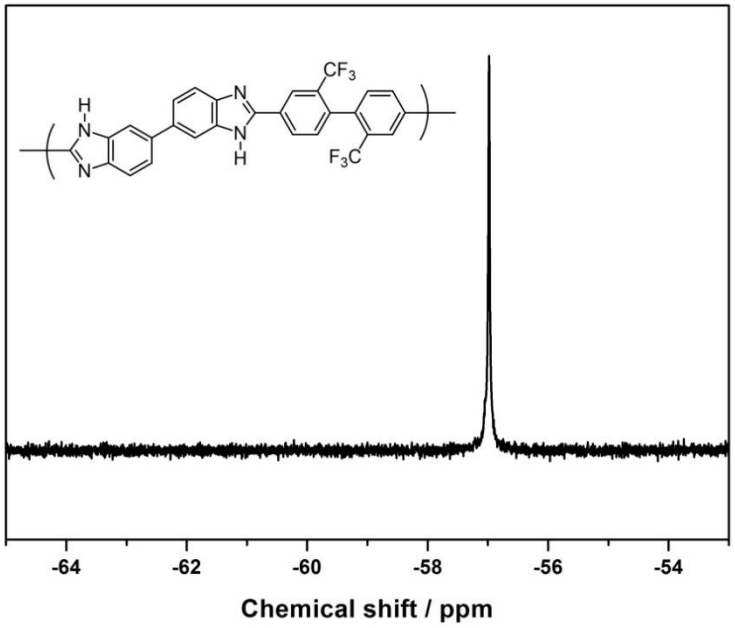

Figure 3.9 ^{19}F NMR spectrum of BTBP-PBI in DMSO-d^{6}.

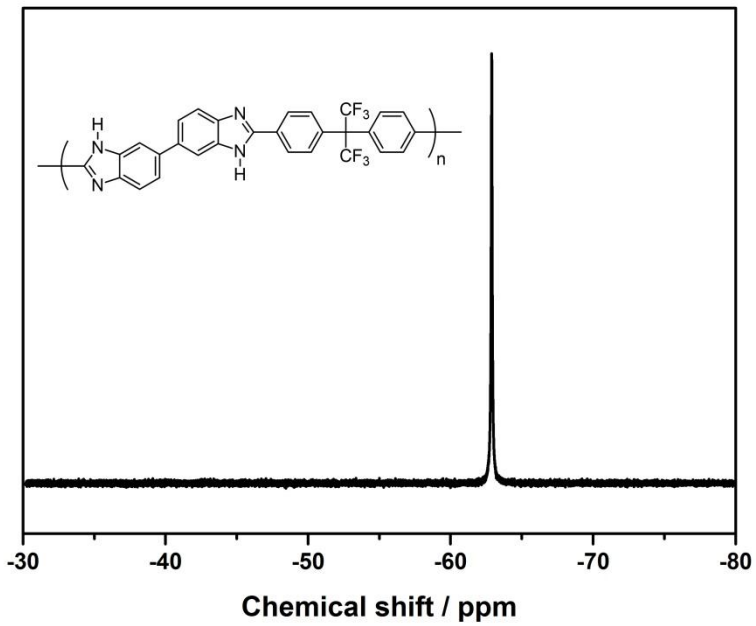

Figure 3.10 ^{19}F NMR spectra of 6F-PBI in DMSO-d^{6}.

3.3.3.2 Thermal Properties

The thermal stability of BTBP-PBI, m-PBI, and 6F-PBI were studied using TGA under nitrogen flow (20 ml/min) at a heating rate of 10 °C /min and the results are shown in Figure 3.11 and Table 3.1(all of the weight loss calculations were based on the dry weight of polymers after water removal). The 7.0 wt% water loss of BTBP-PBI between room temperature and ca. 200 °C was attributed to the hydrophilic characteristics of PBI polymers. This number is comparable to that of 6F-PBI (5.66 wt%) but much smaller than that of m-PBI (16.7 wt%), which is likely caused by the introduction of the more hydrophobic trifluoromethyl groups. The BTBP-PBI was stable up to 277 °C (0.02 wt% loss of the dry polymers) and the decomposition temperatures of TD_5 and TD_{10} (5 wt% and 10 wt% loss of the dry polymers) were 471 °C and 536 °C, respectively. The polymer was completely decomposed at 900 °C. The overall thermal stability of BTBP-PBI was slightly lower than that of m-PBI and 6F-PBI, but sufficiently stable for realistic fuel cell applications [26]. The glass-transition temperature (Tg) of the BTBP-PBI was not detectable by DSC up to 450℃.

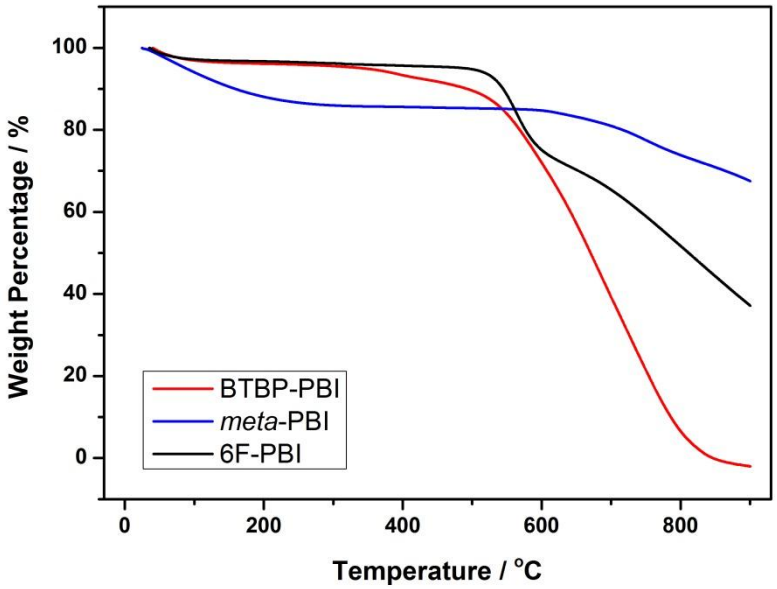

Figure 3.11 TGA thermograms of BTBP-PBI, m-PBI and 6F-PBI in nitrogen atmosphere.

Table 3.1 Thermal stabilities of PBI derivatives.

Polymer	Water wt%	Decomposition Temperature (°C)		
		0.02 wt%	5.0 wt%	10.0 wt%
BTBP-PBI	7.00	277	471	536
meta -PBI	16.7	379	691	754
6F-PBI	5.66	410	478	566

3.3.3.3 Polymer Solubility

The solubility characteristics of all PBIs were determined at ambient conditions and at various polymer concentrations (1.0 wt% - 5.0 wt%) and the results are shown in Table 3.2 The BTBP-PBI polymer showed higher solubility than m-PBI and comparable solubility as 6F-PBI in some polar, aprotic solvents such as DMAc, NMP and DMF, which could be attributed to the introduction of the bulky and twisted biphenyl structure into the polymer backbone. However, it was found for the high concentration solutions (5.0 wt%) that the BTBP-PBI polymers were susceptible to precipitating out of solution

after sitting and formed gels. Further shaking at ambient conditions or slight heating did not convert it back to the solution state. The addition of LiCl (4 wt%) to DMAc as a stabilizer effectively postponed or prevented the polymer precipitation. All polymers were insoluble in common organic solvents such as acetone, THF and MeOH.

Table 3.2 Solubility characteristics of PBI derivatives.

	DMAc		LiCl/DMAc		NMP		DMF		Acetone	THF	MeOH
	1.5 wt%	5.0 wt%	1.5 wt%	5.0 wt%	1.5 wt%	5.0 wt%	1.5 wt%	5.0 wt%	1.0 wt%	1.0 wt%	1.0 wt%
BTBP-PBI	++	++*	++	++	++	++*	++	++*	−	−	−
meta -PBI	+	+	+	+	+	+	+	+	−	−	−
6F-PBI	++	++	++	++	++	++	++	++	−	−	−

DMAc: N,N-dimethylacetamide; LiCl/DMAc: 4 wt% LiCl in DMAc; NMP: N-methyl-2-pyrrolidinone; DMF: N,N-dimethylformamide; THF: tetrahydrofuran; MeOH: methanol.
++: mostly soluble; ++*: mostly soluble, but polymer may precipitate from solution after sitting; +: partially soluble or swelling; -: insoluble.
m-PBI and 6F-PBI were synthesized in house.

3.3.3.4 Oxidative Stability

The oxidative stabilities of all PBIs were investigated by measuring the weight loss of the pre-dried polymer powders which had been immersed into Fenton's reagent for 24 hours at different temperatures. Fenton's reagent (20 ppm Fe (II) in 3% H_2O_2) is an effective method to generate hydroxyl/peroxyl radicals to simulate the oxidative attack during the realistic fuel cell operation [27-28]. Table 3.3 shows the testing results of BTBP-PBI as well as that of Nafion 115 and m-PBI for comparison. It was found that the weight losses of BTBP-PBI at r.t. and 80℃ are 0 wt% and 0.5 wt%, respectively. This result is similar to that of 6F-PBI but lower than that of Nafion 115 and m-PBI tested at similar conditions, indicating the trifluoromethyl groups are very stable from radical attack in harsh conditions.

Table 3.3 Oxidative stability of PBI derivatives and Nafion tested in Fenton's Reagent for 24 hours.

Sample	Weight loss / %	
	r.t.	80℃
Nafion 115	1.3	3.2
meta -PBI	0	0.8
BTBP-PBI	0	0.5
6F-PBI	0[a]	0 (180 ℃)[a]

a. The data was obtained from the literature [14]

3.3.4 Membrane Preparation and Characterization

3.3.4.1 PBI Dense Membrane Preparation

BTBP-PBI dense films were fabricated via a solution casting method. A 3.0 wt% BTBP-PBI solution in DMAc was used for the initial film casting study. However, it was very difficult to obtain high-quality PBI dense films due to the short-term stability of the polymer solution as mentioned in section 3.3.3. Therefore, a more dilute polymer solution (approximately 1.5 wt%) was prepared and poured onto a glass plate with restraints on each side to obtain the dense films with desired thicknesses. When the wet film was dried in air, only opaque and mechanically weak films (Figure 3.12, left) were formed, indicating a strong phase separation which could be attributed to the hydrophilic characteristics of both PBI and DMAc. In comparison, when the film was treated in a dry environment (dry nitrogen atmosphere), mechanically strong and transparent films (Figure 3.12, right) were successfully prepared. The m-PBI and 6F-PBI films were prepared under similar optimized film processing conditions.

Figure 3.12 BTBP-PBI dense films (**left**: dried under air; **right**: dried under nitrogen)

3.3.4.2 PBI Crystallinity

To study the polymer morphology of BTBP-PBI, the dense film prepared was examined using WAXD. Figure 3.13 shows the diffraction pattern of BTBP-PBI. A very broad peak (halo) was clearly observed, indicating the amorphous nature of polymer. It is believed that the introduction of twisted bistrifluoromethyl biphenyl groups effectively suppressed the polymer chain packing and crystallization. The polymer crystallinity of m--PBI and 6F-PBI were reported in the literature and similar amorphous nature was observed [29]. The amorphous morphology is beneficial to improve the polymer's properties such as solubility and proton conductivity.

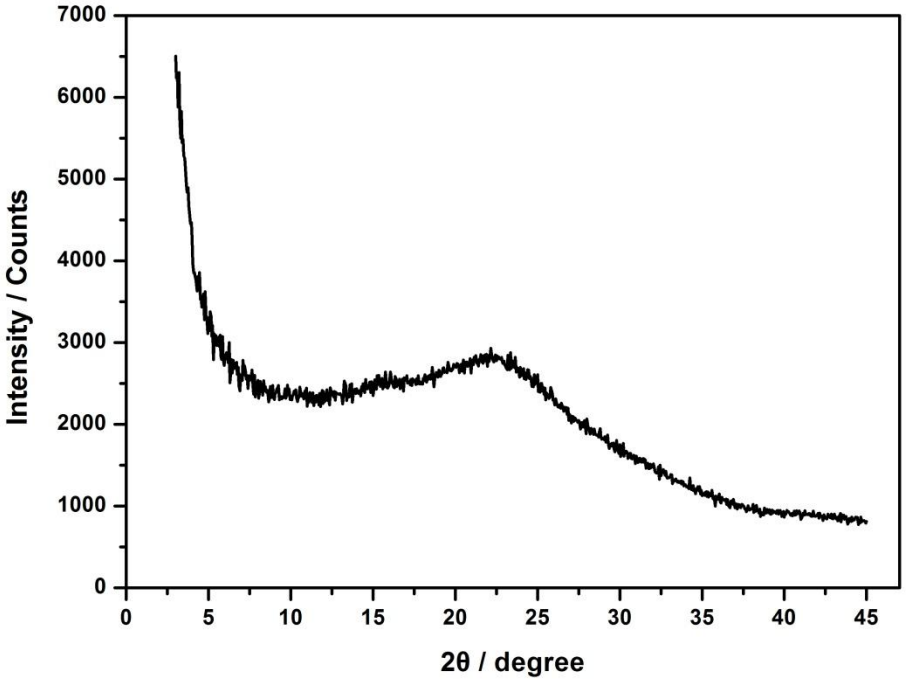

Figure 3.13 WXRD pattern of BTBP-PBI dense film.

3.3.4.3 Acid Absorption

PA-doped BTBP-PBI membranes were prepared by immersing the dense films into PA solutions at ambient conditions for more than 48 hours. The time for PBI membranes to reach maximum acid doping levels was reported to vary (16 h - 50 h), which may be caused by variations in membrane thicknesses [30-31]. A series of PA baths with different concentrations (50% PA – 90% PA) were used to study the polymers' acid absorption and stability behaviors. As shown in Figure 3.14, for BTBP-PBI, a steady increase in PA doping levels was observed with an increase in the PA bath concentrations until 75%. When the concentration reached 80%, the PA doping showed an abrupt increase to 10.70 PA/RU, which was caused by strong swelling of polymer in acid. As evidence, a large increase of membrane thickness from 15 μm to 38 μm was

observed. Beyond this PA concentration, the polymer membrane was found to be partially soluble. The 6F-PBI dense films were also dipped into PA solutions with similar concentrations to help to better understand how the PBI backbone structure could affect its acid uptake behavior. As shown in Figure 3.3, for 6F-PBI there are also two trifluoromethyl groups per polymer repeat unit within its backbone but these two groups are connected by a tetrahedral carbon center, which makes the polymer's backbone relatively more flexible than BTBP-PBI's. It was found these two PBIs exhibited similar doping behavior at low PA concentrations. However, 6F-PBI showed better stability and also a higher PA doping level when it was immersed in high concentration PA (approximately 13.17 PA/RU when soaked in 85% PA). This indicates that the more rigid polymer backbone and decreased chain flexibility of BTBP-PBI could result in the lower swelling ability as compared to 6F-PBI. The acid absorption behavior of m-PBI was also reported and it showed slightly lower acid doping levels than the other two fluorinated PBIs.

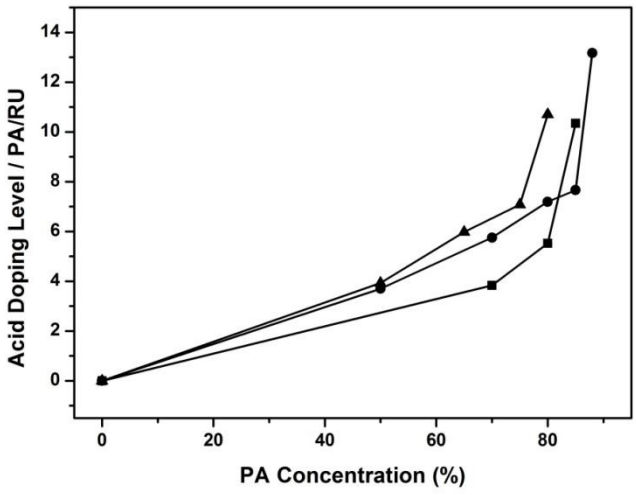

Figure 3.14 PA doping levels of BTBP-PBI membranes (triangles), m-PBI (squares) and 6F-PBI membranes (circles) treated by PA at different concentrations.

3.3.4.4 Mechanical Properties

The tensile properties of BTBP-PBI dense membrane and the membranes with various PA doping levels were measured and the results are shown in Table 3.4. The pure PBI films showed a Young's modulus of 3.62 GPa, a tensile strength of 111 MPa and an elongation at break of 6%. These mechanical properties are higher than the other fluorine-containing PBIs that have been reported (e.g., the Young's modulus and tensile strength of 6F-PBI, 4F-PBI and 14F-PBI are all lower than 1.20 GPa and 55 MPa [12,16]). The mechanical properties of the membrane were reduced drastically when it was doped with PA and further decreased with increased PA doping levels, which is attributed to the increased plasticizing effect of the small molecules (PA and H_2O). The tensile properties of m-PBI and 6F-PBI prepared in our lab were also tested and compared with that of BTBP-PBI as shown in Figures 3.15 and Figure 3.16. They showed similar acid absorption trends and mechanical strength as BTBP-PBI. Figure 3.17 shows the composition percentages of BTBP-PBI membranes doped with different amounts of PA. It was found that as the PA doping level increased to 10.70 PA/RU the polymer percentage dropped to 22.50 wt% whereas the percentages of acid and water increased to 45.35 wt% and 32.14 wt%, respectively. This is consistent with the large decrease in mechanical properties of the BTBP-PBI membranes. Similar trends were also observed from m-PBI and 6F-PBI as shown in Figures 3.18 and Figure 3.19.

Table 3.4 Mechanical properties of BTBP-PBI membranes.

	Young's Modulus / Gpa	Tensile Strength / MPa	Tensile Strain / %
BTBP-PBI	3.617	111.3	6.225
BTBP-PBI - 3.93PA	1.446	46.43	12.58
BTBP-PBI - 5.98PA	0.664	26.59	29.13
BTBP-PBI - 7.08PA	0.394	14.52	30.25
BTBP-PBI - 10.70PA	0.069	3.264	36.19

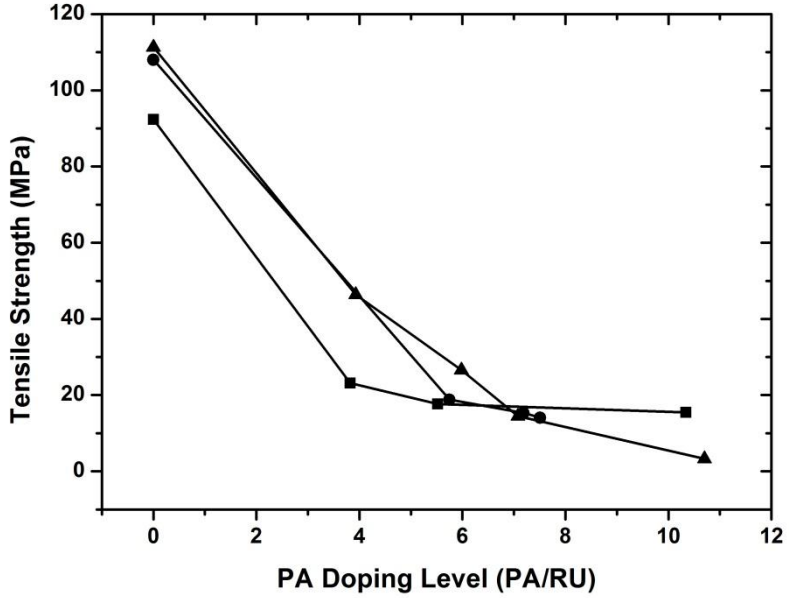

Figure 3.15 Tensile strength of PBI membranes (triangles: BTBP-PBI, squares: m-PBI, circles: 6F-PBI) as a function of PA doping level at ambient temperature.

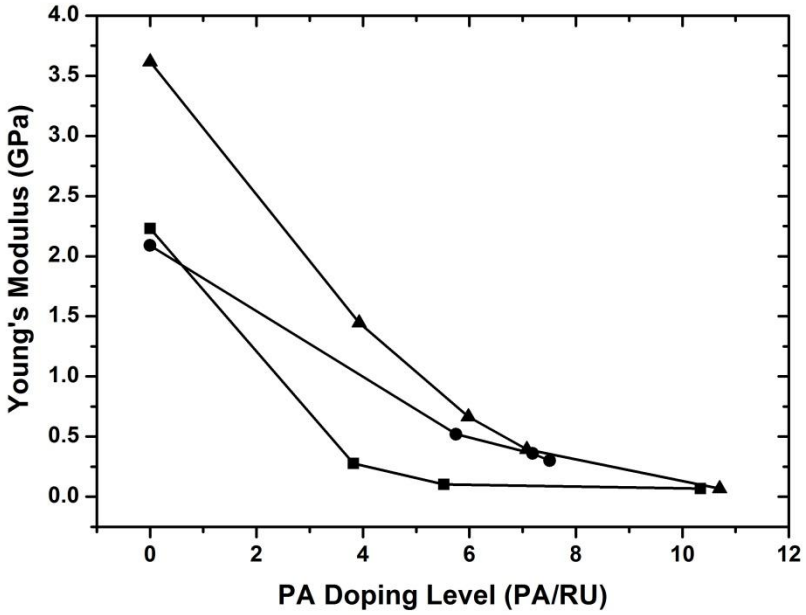

Figure 3.16 Young's modulus of PBI membranes (triangles: BTBP-PBI, squares: m-PBI, circles: 6F-PBI) as a function of PA doping level at ambient temperature.

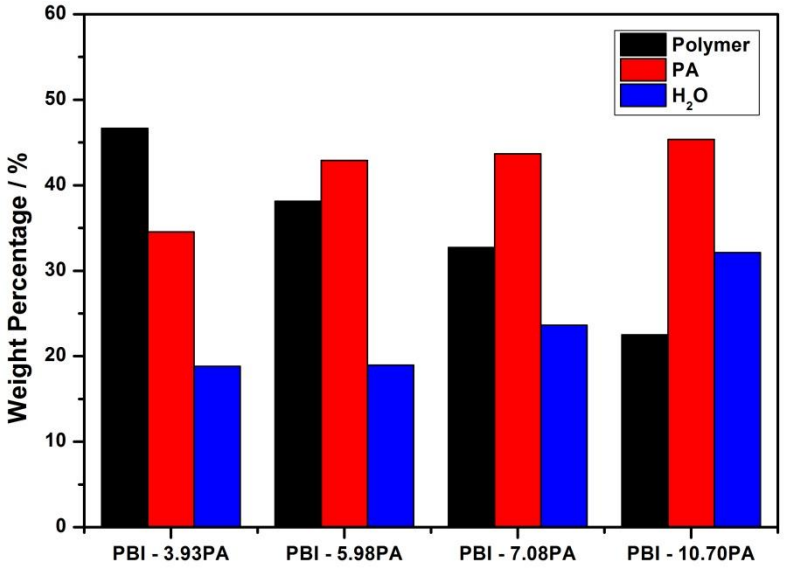

Figure 3.17 Percentage composition of BTBP-PBI membranes treated by PA at different concentrations.

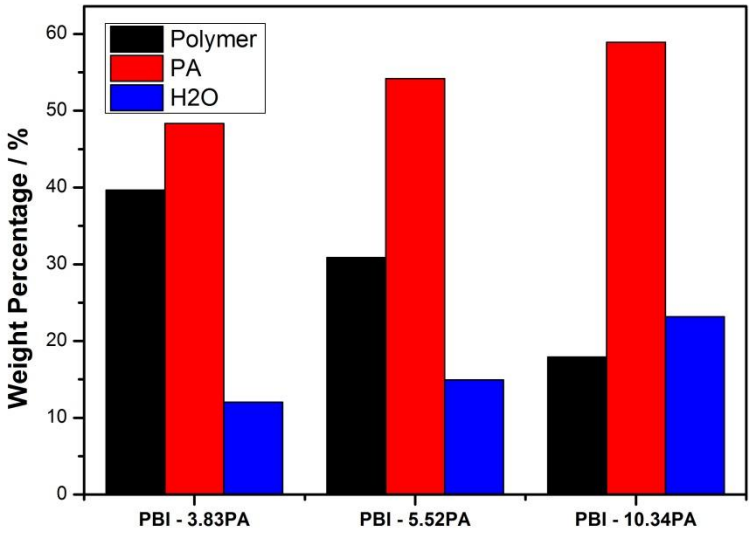

Figure 3.18 Percentage composition of m-PBI membranes treated by PA at different concentrations.

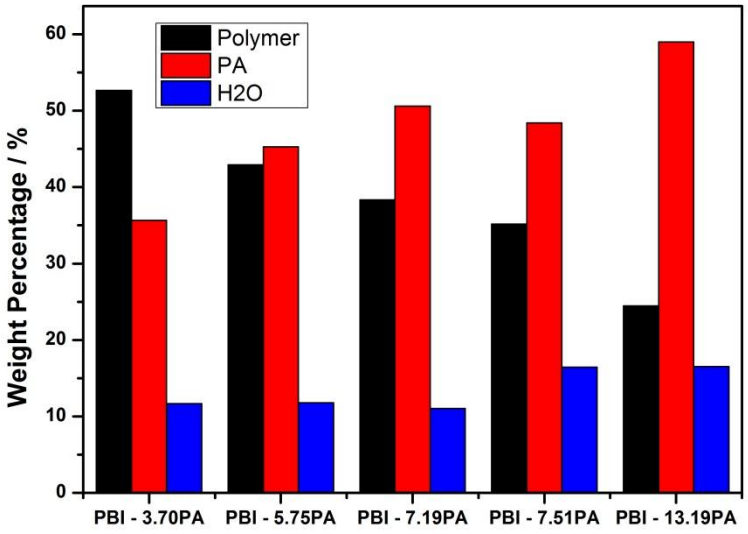

Figure 3.19 Percentage composition of 6F-PBI membranes treated by PA at different concentrations.

3.3.4.5 Proton Conductivity

The proton conductivities of BTBP-PBI membranes with different PA doping levels were measured under anhydrous conditions as a function of temperature from r.t. to 180 °C. It was found that the conductivities increased with the increase in both temperature and acid loading. As shown in Figure 3.20, the conductivity values could be fitted by the Arrhenius equation (Eq. (3)):

$$\sigma = \sigma^0 \, exp\left(\frac{-E_a}{RT}\right) = \frac{A}{T} exp\left(\frac{-E_a}{RT}\right) \quad (3)$$

where σ^0 and A are pre-exponential factors; R is the Boltzmann constant; T is membrane testing temperature and E_a is the activation energy. The activation energy of membrane was found to decrease as the PA doping level increased (47.87 kJ mol^{-1} for doping level of 3.93 PA/RU; 46.58 kJ mol^{-1} for doping level of 5.98 PA/RU; 38.50 kJ mol^{-1} for doping level of 7.08 PA/RU). These values are of similar magnitude and trends to PA-doped m-

PBI membranes (41 KJ mol^{-1} for doping level of 3.00 PA/RU; 34 KJ mol^{-1} for doping level of 4.20 PA/RU; 27.5 KJ mol^{-1} for doping level of 6.0 PA/RU [32]). For the BTBP-PBI membrane with a doping level of 7.08 PA/RU, the maximum proton conductivity at 180 °C was approximately 0.02 S cm^{-1}, which is higher than literature data of some fluorine-containing PBI membranes (6F-PBI, $1.70x10^{-4}$ S cm^{-1}, 3.0 mol PA/RU, 160 °C [33]; 14F-PBI, $3.05x10^{-3}$ S cm^{-1}, 7.0 mol PA/RU, 150 °C [16]; 4F-PBI, ~$6.31x10^{-4}$ S cm^{-1}, 7.0 mol PA/RU, 150 °C [16]) and also m-PBI (6.0 mol PA/PBI, ~$1.0x10^{-2}$ S cm^{-1}, 160 °C, relative humidity=0 [32]). It is noteworthy that the membrane with a PA doping level of 10.70 PA/RU (immersed in 80% PA) could not be tested accurately since it became very soft and underwent large deformation at elevated temperatures. In realistic fuel cell applications, it is important to find the best combination of proton conductivity and mechanical strength of the membrane.

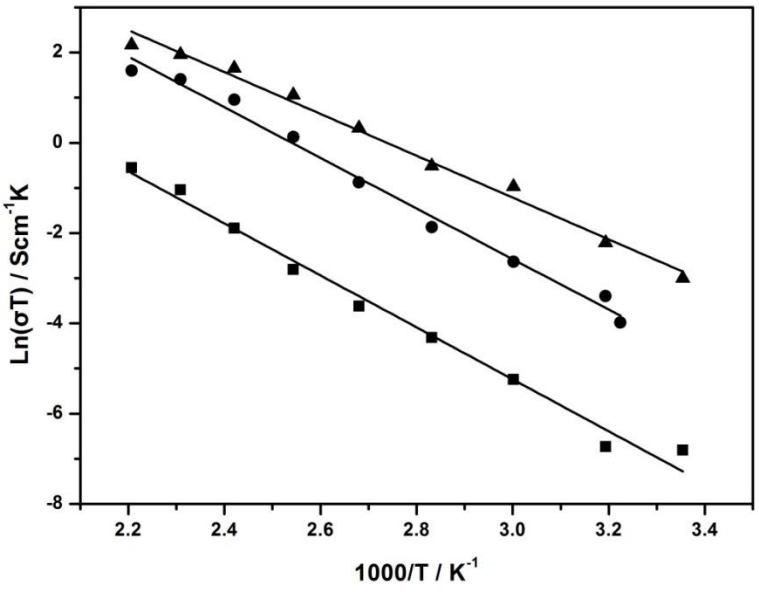

Figure 3.20 Temperature dependence of proton conductivity of BTBP-PBI membranes without humidification. PA doping levels of PTBP-PBI membranes: (squares) 3.93 PA/RU; (circles) 5.98 PA/RU; (triangles) 7.08 PA/RU.

3.3.4.6 Fuel Cell Testing

The BTBP-PBI membrane with a PA doping level of 7.08 PA/RU was chosen for the MEA preparation. Just prior to MEA fabrication, the membrane was dipped into a 85% PA solution for approximately 10 - 20 seconds, which was performed to decrease the interface resistance between membrane and electrodes. This acid pre-treatment was found to be effective in improving the ultimate fuel cell performance and the detailed mechanism is still under investigation. The fuel cell performance of BTBP-PBI was then investigated in a 10.15 cm^2 single cell fuel cell and Figure 3.21 shows the polarization curves of BTBP-PBI tested at 180 °C under H_2/Air and H_2/O_2. The open circuit voltages (OCV) of the membrane at both gas conditions were found to be low (0. 754 V and 0.813 V under H_2/Air and H_2/O_2, respectively), which could be attributed to the relatively low membrane thicknesses (15 μm - before acid doping; and 24 μm - after acid doping) and non-optimized hot-pressing conditions (e.g., compression pressure, temperature, time, etc.). However, the membrane still operated reliably and, at a current density of 0.2 A/cm^2, the cell voltage of BTBP-PBI in H_2/Air operation was approximately 0.649 V. It then increased to 0.728 V when the gas pair was switched to H_2/O_2, which is due to the higher O_2 partial pressure at the cathode side. The maximum power densities that BTBP-PBI obtained under H_2/Air and H_2/O_2 were 0.462 W/cm^2 and 0.574 W/cm^2, respectively. The overall fuel cell performance of BTBP-PBI was comparable to that of m-PBI (190 °C, H_2/O_2, 0.55 W cm^{-2} at 1.2 A cm^{-2} [34]) and much better than that of 6F-PBI (160 °C, H_2/O_2, 0.43 W cm^{-2} at 1.0 A cm^{-2} [14]) reported in the literature.

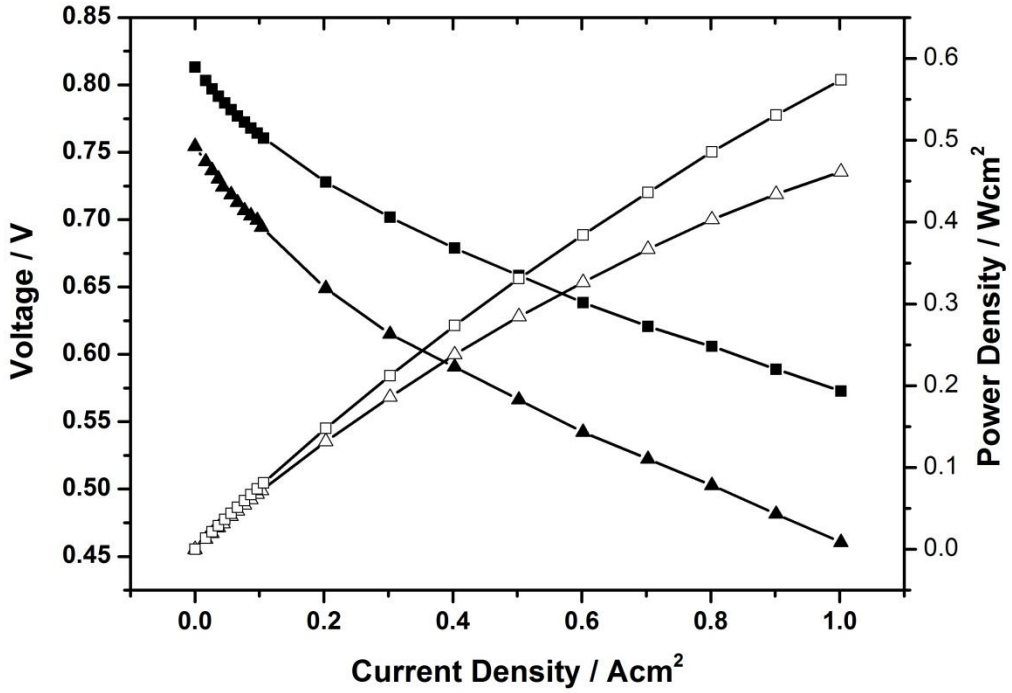

Figure 3.21 Polarization curves (filled symbols) and power density curves (unfilled symbols) for MEA using BTBP-PBI membrane. (Fuel cell operation conditions: 1 atm, 180 °C, constant stoichiometry H_2 (λ=1.2)/air (λ=2.0) (triangles) or (λ=1.2)/O_2 (λ=2.0) (squares), no external humidification).

3.4 Conclusions

A novel high molecular weight, thermally stable and organo-soluble BTBP-PBI containing electron-withdrawing trifluoromethyl groups at the 2 and 2' positions of a biphenyl moiety was successfully synthesized by solution polymerization in Eaton's reagent. A diacid, namely 2,2'-bis(trifluoromethyl)-4,4'-biphenyldicarboxylic acid, was synthesized and purified by a new simplified two-step method. The introduction of a tetrahedral copper-cyano complex ($Na_3[Cu(CN)_3]$) as cyanating reagent moderately increased the reaction yield from 15.2% to 25.6%. Optimization of polymerization conditions to achieve high molecular weight polymers was explored by varying the initial

monomer concentrations. The TGA results showed that the polymer had excellent thermal stability up to 471 °C (5 wt% loss of dry polymer). The polymer exhibited good solubility in some polar, aprotic solvents such as DMAc due to the introduction of steric repulsion of the trifluoromethyl groups at the biphenyl moiety. Due to the presence of fluorine, the polymer also showed high resistance of hydroxyl/peroxyl radical attack in Fenton reagent testing at both low and high temperatures. The PA-doped BTBP-PBI membranes were prepared by a traditional imbibing process. With increasing acid bath concentration, the PA doping levels of the membrane also increased whereas the mechanical properties decreased. It was found that BTBP-PBI membranes could be doped to 7.08 PA/RU in 75% PA solution and exhibit a proton conductivity of approximately 0.02 $S \cdot cm^{-1}$, which is higher than m-PBI and some other fluorine-containing PBIs prepared by the same method and with similar doping levels. The MEA fabricated from the PA-doped BTBP-PBI membrane was tested in a fuel cell and showed approximately 0.65 V at 0.2 A/cm^2 at 180 °C under H_2/Air, which is potentially useful in high temperature (120 °C – 200 °C) PEMFC applications.

3.5 References

[1] Q. Li; R. He; J. O. Jensen; N. J. Bjerrum, *Fuel Cells* **2004,** 4, 147.

[2] R. Savinell; E. Yeager; D. Tryk; U. Landau; J. Wainright; D. Weng; K. Lux; M. Litt; C. Rogers, *J Electrochem Soc* **1994,** 141, L46.

[3] L. Xiao; H. Zhang; E. Scanlon; L. S. Ramanathan; E. W. Choe; D. Rogers; T. Apple; B. C. Benicewicz, *Chem Mater* **2005,** 17, 5328.

[4] J. T. Wang; R. F. Savinell; J. Wainright; M. Litt; H. Yu, *Electrochim Acta* **1996,** 41, 193.

[5] S. R. Samms; S. Wasmus; R. F. Savinell, *J Electrochem Soc* **1996,** 143, 1498.

[6] S. Yu; H. Zhang; L. Xiao; E. W. Choe; B. C. Benicewicz, *Fuel Cells* **2009,** 9, 318.

[7] M. G. Dhara; S. Banerjee, *Prog Polym Sci* **2010,** 35, 1022.

[8] S. Ando, *J Photopolym Sci Tec* **2004,** 17, 219.

[9] K. Xie; J. G. Liu; H. W. Zhou; S. Y. Zhang; M. H. He; S. Y. Yang, *Polymer* **2001,** 42, 7267.

[10] D. J. Liaw; K. L. Wang, *J Polym Sci Part A: Polym Chem* **1996,** 34, 1209.

[11] D. X. Yin; Y. F. Li; H. X. Yang; S. Y. Yang; L. Fan; J. G. Liu, *Polymer* **2005,** 46, 3119.

[12] S. H. Hsiao; C. P. Yang; S. C. Huang, *J Polym Sci Part A: Polym Chem* **2004,** 42, 2377.

[13] S. Banerjee; G. Maier; R. Burger, *Macromolecules* **1999,** 32, 4279.

[14] G. Qian; B. C. Benicewicz, *J Polym Sci Part A: Polym Chem* **2009,** 47, 4064.

[15] G. Qian; D. W. Smith Jr; B. C. Benicewicz, *Polymer* **2009,** 50, 3911.

[16] H. T. Pu; L. Wang; H. Y. Pan; D. C. Wan, *J Polym Sci Part A: Polym Chem* **2010,** 48, 2115.

[17] R. A. Gaudiana; R. A. Minns; R. Sinta; N. Weeks; H. G. Rogers, *Prog Polym Sci* **1989,** 14, 47.

[18] H. G. Rogers; R. A. Gaudiana; R. A. Minns, US Patent, 4, 628, 125, 1986.

[19] H. G. Rogers; R. A. Gaudiana; R. A. Minns, US Patent, 4, 433, 132, 1984.

[20] P. E. Eaton; G. R. Carlson; J. T. Lee, *J Org Chem* **1973,** 38, 4071.

[21] H. Zhang, Novel phosphoric acid doped polybenzimidazole membranes for fuel cells. Ph.D. Thesis, Rensselaer Polytechnic Institute, 2004.

[22] J. C. Chen; C. J. Chiang; Y. C. Liu, *Synthetic Metals* **2010,** 160, 1953.

[23] H. G. Rogers; R. A. Gaudiana; W. C. Hollinsed; P. S. Kalyanaraman; J. S. Manello; C. McGowan; R. A. Minns; R. Sahatjian, *Macromolecules* **1985,** 18, 1058.

[24] N. Yonezawa; T. Namie; T. Ikezaki; T. Hino; H. Nakamura; Y. Tokita; R. Katakai, *React Funct Polym* **1996,** 30, 261.

[25] N. Yonezawa; T. Hino; T. Namie; R. Katakai, *Synthetic Commun* **1996,** 26, 1575.

[26] A. S. Buckley; D. E. Stuetz; G. A. Serad, *Encycl Polym Sci Eng* **1987,** 11, 572.

[27] E. Graf; J. R. Mahoney; R. G. Bryant; J. W. Eaton, *J Biol Chem* **1984,** 259, 3620.

[28] V. A. Sethuraman; J. W. Weidner; A. T. Haug; L. V. Protsailo, *J Electrochem Soc* **2008,** 155, B119.

[29] A. Carollo; E. Quartarone; C. Tomasi; P. Mustarelli; F. Belotti; A. Magistris; F. Maestroni; M. Parachini; L. Garlaschelli; P. P. Righetti, *J Power Sources* **2006,** 160, 175.

[30] S. Kumbharkar; M. N. Islam; R. Potrekar; U. Kharul, *Polymer* **2009,** 50, 1403.

[31] Q. Li; R. He; R. W. Berg; H. A. Hjuler; N. J. Bjerrum, *Solid State Ionics* **2004,** 168, 177.

[32] Y. L. Ma; J. S. Wainright; M. H. Litt; R. F. Savinell, *J Electrochem Soc* **2004,** 151, A8.

[33] S. W. Chuang; S. L. C. Hsu, *J Polym Sci Part A: Polym Chem* **2006,** 44, 4508.

[34] Q. Li; H. A. Hjuler; N. J. Bjerrum, *J Appl Electrochem* **2001,** 31, 773.

CHAPTER 4

INFLUENCE OF POLYBENZIMIDAZOLE MAIN CHAIN STRUCTURE ON H2/CO2 SEPARATION AT ELEVATED TEMPERATURES[3]

[3] X. Li, R.P. Singh, K.W. Dudeck, K.A. Berchtold, and B.C. Benicewicz. Submitted to *Journal of Membrane Science*, 11/10/2013

4.1 Introduction

H_2 is a fast-growing market not only because of its significant applications in traditional areas such as ammonia production and oil refining but also its great potential as a clean energy carrier for renewable energy devices such as fuel cells and to address issues related to the world's oil consumption and environmental concerns [1-4]. As a result, great attention has been placed on improving H_2 production technologies with lower cost and higher efficiency. Although there are a variety of novel approaches for hydrogen production such as photoelectrochemical water splitting and biological hydrogen production processes that are being explored, for the foreseeable future, natural gas reforming and coal gasification will remain the dominant methods to produce hydrogen industrially [5-8].

H_2/CO_2 separation is a critical step in hydrocarbon fuel processing for clean H_2 production while mitigating CO_2 emissions in electricity, power and fuels production process schemes. In a typical hydrocarbon processing scheme for H2 production, post water-gas-shift reaction ($CO + H_2O \rightarrow CO_2 + H_2$), synthesis (syn) gas is separated into H_2 and CO_2 rich streams. Industry standard H2/CO2 separation techniques are highly energy inefficient due to high parasitic energy losses associated with syngas heating and cooling, and sorbent regeneration [9, 10]. Therefore, in recent years considerable research has been focused on investigating novel H_2/CO_2 separation technologies which could achieve improvements in both economics and performance [11-14].

Polymer membrane-based gas separation has emerged as a promising alternative to replace or use in combination with conventional gas separation techniques which could lead to processes that are more cost-effective, efficient, and less energy-intensive [15,

16]. One widely recognized challenge that exists with polymer membrane based separation approaches is the trade-off relationship between gas permeability and selectivity. However, an increasing number of studies have shown that both gas permeability and selectivity characteristics can be improved through new polymer material design and/or polymer structure modification [17]. A successful gas separation membrane must be applicable to industrially realistic gas processing conditions including temperature, pressure, and tolerance to impurities while maintaining efficiency and providing economic benefit. H_2 selective membranes applicable for use under syngas processing conditions at high temperatures (>150 °C) are highly desirable since they would not require intermediate cooling procedures prior to treatment [18]. However, commercially available polymer membrane materials either do not meet these stability requirements or exhibit very poor gas separation performance at the desired elevated temperature condition.

Polybenzimidazoles (PBIs) are a class of heterocyclic polymers which possess extremely high thermal stability, excellent chemical and moisture resistance, and can be fabricated into fibers and films with outstanding mechanical stability [19, 20]. For these reasons, PBIs have been widely studied in recent years as polymer electrolyte membrane (PEM) materials for high temperature fuel cell applications [21, 22]. These properties also make PBI a promising candidate among the class of glassy thermoplastics in the application of H_2/CO_2 separation at elevated temperatures. Some preliminary work has been reported on evaluating the gas transport properties of commercially available poly(2,2'-(m-phenylene)-5,5'-bibenzimidazole) (m-PBI). For example, Pesiri et al. successfully prepared m-PBI meniscus membranes with a rough thickness of 4 μm at the

film centers and demonstrated H_2/CO_2 separations at elevated temperatures [23]. Berchtold et al. tested the long-term gas separation performance using m-PBI/zirconia/stainless steel composite membranes under pure and simulated dry syngas environments and reported good H_2/CO_2 selectivities and excellent thermo-chemical stability [24]. Kumbharkar et al. prepared m-PBI based hollow fiber membranes and measured the gas transport properties for H_2/CO_2 in the temperature range of 100-400 °C [25]. Although m-PBI exhibits industrially attractive H_2/CO_2 selectivity at high temperatures, its low H_2 permeability mandates ultrathin selective layer for commercially attractive H_2 fluxes. This low permeability is attributed to the small free volume of m-PBI resulting from efficient polymer chain packing due to pi-pi stacking and strong H-bonding interactions [26, 27]. Therefore, strategies to improve the hydrogen permeability while simultaneously maintaining high H_2/CO_2 selectivity are needed to make this class of materials more industrially attractive.

Molecular structure modification is an effective way to manipulate aspects of polymer morphology such as chain packing efficiency and free volume architecture and to ultimately tune the gas diffusivity within the glassy polymers [28]. During the past few decades, tremendous work has been done on modifying the structures of known polymers such as polyimides to achieve a better balance between gas permeability and selectivity [29, 30]. Although PBI represents a large family of heterocyclic polymers with the benzimidazole ring in its polymer repeat unit, very little work has been focused on investigating the structure-property relationships within this type of materials, especially with detailed studies of their corresponding gas separation characteristics at elevated temperatures [26, 27]. In this work, PBI polymers with different backbone structures

have been prepared using four different dicarboxylic acid monomers and evaluated as films for high-temperature H_2/CO_2 separations. Some general structural strategies that have been widely applied in other polymers to improve their gas separation performance have been introduced and applied to the PBI structural modifications. A detailed study of their corresponding physicochemical properties was conducted and the results showed that PBI main chain structure modification is an effective method to increase the gas permeability at high temperatures. The gas transport properties of these new PBI derivatives were compared to the commercially available m-PBI material.

4.2 Experimental

4.2.1 Materials

2,2-Bis(4-carboxyphenyl)-hexafluoropropane (6F-diacid, 98.0 %) was purchased from TCI America. 4,4'-((1,2,3,3,4,4-Hexafluorocyclobutane-1,2-diyl)bis(oxy))dibenzoic acid (PFCB-diacid, 99.0 %) was obtained from Tetramer Technologies (distributed through Oakwood Chemical, Columbia, SC). 2,2'-Bis(trifluoromethyl)benzidine (98.5 %) used in BTBP-diacid synthesis was purchased from Akron Polymer Systems. 1,1,3-Trimethyl-3-phenylindan-4',5-dicarboxylic acid (phenylindane-diacid, 98 %) was purchased from Amoco Chemicals. 3,3',4,4'-Tetraaminobiphenyl (TAB, polymer grade, ~97.5%) was donated by BASF Fuel Cell, Inc. Polyphosphoric acid (PPA, 115%) was purchased from InnoPhos. The m-PBI used in this study as the benchmark PBI material was obtained from PBI Performance Products, Inc. and used as received. All other reagents (e.g. sodium cyanide, sodium nitrite, lithium chloride, etc.) and solvents (e.g. N,N-dimethylacetamide (DMAc), ammonium hydroxide, etc.) were purchased from

Fisher Scientific. Unless otherwise specified, all chemicals were used without further purification.

4.2.2 PBI Polymer Synthesis

The detailed synthetic procedures of 2,2'-bis(trifluoromethyl)-4,4'-biphenyldicarboxylic acid (BTBP-diacid) and four different PBI variants (6F-PBI, PFCB-PBI, BTBP-PBI, and phenylindane-PBI) were reported previously [31-34]. Herein, 6F-PBI is used as an example to describe the general synthetic procedure of PBI polymers. To a 100 ml, three-necked, round-bottom flask, TAB (1.071 g, 5 mmol) and 6F-diacid (1.961 g, 5 mmol) were added under nitrogen protection in a glove box, followed by approximately 98.0 g PPA. The reactor was then equipped with an overhead mechanical stirrer and a nitrogen purge. The reaction mixture was stirred at 50 rpm under nitrogen purge during the entire reaction procedure. The reaction temperature was controlled by a programmable temperature controller with ramp and soak capabilities. The typical final polymerization temperatures were 195-220 °C for 10-40 hours. As the reaction proceeded, the solution developed a dark brown color and became viscous. At the end of the reaction, the polymer solution was poured into water to stop the reaction, pulverized in a blender, neutralized with ammonium hydroxide, filtered, washed with water, and dried in a vacuum oven at 110 °C to obtain the final 6F-PBI polymer powders.

4.2.3 PBI Dense Film Preparation

The general free-standing polymer film casting procedure for the PBI derivatives is described as follows. To a 100 ml round-bottom flask, 1.00 g (applied to 6F-PBI, PFCB-PBI, and phenylindane-PBI) or 0.500 g (applied to BTBP-PBI) dry PBI powder and approximately 33 ml DMAc were added. The reaction mixture was heated to reflux

at ca. 180 °C (oil bath temperature) for 3-4 hours until most of the PBI powder was dissolved. The PBI solution was then cooled down to ambient temperature and centrifuged at 5500 rpm for 30 min to remove any undissolved or swollen polymer. The clean, brown color PBI solution was then transferred to a glove bag with nitrogen purge. The PBI solution was poured on a clean glass substrate (in the case of BTBP-PBI, the polymer solution is very dilute, so a glass substrate with glass slides taped on each side was used to restrict the movement of the solution) and heated to 40 - 50 °C on a hot-plate overnight to remove the solvent. Then, the glass plate was transferred to the vacuum oven and heated at 110 °C for 24-48 hours to obtain the final dry, dense PBI films.

4.2.4 Characterization

^{1}H NMR and ^{19}F NMR spectra were recorded on a Varian Mercury 400 spectrometer. FT-IR spectra were recorded on a PerkinElmer Spectrum 100 FT-IR spectrometer with a three reflection diamond/ZnSe crystal. PBI inherent viscosities (IVs) were measured by a Cannon Ubbelohde viscometer with a 0.2 g/dL PBI solution dissolved in concentrated sulfuric acid (96%) at 30.0 °C. Thermogravimetric analysis (TGA) was conducted on polymer powders using a TG 209 F1 Iris from Netzsch Inc. The samples were heated at 200 ºC for 12 hours to ensure residual solvent and adsorbed water removal prior to thermal analysis. After the drying step, samples were heated at a ramp rate of 2 ºC/min in N_2 from 75 to 1000 ºC. The densities of the PBIs were measured with a Kimble® Kimax® specific gravity bottle using cyclohexane as the solvent at 30.0 °C and a Micromeritics Accupyc 1330 gas displacement pycnometer using 99.999% purity helium at ambient conditions. The detailed gravity bottle density measurement protocols are shown as follows:

Kimble® Kimax® Specific Gravity Bottle, Pycnometer (10 ml)

Procedures:

1. Dry the PBI powders in vacuum oven at 110 ºC overnight before using.

*2. Thoroughly clean, dry, assemble, and weigh the empty gravity bottle (including thermometer and cap) and record (**M_1**).*

3. Fill the gravity bottle with cyclohexane and insert the thermometer into the bottle, forcing cyclohexane through the overflow tube.

4. Place the gravity bottle in the water bath and when the desired temperature is reached, wipe off excess cyclohexane from the overflow tube tip and put the cap on.

*5. Remove the gravity bottle rapidly from the bath, wipe dry, weigh and record (**M_2**).*

*6. Pour ~100mg PBI powders into the bottle carefully, weigh and record. (**M_3**)*

*7. Repeat step 3 to 5. (**M_4**) (**M_2** and **M_4** should be tested at the same temperature)*

8. Check the cyclohexane density at specified temperature and calculate the density with following equation. (Cyclohexane density (ref) =0.76919 g cm^{-3})

$$R = \frac{D_{PBI}}{D_{cyclohexane}} = \frac{M_3 - M_1}{(M_3 - M_1) - (M_4 - M_2)} \quad (1)$$

$$D_{PBI} = R \times D_{cyclohexane} \quad (2)$$

PBI powder and cast film samples were used for density measurement using the gravity bottle and gas pycnometer, respectively. The PBI film samples were annealed at 100 and 250 °C in a vacuum oven for 24 hours prior to density measurement. The same samples were subjected to annealing at two temperatures with cool down to 30 °C under vacuum and density measurement in between the two annealing steps. PBI solubilities were measured at both ambient and reflux conditions. For ambient temperature solubility testing, the PBI powders were mixed with each solvent and shaken on a wrist action

shaker for 24 – 48 hours. For elevated temperature solubility testing, the PBI powders were mixed with each solvent and refluxed for 2-4 hours.

4.2.5. Gas Permeation Testing

The PBI membranes were tested in a custom stainless steel housing using high temperature o-rings (Kalrez^{TM}) in a constant-volume variable-pressure test system. The module was configured for continuous feed gas flow using a dip tube and use of vacuum on the permeate side of the module housing for the permeance measurement. The pure gas permeation experiments were performed with H_2, CO_2, and N_2 at feed pressures and operating temperatures from 20 to 50 psi and 30 to 250 ºC, respectively. A 1 ºC/min temperature ramp rate was typically used in this work for both ramp-up and ramp-down cycles. The permeability data reported here was collected during temperature ramp-down cycle following a 10 hr dwell at 250 °C. The upstream and downstream pressures were measured using high accuracy (± 0.25 % FS) pressure transducers (MKS Instruments, Inc.). The permeance (GPU=10^{-6} cm^3 cm^{-2} $cmHg^{-1}$ s^{-1}) was calculated from the slope of the linear part of the permeate pressure rise versus time curve using Eq. (3):

$$Permeance, P = 10^6 \frac{dp}{dt} \left(\frac{V*22400}{R*T*\Delta p*A}\right) \quad (3)$$

where dp/dt (Torr/sec) is the pressure rise; R (62.363 Torr L K^{-1} mol^{-1}) is the universal gas constant, V (L) is the downstream volume; Δp (cmHg) is the pressure difference between membrane upstream and downstream side; T(K) is the permeate temperature; and A (cm^2) is the effective membrane surface area. The permeability was calculated using film thicknesses measured using scanning electron microscopy after testing. The ideal selectivity for a gas pair is calculated by taking the ratio of their gas permeances.

4.3 Results and Discussion

4.3.1. Polymer Synthesis and Characterization

4.3.1.1. Polymer Synthesis

As shown in Figure 4.1, five different PBI variants were chosen and prepared for the gas separation study. For comparison, m-PBI was obtained commercially (PBI Performance Products, Inc.) in both powder form (100 mesh PBI powders) and solution form (26.2 wt% PBI solution in N,N-dimethylacetamide (DMAc) containing 2 wt% lithium chloride as a phase stabilizer). Industrially, m-PBI is produced by a two-stage melt-solid polycondensation reaction (Fig. 1a) which is more convenient for large-scale production but usually produces lower molecular weight polymer due to the heterogeneous reaction conditions. The other four PBI variants were synthesized in this study by solution polymerization (Fig. 1b) in either PPA or Eaton's reagent. The solution polymerization in PPA is a convenient laboratory procedure for many PBIs since PPA serves as both solvent and condensation reagent and can produce high molecular weight polymer. This PPA-based procedure produced high molecular weight 6F-PBI and phenylindane-PBI. However, this procedure did not work for the synthesis of PFCB-PBI or BTBP-PBI as the PFCB-diacid monomer showed low PPA solubility and BTBP-PBI appeared to cross-link in PPA at elevated temperatures. Thus, these two PBIs were prepared using Eaton's reagent as a convenient alternative to PPA. One important criterion for PBI synthesis is the polymer molecular weight (or IV) since high IV PBIs typically exhibit improved thermal stability and film forming properties in comparison to their lower IV analogs. The detailed discussion and optimization of PBI polymerization conditions was reported previously [31-34] and the general conditions used in this study

are given in Table 4.1. 6F-PBI, PFCB-PBI, BTBP-PBI, and phenylindane-PBI were prepared with IVs of 1.40, 0.73, 1.60, and 0.81 dL/g, respectively, indicating relatively high polymer molecular weights. PBI structures were confirmed by FTIR, ^{1}H NMR and ^{19}F NMR and the spectra are shown in Figure 4.2, Figure 4.3 and Figure 4.4.

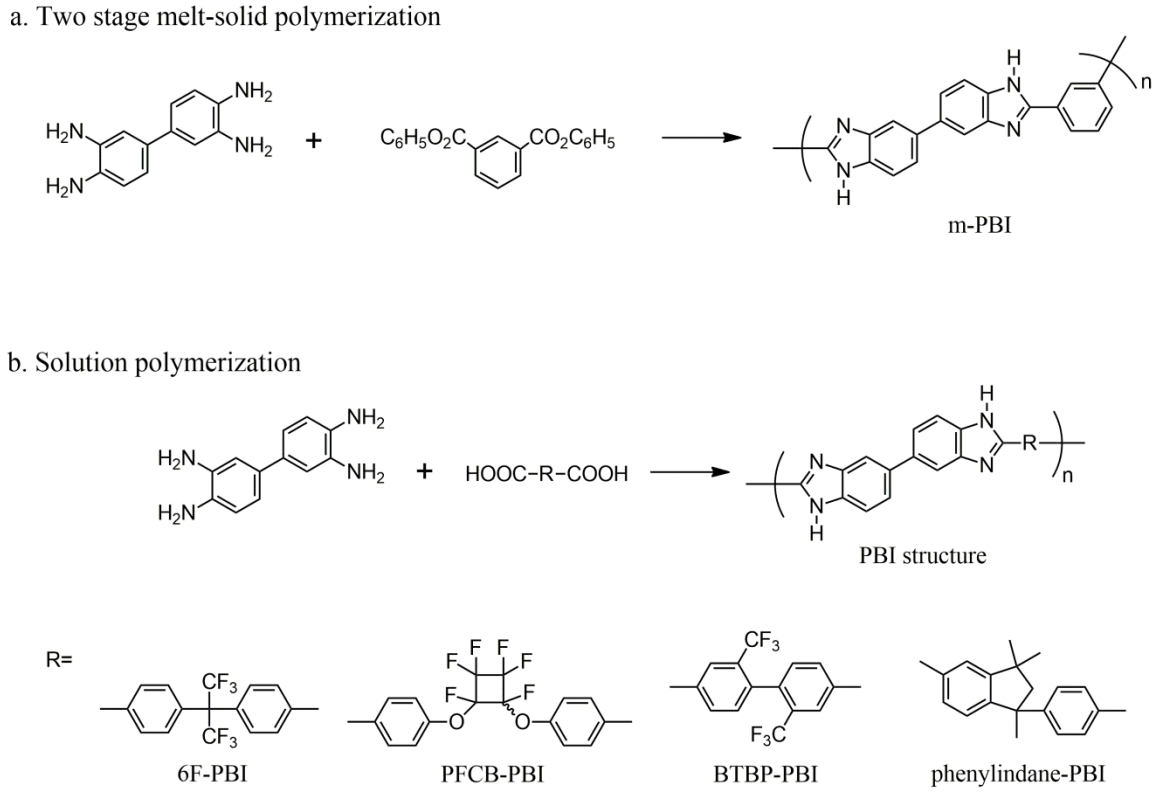

Figure 4.1 Synthetic schemes of PBI derivatives (a. m-PBI; b. 6F-PBI, PFCB-PBI, BTBP-PBI, and phenylindane-PBI).

Table 4.1 Polymerization conditions of PBI derivatives.

Polymer	HOOC-R-COOH	Polymerization Solvent	Monomer Charge	Polymerization Temperature (℃)	Polymerization Time (h)	IV (dL g^{-1})
6F-PBI	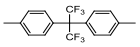	PPA	2.89 wt%	220	24	1.4
PFCB-PBI	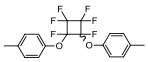	Eaton's Reagent[a]	1 mmol: 5 ml[b]	140	24	0.73
BTBP-PBI	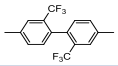	Eaton's Reagent[a]	1 mmol: 5.5 ml[b]	140	42	1.6
phenylindane-PBI	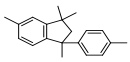	PPA	6.11 wt%	195	35	0.8

a. Eaton's Reagent: a solvent mixture of methanesulfonic acid (MA) and phosphorous pentoxide (PP) (MA:PP=10:1, w:w).
b. x mmol: y ml: means x mmol each monomer dissolved in y ml Eaton's Reagent.

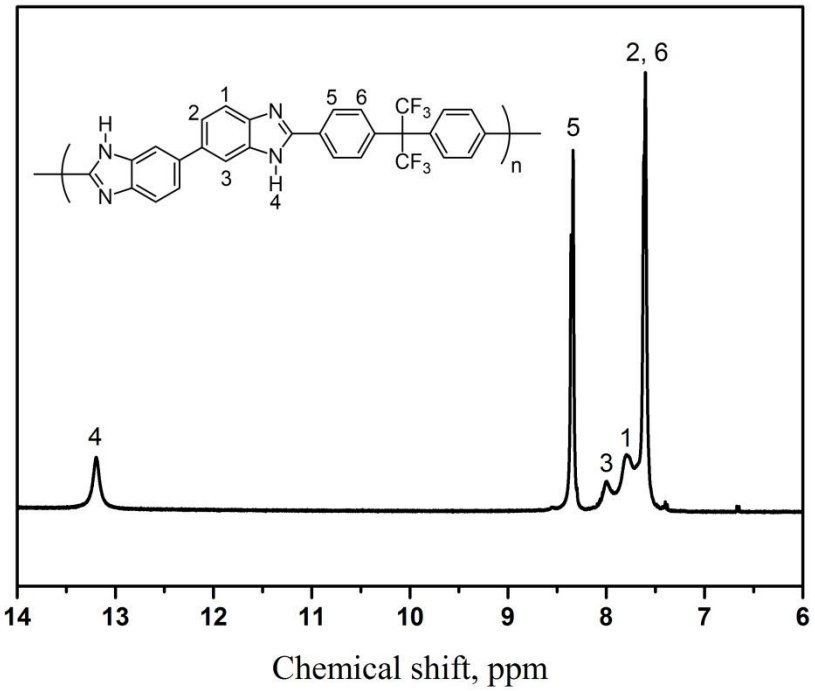

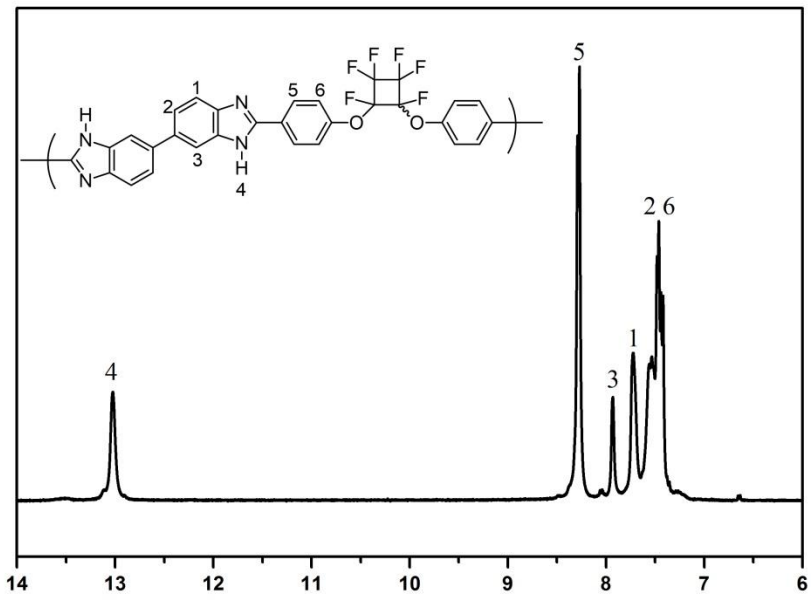
5
2 6
1
3
4
14
13
12
11
10
9
8
7
6
Chemical Shift, ppm

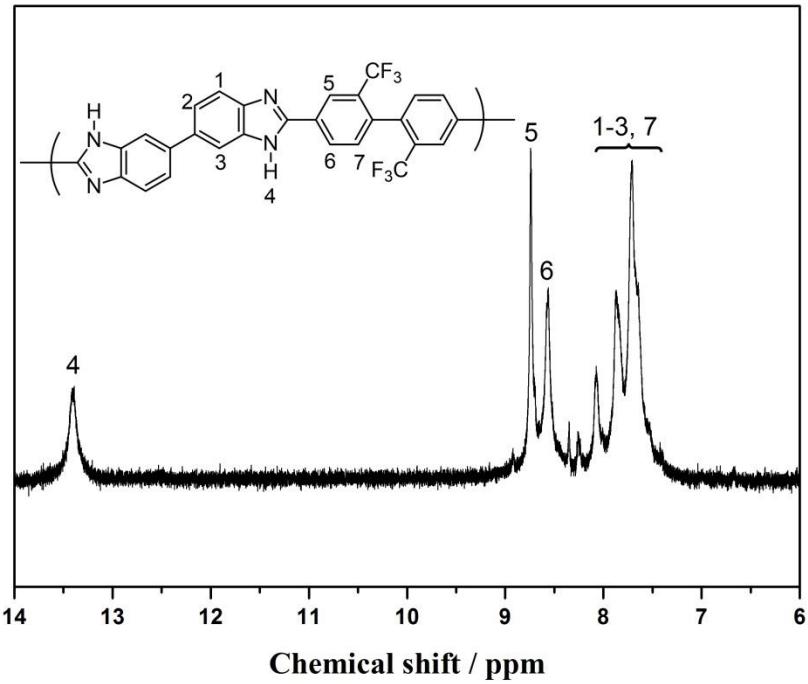
5
1-3, 7
6
4
14
13
12
11
10
9
8
7
6
Chemical shift / ppm

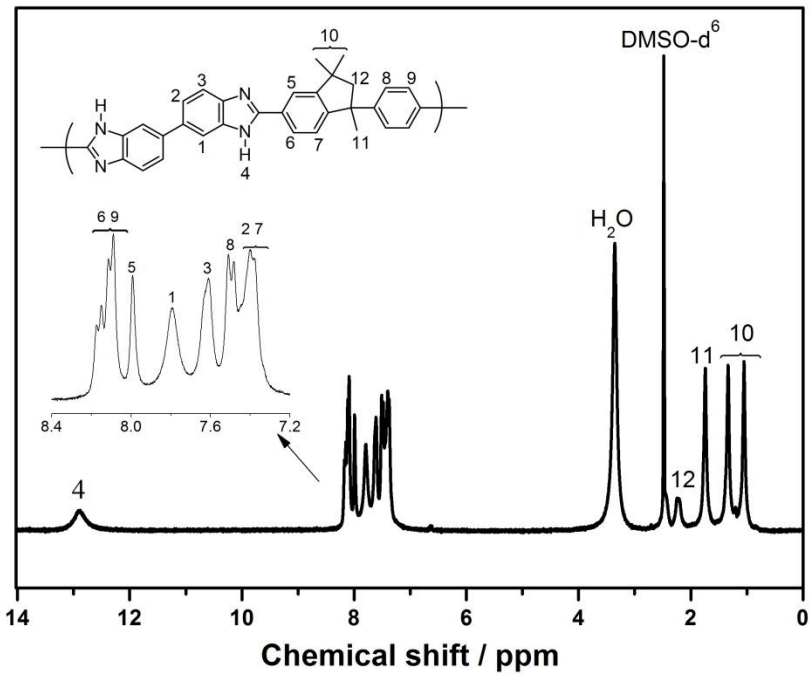

Figure 4.2 ^{1}H NMR spectra of 6F-PBI (top), PFCB-PBI (second), BTBP-PBI (third), and phenylindane-PBI (bottom).

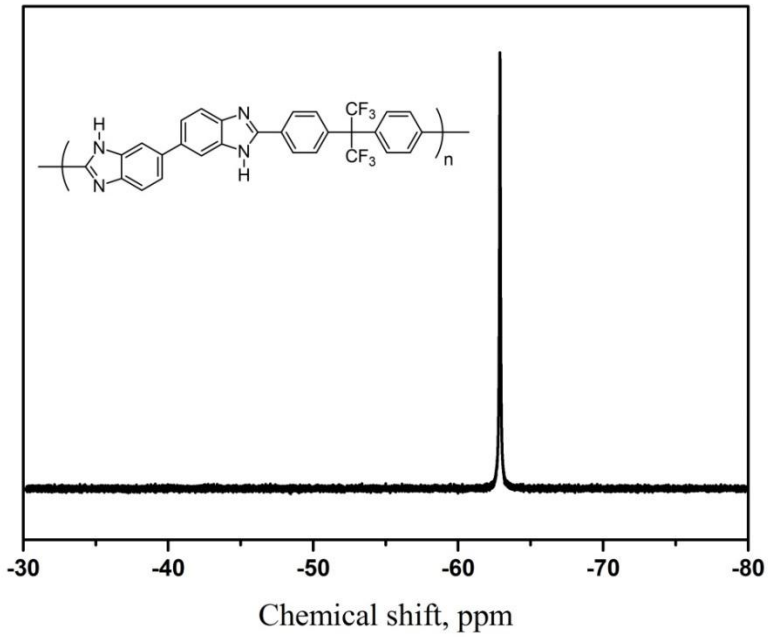

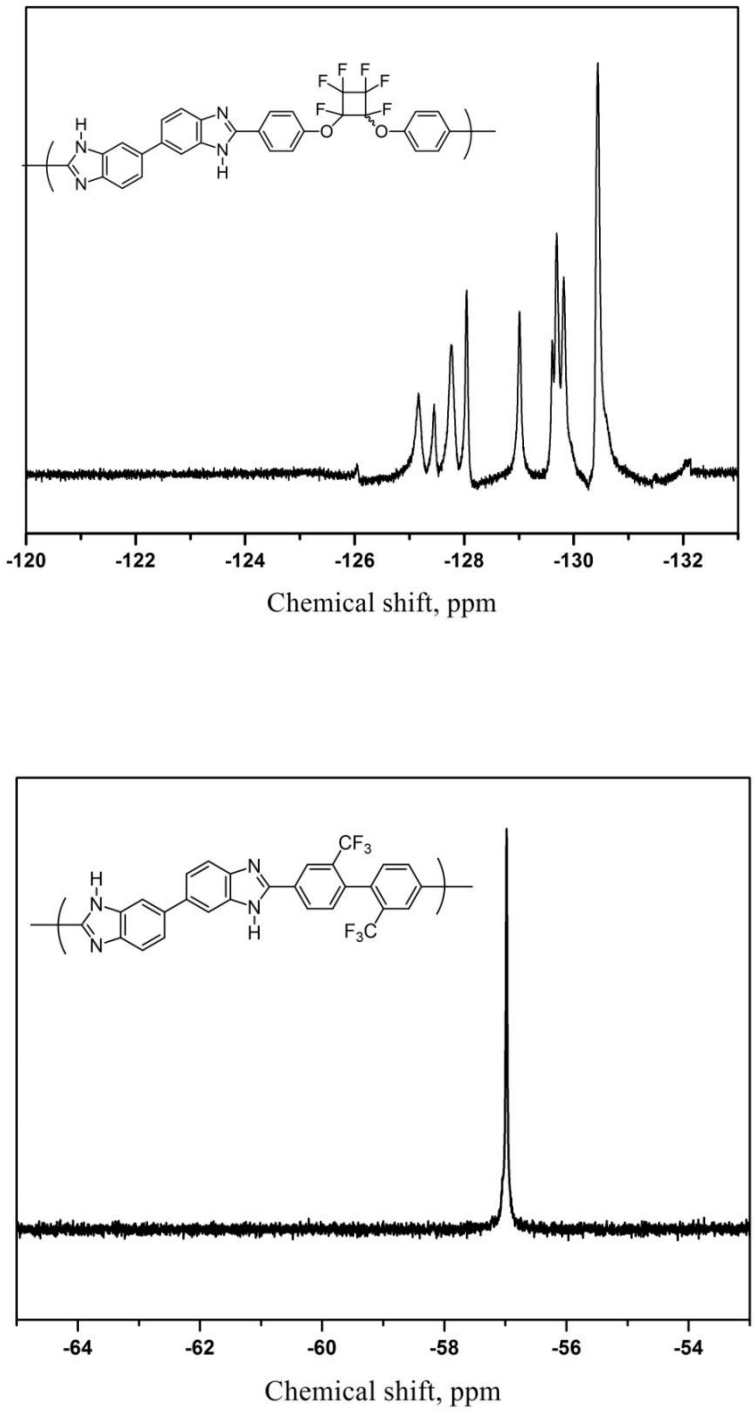

Figure 4.3 ^{19}F NMR spectra of 6F-PBI (top), PFCB-PBI (middle), and BTBP-PBI (bottom).

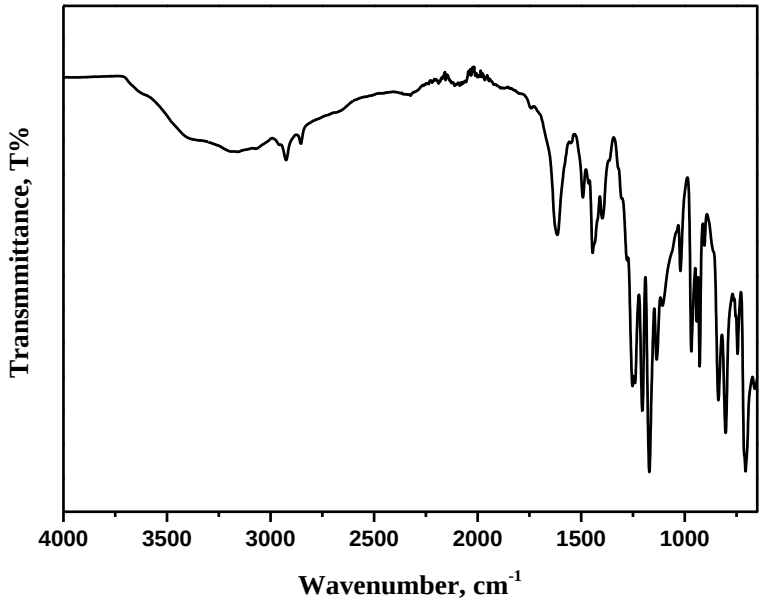
Transmmittance, T%
4000
3500
3000
2500
2000
1500
1000
Wavenumber, cm-1

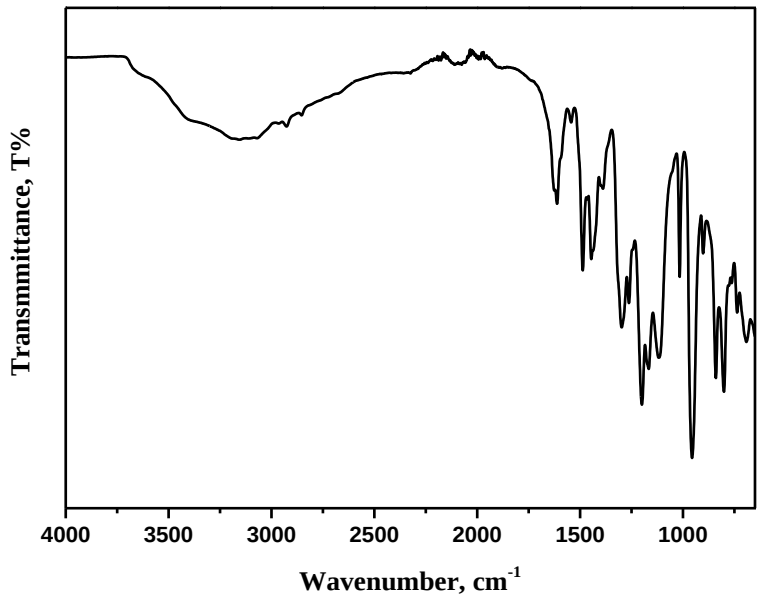
Transmmittance, T%
4000
3500
3000
2500
2000
1500
1000
Wavenumber, cm-1

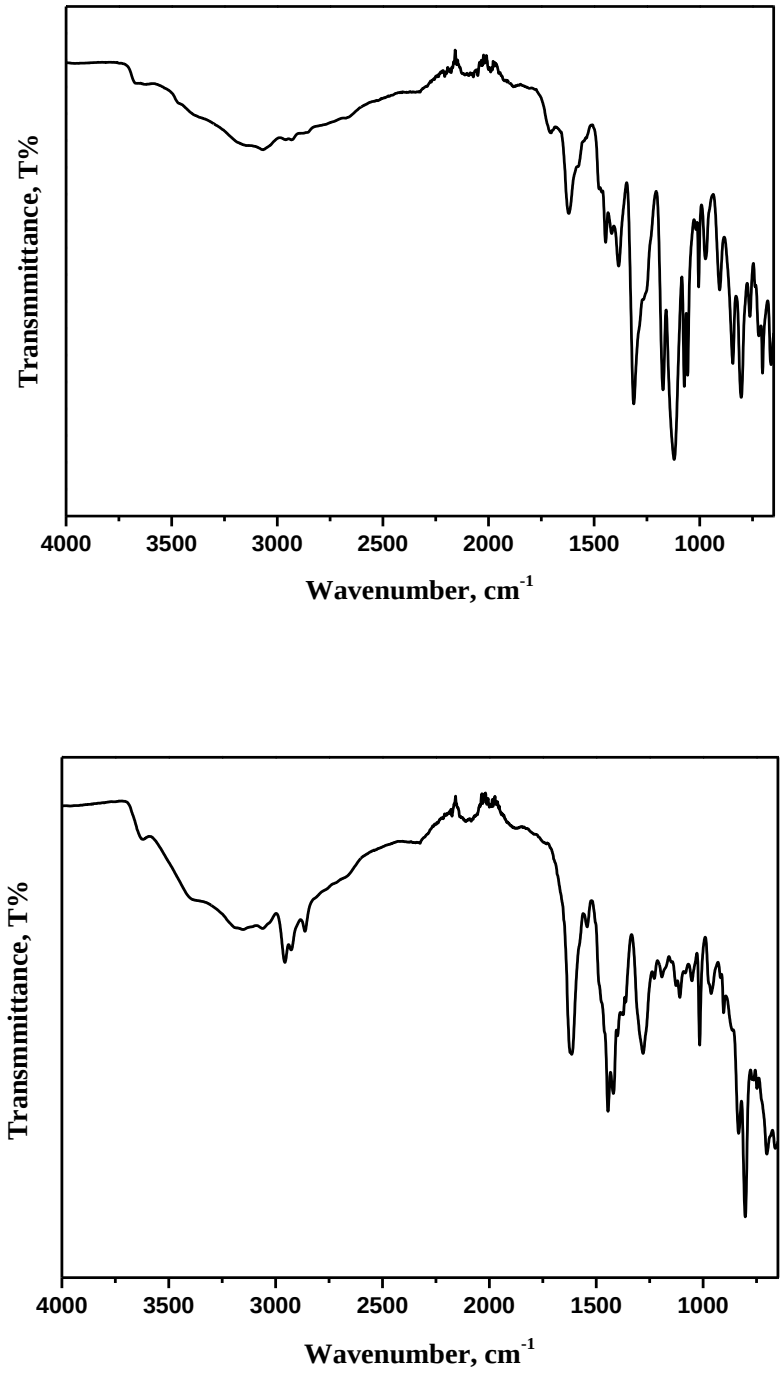

Figure 4.4 FTIR spectra of 6F-PBI (top), PFCB-PBI (second), BTBP-PBI (third), and phenylindane-PBI (bottom).

4.3.1.2 Thermal Properties

PBI thermal stability was studied using TGA under N_2. Polymer powders were pre-treated at 200 °C for 12 hours in the TGA to remove residual solvents and absorbed water. As shown in Figure 4.5, all PBIs exhibited excellent thermal stabilities and no obvious weight losses (> 1 wt%) were observed at temperatures up to 300 °C, a common feature of PBI polymers. Decomposition temperatures at different weight losses (1 wt%, 5 wt%, and 10 wt%) are given in Table 4.2. It was found that all four modified PBI derivatives exhibited lower thermal stabilities than m-PBI, which was likely caused by the introduction of less stable functional groups (e.g. polar groups, hydrocarbon rings, etc.) or the strong disruption of the chain pi-pi stacking and H-bonding interactions. However, all PBIs were stable enough for the desired gas permeation testing conditions (up to 250 °C).

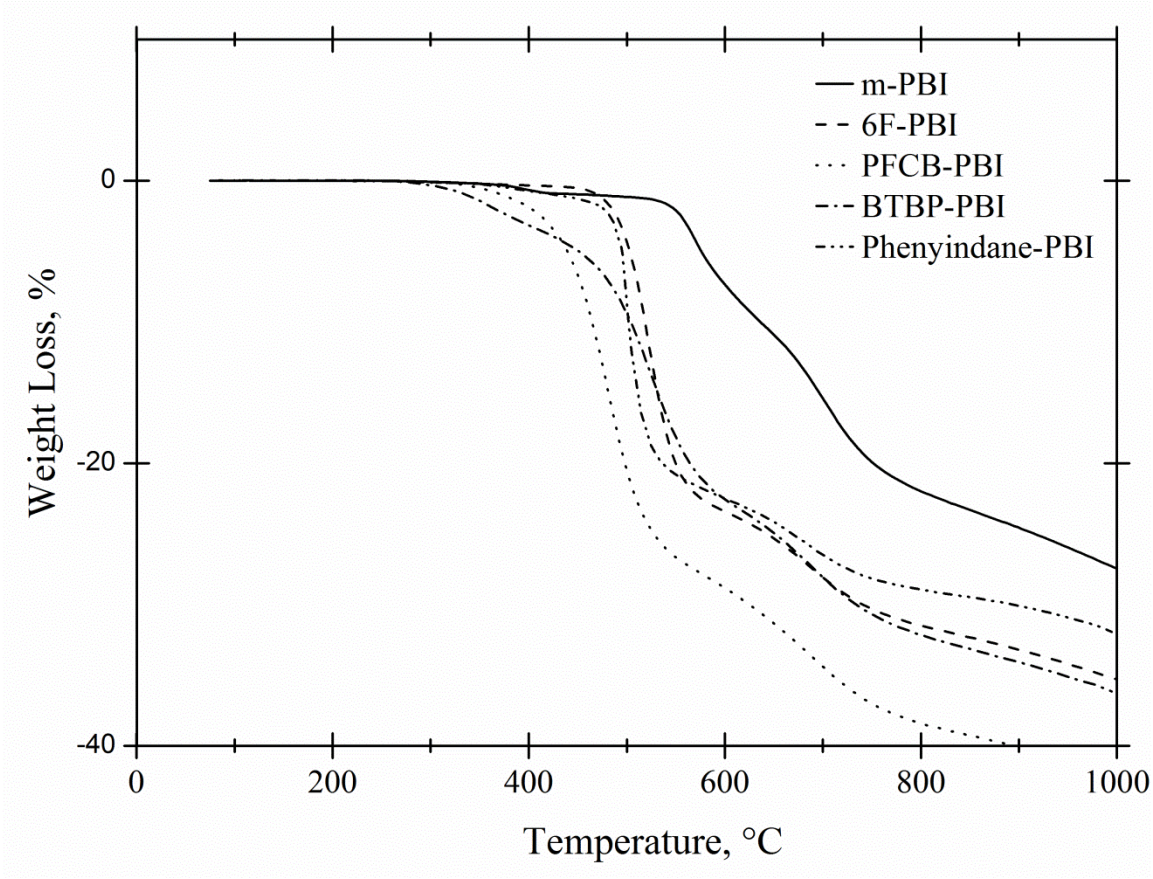

Figure 4.5 TGA thermograms for PBI derivatives in N_2.

Table 4.2 Physical properties of PBI polymers.

Polymer	Density (g cm^{-3})			FFV[d]	Decomposition Temperature (°C)[e]		
	method a[a]	method b[b]	method c[c]		1.0 wt%	5.0 wt%	10.0 wt%
m-PBI	1.37	1.28	1.31	0.145	463	576	637
6F-PBI	1.41	1.44	1.44	0.145	474	507	523
PFCB-PBI	1.45	1.47	1.43	0.175	373	439	465
BTBP-PBI	1.47	1.52	1.52	0.098	355	488	500
phenylindane-PBI	1.16	0.95	1.21	0.142	424	490	502

a. Density data of PBI powders measured by specific gravity bottle after annealing the sample at 110 °C in vacuum oven overnight.
b and c. Density data of PBI films measured by gas displacement pycnometry after annealing the samples in vacuum oven for 24 hours at 100 and 250 °C, respectively.
d. Fractional free volume (FFV) calculated using polymer densities obtained from method c and Bondi's group contribution approach [37, 38].
e. Temperature where the noted weight loss percentage was observed.

The density values obtained on PBI polymers synthesized in this work using gravity bottle and gas displacement pycnometry on powder and cast film samples after vacuum drying at 100-110 °C are in close agreement except for phenylindane-PBI, Table 4.2. In the case of phenylindane-PBI, a lower density value was observed for the cast film as compared to the powder sample. However, the density of phenylindane-PBI film increased after annealing at 250 °C. This density increase upon annealing at higher temperature might be indicative of residual solvent and water removal and/or structural rearrangement. It is anticipated that polymer processing history, especially in the case of PBI-based polymers due to their tight chain packing, can have significant effect on the polymer physical characteristics. The densities of all cast films were also measured after annealing at 250 °C in vacuum oven for 24 hours. The density differences obtained after annealing at 100 and 250 °C were small except for phenylindane-PBI as discussed above.

4.3.1.3 Solubility

PBI solubility characteristics were determined under two different dissolution conditions (a. 1.5 wt% polymer concentrations at ambient temperature; b. 3.0 wt% polymer concentration at reflux temperature) and the results are given in Table 4.3. At ambient conditions, all PBIs exhibited complete or partial dissolution in polar aprotic solvents such as DMAc and DMF. The modified PBI derivatives demonstrated improved solubility compared to m-PBI, which was attributed to the introduction of bulky, high mobility or twisted functional groups into the polymer backbones. At elevated temperatures, all PBIs showed improved solubility in DMAc and LiCl/DMAc at the higher solids concentration. However, for BTBP-PBI, the polymer solution in DMAc was found to exhibit poor long-term stability. BTBP-PBI precipitation was observed and the

homogeneous solution became a swollen gel after sitting for 2-3 hours at ambient conditions. Decreasing the polymer concentration or adding lithium chloride as a phase stabilizer was found to suppress the phase separation [33]. All PBIs were insoluble in common organic solvents such as acetone, THF, or MeOH.

Table 4.3 Solubility characteristics of PBI derivatives.

	Ambient Temperature							Reflux Temperature	
Polymer	DMAc	LiCl/DMAc	NMP	DMF	Acetone	THF	MeOH	DMAc	LiCl/DMAc
m-PBI (100 mesh)	+	+	+	+	−	−	−	++	++
6F-PBI	++	++	++	++	−	−	−	++	++
PFCB-PBI	++	++	++	++	−	−	−	++	++
BTBP-PBI	++	++	++	++	−	−	−	++*	++
Phenylindane-PBI	++	++	++	++	−	−	−	++	++

DMAc: N,N-dimethylacetamide; LiCl/DMAc: 4 wt% LiCl in DMAc; NMP: N-methyl-2-pyrrolidinone; DMF: dimethylformamide; THF: tetrahydrofuran; MeOH: methanol.
++: mostly soluble; ++*: mostly soluble, but polymer precipitated after cooling; +: partially soluble or swelling; -: insoluble.

4.3.2. PBI Dense Film Preparation

Free-standing dense PBI films with thicknesses ranging from 5 μm to 20 μm were fabricated for pure gas permeation measurements. Several important factors potentially affecting the film quality and gas permeation characteristics were studied. These factors included humidity, LiCl stabilizer, and solvent evaporation rate.

Humidity: It was noted that the PBI solution systems (PBI/DMAc or PBI/LiCl/DMAc) were very hygroscopic and thus, for the films cast and dried in the open air, water from the surrounding environment was absorbed by the polymer solutions and caused phase separation in the PBI films. As a result, the PBI polymer precipitated prematurely and formed a porous film with large pores and voids. These features both reduced the film mechanical properties and gas separation performance. Figure 4.6 (left) shows an example of a 6F-PBI film cast in the open air where the film opacity was a

direct result of the strong phase separation. To eliminate the influence of humidity, the PBI films were cast and dried under dry nitrogen in a glove bag, and then transferred to a vacuum oven. The final film, as shown in Figure 4.6 (right), was much stronger and transparent, indicating that a high-quality PBI dense film was formed.

Figure 4.6 6F-PBI free-standing films prepared by various methods (**left**: prepared with 3 wt% 6F-PBI/DMAc solution in open air; **middle**: prepared with 3 wt% 6F-PBI/LiCl/DMAc (PBI: LiCl=1:0.3, w:w) under dry nitrogen protection; **right**: prepared with 3 wt% 6F-PBI/DMAc solution under dry nitrogen protection).

LiCl addition: The addition of LiCl to the PBI/DMAc solution has been commonly used in PBI processing to improve both the polymer solubility and solution stability. It was postulated that Li^+ cation could react with DMAc to form a $[DMAc+Li]^+$ macrocation, thus allowing the Cl^- anion more freedom to disrupt the intra- and inter-molecular hydrogen bonding and suppress PBI aggregation in solution [37-39]. Therefore, LiCl was added to the PBI DMAc solution for initial film casting studies. It was found that even a small amount of LiCl added to the 6F-PBI solution (6F-PBI:LiCl=1:0.3, w:w) caused the cast film (LiCl was washed out by boiled water) (Figure 4.6 (middle)) to become translucent and much weaker than the film cast from pure

DMAc (Figure 4.3 (right)). It is proposed that LiCl aggregation may occur during the solvent evaporation and subsequently affect the polymer morphology, although a detailed mechanism study is still under investigation. In this work, pure DMAc was chosen as the solvent to eliminate the influence of LiCl and obtain accurate correlations between PBI structure and gas permeation properties.

Rate of evaporation: The film drying procedure in this study was divided into two stages: 1) the initial solvent evaporation in a glove bag under dry nitrogen and 2) final heating in a vacuum oven. It was found the initial solvent evaporation speed in a nitrogen environment greatly affected the film quality. For PBIs such as PFCB-PBI, a high initial heating temperature (75-110 °C, hot-plate temperature) resulted in defects such as patterns or uneven thickness in the films. Therefore, lower heating temperatures (40-50 °C, hot-plate temperature) were applied and homogeneous films could be routinely prepared. Figure 4.7 shows the fabrication strategy that facilitated the fabrication of PBI films for all the polymers tested which resulted in consistent quality for gas transportation studies.

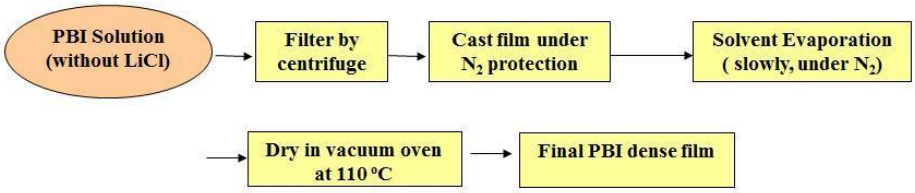

Figure 4.7 Optimized PBI dense film preparation conditions.

4.3.3 Gas Transport Properties

4.3.3.1. Membrane Fundamentals

In an ideal gas separation model, when the upstream pressure (p_1) is significantly larger than downstream pressure (p_2), the permeability (P) of penetrant gas through a

dense polymer membrane can be expressed as the product of the diffusion coefficient (D) and solubility coefficient (S) as shown in Eq. (4):

$$P = D \times S \tag{4}$$

By calculating the permeability ratio of two different gases, for instance P_{H_2}/P_{CO_2} in this work, the ideal gas selectivity (α_{H_2/CO_2}) is obtained, providing an assessment of the polymer film's ability to separate these gases from a mixed gas system. Also according to Eq. (4), when factoring the permeability into diffusivity and solubility, the ideal H_2/CO_2 selectivity can be obtained from the product of the mobility selectivity (D_{H_2}/D_{CO_2}) and sorption selectivity (S_{H_2}/S_{CO_2}) as shown in Eq. (5):

$$\alpha_{H_2/CO_2} = \frac{P_{H_2}}{P_{CO_2}} = \left[\frac{D_{H_2}}{D_{CO_2}}\right]\left[\frac{S_{H_2}}{S_{CO_2}}\right] \tag{5}$$

In general, the mobility selectivity of polymer films to separate gas mixtures is based on their ability to act as "molecular sieves". Therefore, the polymer film preferentially transports the smaller sized H_2 molecules (kinetic diameter=2.89 Å) rather than the larger CO_2 molecules (kinetic diameter=3.30 Å). Comparatively, the sorption selectivity of polymer films is mainly determined by the relative gas condensabilities (or gas critical temperature/boiling point), so CO_2 (boiling point=195 K) usually exhibits higher solubility than H_2 (boiling point=20 K) in polymeric membranes. Generally in glassy polymers, large segmental chain movements are relatively limited so gas diffusion plays the dominant role in deciding the overall gas transport properties. Therefore, in this specific application, increasing penetrant mobility and mobility selectivity in the polymers are the most important criteria to design commercially attractive H_2-selective polymeric membranes.

4.3.3.2. Gas Permselectivity at Elevated Temperatures

The pure gas permselectivities of the PBI derivatives tested at 250 °C and 50 psia are reported in Table 4.4. For m-PBI, the H_2 permeance is 3.6 GPU (3.6×10^{-6} cm^3 cm^{-2} s^{-1} cm Hg^{-1}) and the H_2/CO_2 and H_2/N_2 ideal selectivities are 23.0 and 98.3, respectively. The PBI film thicknesses were measured using SEM after gas permeation testing. The film thickness of m-PBI was approximately 21.6 μm and thus, the corresponding H_2 permeability is 76.8 barrer (76.8×10^{-10} cm^3 cm cm^{-2} s^{-1} cm Hg^{-1}). Previously Berchtold et.al. reported H_2 permeability of 58 barrer and H_2/CO_2 selectivity of 43 for m-PBI [24]. They evaluated a PBI/ceramic composite membrane for one year at 250 °C. The effects of long term membrane exposure to elevated temperature are likely the major contributing factor in the observed differences in H_2 permselectivity characteristics measured in this work as compared to that reported by Berchtold et.al.. The lower H_2 permeability and higher H_2/CO_2 selectivity reported there are consistent with polymer structure tightening due to long term exposure to elevated temperatures.

Table 4.4 Perm-selectivity for the PBI membrane derivatives tested at 250 °C and 50 psia.

	Gas Permeance (GPU)[a]			Gas Permeability (Barrer)[a]			Gas Selectivity[a]		Ep (KJ mol^{-1})[b]		
Polymers	H_2	CO_2	N_2	H_2	CO_2	N_2	H_2/CO_2	H_2/N_2	H_2	CO_2	N_2
6F-PBI	162.1	31.34	8.661	997.2	192.7	53.26	5.174	18.72	8.36	0.39	11.02
BTBP-PBI	89.07	12.53	3.802	710.4	99.91	30.33	7.111	23.43	10.9	4.28	13.62
Phenylindane-PBI	24.55	3.765	0.9329	480.6	73.69	18.26	6.522	26.32	10.4	3.11	14.01
PFCB-PBI	22.55	3.415	0.9617	323.1	48.92	13.79	6.604	23.45	13.1	6.72	17.64
m-PBI	3.564	0.1548	0.03625	76.81	3.335	0.7812	23.03	98.32	19.4	17.1	27.48

a. All date was measured based on pure gas testings.
b. E_p is the activation energy of the permeabilities obtained from the slope of permeability versus inverse temperature.

As shown in Table 4.4, all the modified PBIs exhibited significantly higher gas permeabilities than m-PBI, indicating the chain functionalization effectively changed the

polymer chain packing (e.g. free volume architecture) and ultimately improved the gas transport properties. The H_2 permeability of 6F-PBI was 997.2 barrer (997.2×10^{-10} cm^3 cm cm^{-2} s^{-1} cm Hg^{-1}) at 250 °C, which was approximately 13x higher than m-PBI and was also the highest among all the synthesized PBI derivatives. PBI gas permeabilities correlated well with gas molecule size (kinetic diameter: H_2 (2.89 Å) <CO_2 (3.30 Å) <N_2 (3.64 Å)), indicating that a diffusion-based selectivity (or size sieving effect) plays the dominant role in the gas transport properties at elevated temperatures. The polymer densities were measured by pycnometry at ambient temperature after annealing the film samples at 250 °C and used for polymer fractional free volume (FFV) calculations (Table 4.2). No direct correlation was found between FFV data and polymer gas transport characteristics. Numerous factors including polymer FFV, molecular weight, gas-polymer interactions, and polymer glass transition temperature in relation to operating temperature (i.e., polymer molecular mobility at use conditions) influence the gas transport characteristics of polymer materials. The interplay between these influencing factors and convolution of their ultimate property influences makes one-to-one chemistry-property or structure-property relationship identification a daunting task. Further targeted chemistry-structure-property relationship exploration, building on the work presented here, is required to gain additional insight and specificity regarding the complex interplay of influencing factors in these PBI-based materials.

This work explored several strategies for PBI main chain modifications with the goal of increasing polymer gas permeability. In general, these strategies or factors are correlated so it is difficult to isolate one effect from the others. For instance, incorporating bulky and rigid functional moieties could help to “stiffen” the chain and

decrease the chain packing efficiency (i.e. increase free volume), which would generally increase gas diffusivity. However, these rigid functionalities could also increase the energy barrier for, and thus restrict, chain torsional mobility which would lead to decrease in gas diffusivity. One example of this complex interplay of influencing factors is observed in the comparison of 6F-PBI and PFCB-PBI. Both of these materials possess bulky and relatively flexible chain connectors compared with m-PBI. As a result, both 6F-PBI and PFCB-PBI have, as anticipated, significantly higher H_2 permeability than m-PBI. Based on the calculated FFVs for these same polymers alone, it is anticipated that PFCB-PBI would exhibit a higher H_2 permeability. However, in practice the H_2 permeability of PFCB-PBI is lower than that of 6F-PBI. This permeability differential is attributed to the increased rigidity of the PFCB functionality over that of the 6F functionality. A second illustrative example is found in the comparison of BTBP-PBI with phenylindane-PBI. The BTBP-PBI has a rigid-rod but also twisted backbone conformation (caused by the steric repulsion of bistrifluoromethyl groups), which suppresses the chain packing efficiency. Phenylindane-PBI possesses a bulky, rigid bent moiety in the polymer backbone which could also decrease chain packing density. The calculated FFVs for BTBP-PBI and phenylindane-PBI are both lower than that calculated for m-PBI indicating tighter chain packing. However, the higher H_2 permeability of BTBP-PBI and phenylindane-PBI indicates contrary. Therefore, further quantitative and direct FFV analysis of PBI-based polymers using analytical techniques such as positron annihilation lifetime spectroscopy (PALS) is required to further correlate gas permselectivity characteristics with polymer microstructure.

The increase in H_2 permeability resulted in a significant decrease of ideal gas selectivities for all the modified PBIs. The H_2/CO_2 selectivity decreased from 23 (m-PBI) to approximately 5-7 (all other PBIs), indicating a much more open chain packing structure for the modified PBIs.

4.3.3.3. Effect of Temperature on Gas Permselectivity

The effect of operating temperature on gas permselectivities is very important since it can be used to attain an optimum set of permeability and selectivity characteristics and to select the proper materials for a specific application (e.g. H_2/CO_2 separation at elevated temperatures). m-PBI is considered a poor material for ambient temperature H_2 separation due to its low permeability [23]. This is attributed to the extremely tight and close chain packing characteristics of m-PBI caused by strong pi-pi interactions and interchain hydrogen bonding. However, the rigid structure and excellent thermal resilience of m-PBI make it promising candidate for H_2/CO_2 separation at extreme conditions [23]. For polymer materials, the temperature dependence of the gas diffusion coefficient and solution coefficient can be expressed as follows (Eqs. (6) and (7)):

$$\mathrm{D} = D_0 e^{-\Delta E_d/RT} \tag{6}$$

$$\mathrm{S} = S_0 e^{-\Delta Hs/RT} \tag{7}$$

where E_d is the activation energy of diffusion; ΔH_s is the partial molar enthalpy of sorption; D_0 and S_0 are constants; R is the universal gas constant; and T is the operating temperature. In general, the diffusion coefficient increases with temperature whereas the solubility coefficient decreases with temperature. For glassy PBI polymers, diffusion coefficients are strongly dependent on temperature with minimal solubility contributions

to permeability. Thus, their permeability behavior is typically consistent with activated diffusion, i.e., as operating temperature increases all gas diffusivity coefficients increase resulting in increased gas permeabilities. Figure 4.8 shows the temperature dependence of the gas permeabilities (H_2, CO_2, and N_2) for all the PBI derivatives. It was found that the gas permeabilities of all PBIs increased with temperature, indicating a diffusion-dominated gas transport mechanism in the temperature range tested. Also, the activation energy of permeability (E_p) was calculated from this data and the results are shown in Table 4. The order of E_p value is $N_2>H_2>CO_2$ indicating greatest influence of temperature on N_2 permeability.

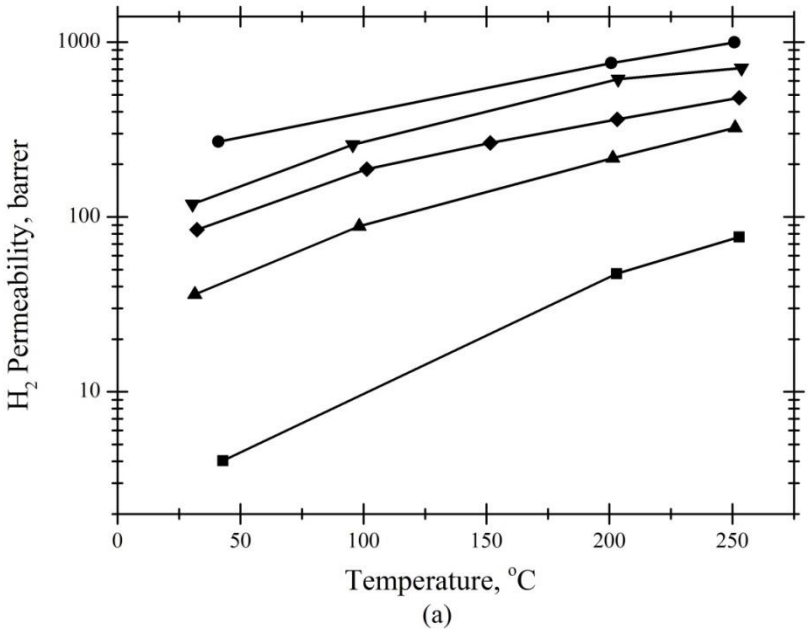

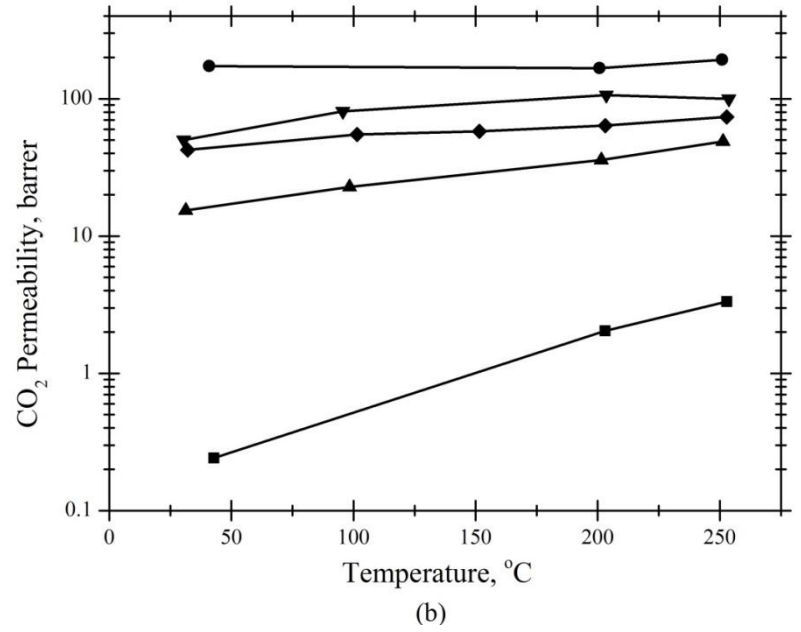

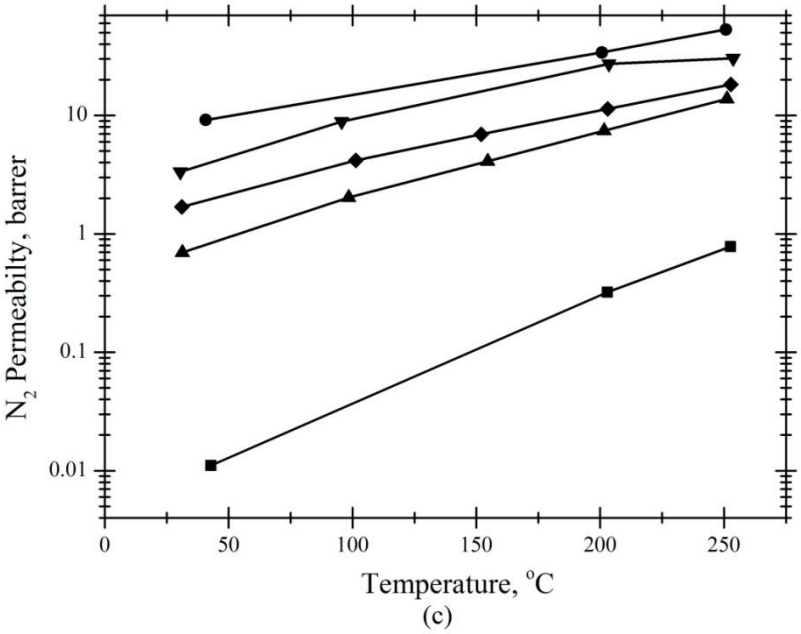

Figure 4.8 Effect of operating temperature on pure gas permeabilities ((a). H_2; (b). CO_2; (c). N_2) of PBI derivative membranes (circles: 6F-PBI; downtriangles: BTBP-PBI; diamonds: phenylindane-PBI; uptriangles: PFCB-PBI; squares: m-PBI). The lines are drawn to guide the eye.

Fig. 4.9 shows the temperature dependence of the ideal selectivities for H_2/N_2 (a) and H_2/CO_2 (b) for the evaluated polymers. The selectivity of glassy polymers often decreases with temperature as less permeable gas component often possesses higher activation energies, i.e., these less permeable gases realize relatively larger increases in permeability with increasing temperature. The temperature dependence of the ideal H_2/N_2 selectivity for these PBI membranes follows this general trend. Furthermore, the polymer chain motion (rotational and vibrational) is significantly influenced at elevated temperatures. Since polymer free volume is a function of polymer chain packing and inter-segmental motion, the increased N_2 permeability is also influenced by the effect of elevated temperature on these aforementioned polymer macromolecular characteristics. In contrast, the H_2/CO_2 ideal selectivities increase with temperature indicating that the increase in H_2 permeability as a function of temperature is greater than that of CO_2. The effect of temperature on permeability is quantitatively shown in the values of E_p (Table 4.4), which are significantly larger for H_2 than for CO_2. The large increase in H_2 permeability compared to that of CO_2 with temperature is attributed to its smaller size consistent with the size sieving characteristics of PBI. In addition, the solubility driven permeability component, the minor component in these PBI materials, is expected to be higher for CO_2 as compared to H_2 due to higher CO_2 solubility in the polymer. However, this solubility component will decrease with increasing temperature thereby further contributing to an increase in H_2/CO_2 selectivity.

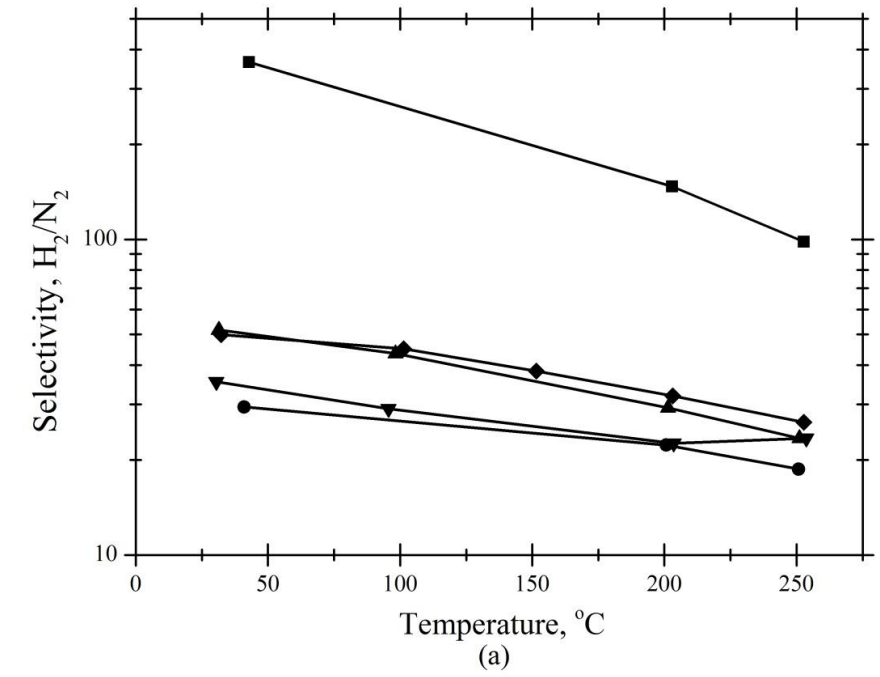

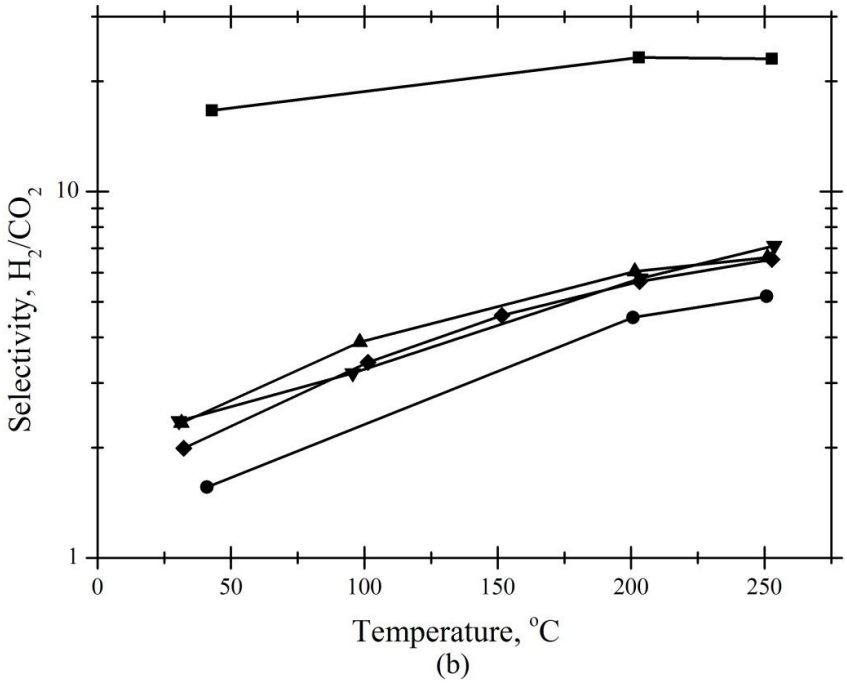

Figure 4.9 Effect of operating temperature on H_2/N_2 (a) and H_2/CO_2 (b) ideal selectivities of the PBI derivative membranes (circles: 6F-PBI; down-triangles: BTBP-PBI; diamonds: phenylindane-PBI; up-triangles: PFCB-PBI; squares: m-PBI). The lines are drawn to guide the eye.

An exception to the general increase in permeability as a function of temperature is observed for 6F-PBI membrane. In contrast to the other PBI-derivatives studied here, as the operating temperature is increased from near-ambient to 250 °C, the CO_2 permeability remained nearly constant for 6F-PBI membranes. This 6F-PBI membrane behavior can be attributed to strong CO_2-polymer interactions in this highly fluorinated material combined with its activated diffusion character. In general, CO_2 has significantly higher solubility in polymers as compared to H_2 and N_2 due to dipole-dipole interaction between CO_2 and the polymer [40]. This CO_2-polymer interaction is expected to be significant for 6F-PBI due to presence of highly electronegative 6F group. However, the gas solubility decreases as temperature increases (Eq. (7)). Therefore, the solubility contribution to permeability decreases while the diffusivity contribution increases with operating temperature. This interplay between diffusivity and solubility results in a near constant 6F-PBI CO_2 permeability over the evaluated temperature range.

4.3.3.4 Effect of Pressure on Gas Permselectivity

The relationship between gas permeability and transmembrane pressure was also investigated. Figure 4.10 shows the H_2 permeability at 250˚C for the PBIs at different trans-membrane pressures from 20 to 50 psi. A fairly constant H_2 permeability was observed for all of the polymers, indicating the absence of viscous flow and correspondingly, defects in the tested dense membranes.

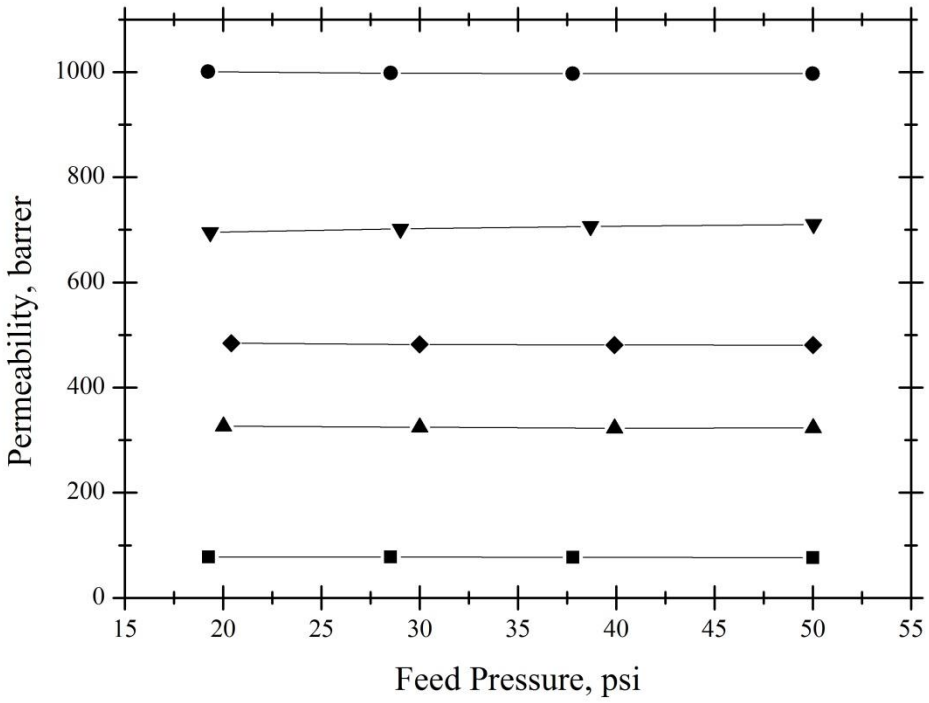

Figure 4.10 Effect of trans-membrane pressure on the H_2 permeability of the PBI derivative membranes. (Circles: 6F-PBI; down-triangles: BTBP-PBI; diamonds: phenylindane-PBI; up-triangles: PFCB-PBI; squares: m-PBI). The lines are drawn to guide the eye.

4.3.3.5 Comparison to Other Polymeric Membranes

As discussed previously, the gas separation performance of polymeric membrane materials is generally subjected to a trade-off relationship between gas permeability and gas selectivity. Tremendous work has been done on exploring the gas separation performance of various kinds of polymeric materials in the past few decades and these experimental results were collected and organized by Robeson to draw a series of upper-bound curves based on different gas pairs [17, 41]. Figure 4.11shows Robeson's upper-bound curve for the H_2/CO_2 gas pair published in 2008. Polymeric materials with gas separation capabilities surpassing the upper-bound and located in the upper right hand quadrant of Figure 4.11 are considered as attractive candidates for H_2/CO_2 separation.

However, the literature data shown in Figure 4.11 by Robeson were acquired at relatively low temperature (35 °C). While the use of near-ambient temperature conditions is a standard test protocol, it does not provide sufficient information to assess the technical viability of a membrane for H_2/CO_2 separation at typically encountered syngas processing conditions. Very few data or reports could be found in the literature for H_2/CO_2 separation at elevated temperatures (>150 °C) largely due to the low thermal degradation temperatures of most polymer-based materials. The gas separation performance of the PBIs evaluated in this work at both ambient temperature and 250 °C was incorporated into the H_2/CO_2 Robeson plot (Figure 4.11). The permselectivities of all PBIs at 250 ºC exceeded the Robeson upper bound indicating the potential utility of these PBI-based materials for H_2 separation from syngas at elevated temperatures. However, more effort is required to further optimize this class of materials for industrially attractive H_2/CO_2 separations.

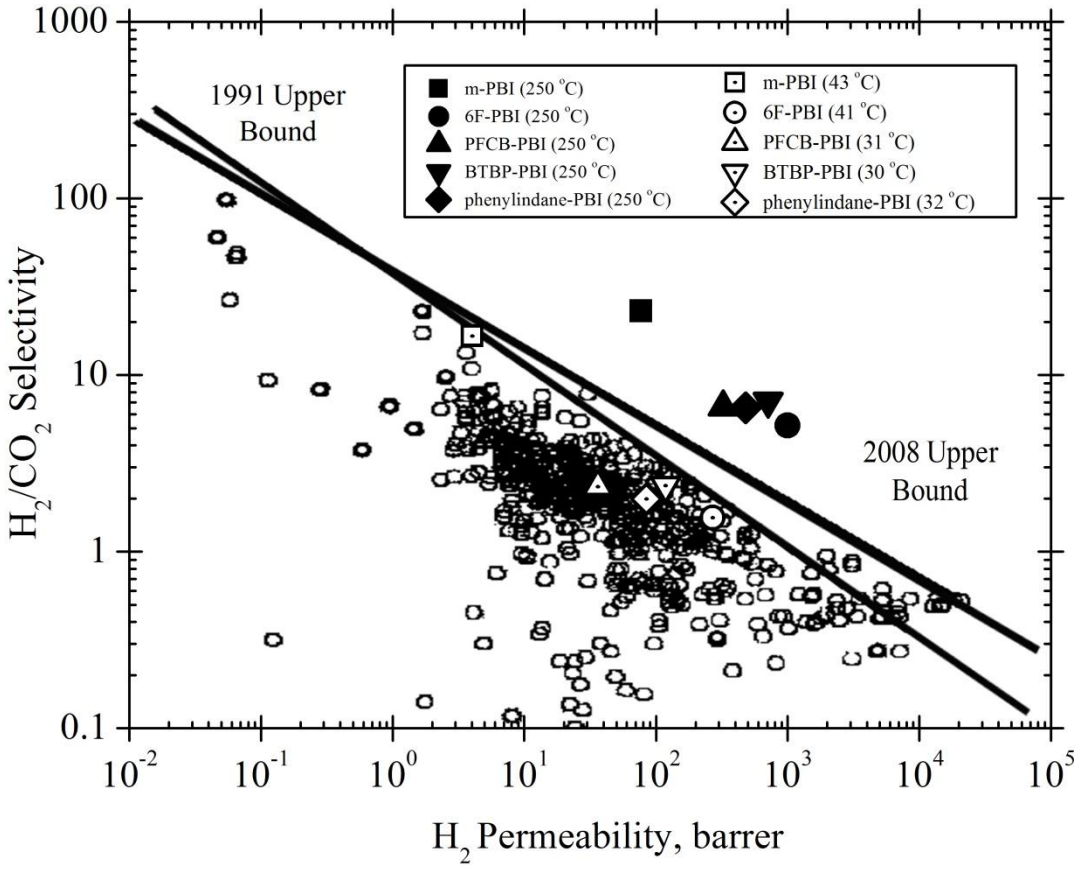

Figure 4.11 Robeson plot comparing the PBI derivative membranes with other polymeric membranes tested for the H_2/CO_2 separation. The lines represents the 1991 and 2008 Robeson upper bounds and the open circles represent literature data for polymeric gas separation membranes [17].

4.4 Conclusions

A series of high molecular weight PBI derivatives with modified bulky/flexible/frustrated backbone structures were successfully prepared by solution polymerization in PPA or Eaton's Reagent and compared to commercially available m-PBI for H_2/CO_2 gas separation. The modified PBIs exhibited slightly decreased thermal stabilities and better organo-solubilities compared to m-PBI, which was attributed to the ability of the various functional groups to "open up" or disrupt the polymer chain packing. The PBI derivatives were fabricated into free-standing films by solution casting.

Film casting protocols were optimized for film quality, including mechanical properties and defect levels. H_2/CO_2 separation testing was performed on the cast membranes at temperatures ranging from ca. 30 °C to 250 °C and varied pressure. It was found that the PBI films exhibited improved gas separation properties (H_2 permeability and H_2/CO_2 selectivity) with an increase in operating temperature. Also, the introduction of bulky/flexible/frustrated functionalities into the PBI backbone effectively disrupted the polymer close chain packing and provided materials with much higher H_2 permeability (up to 997.2 barrer) compared to m-PBI (76.81 barrer) at 250 °C. However, decreases in H_2/CO_2 selectivities from 23.03 (m-PBI) to 5-7 (other PBIs) were also observed at 250 °C in these materials. No direct correlations were found between the calculated FFV data and the gas separation characteristics within the PBI derivatives. All PBIs exhibited elevated temperature (250 °C) gas separation performance exceeding the Robeson upper-bound , indicating their promise for application as membranes for H_2 purification from syngas.

4.5 References

[1] G. Marbán; T. Valdés-Solís, *Int J Hydrogen Energy* **2007**, 32, 1625.

[2] J. A. Turner, *Science*, **2004**, 305, 972.

[3] A. Midilli; M. Ay; I. Dincer; M. A. Rosen, *Renew Sust Energy Rev* **2005**, 9, 255.

[4] P. P. Edwards; V. L. Kuznetsov; W. I. F. David, *Philos Trans R Soc A-Math Phys Eng Sci* **2007**, 365, 1043.

[5] J. Turner; G. Sverdrup; M. K. Mann; P. C. Maness; B. Kroposki; M. Ghirardi; R. J. Evans; D. Blake, *Int J Energy Res* **2008**, 32, 379.

[6] S. K. Ngoh; D. Njomo, *Renew Sust Energy Rev* **2012**, 16, 6782.

[7] R. M. Navarro; M. A. Pena; J. L. G. Fierro, *Chem Rev* **2007**, 107, 3952.

[8] J. D. Holladay; J. Hu; D. L. King; Y. Wang, *Catal Today* **2009**, 139, 244.

[9] E. S. Rubin; H. Mantripragada, *Prog. Energy Combust. Sci.* **2012**, 38, 630.

[10] A. A. Olajire, *Energy* **2010**, 35, 2610.

[11] D. Grainger; M. -B. Hägg, *Fuel*, **2008**, 87, 14.

[12] G. Krishman; D. Steel; K. C. O'Brien; R. Callahan; K. A. Berchtold; J. D. Figueraa, *Energy Proc*, **2009**, 1, 4079.

[13] H. Li; Z. Song; X. Zhang; Y. Huang; S. Li; Y. Mao; H. J. Ploehn; Y. Bao; M. Yu, *Science*, **2013**, 342, 95.

[14] H, Lin; E. Van Wagner; B. D. Freeman; L. G. Toy; R. P. Gupta, *Science*, **2006**, 311, 639.

[15] S. A. Stern, *J. Membr. Sci.*, **1994**, 94, 1.

[16] K. Ghosal; B.D. Freeman, *Polym Adv Technol* **1994**, 5, 673.

[17] L. M. Robeson, *J Membr Sci* **2008**, 320, 390.

[18] T. C. Merkel; M. Zhou; R. W. Baker, *J Membr Sci* **2012**, 389, 441.

[19] H. Vogel; C. S. Marvel, *J Polym Sci* **1961**, 50, 511.

[20] A. S. Buckley; D. E. Stuetz; G. A. Serad, *Encycl Polym Sci Eng* **1987**, 11, 572.

[21] J. T. Wang; R. F. Savinell; J. Wainright; M. Litt; H. Yu, *Electrochim Acta* **1996**, 41, 193.

[22] L. Xiao; H. Zhang; E. Scanlon; L. S. Ramanathan; E. W. Choe; D. Rogers; T. Apple; B. C. Benicewicz, *Chem Mater* **2005**, 17, 5328.

[23] D. R. Pesiri; B. Jorgensen; R. C. Dye, *J Membr Sci*, **2003**, 218, 11.

[24] K. A. Berchtold; R. P. Singh; J. S. Young; K. W. Dudeck, *J Membr Sci* **2012**, 415, 265.

[25] S. C. Kumbharkar; Y. Liu; K. Li, *J Membr Sci* **2011**, 375, 231.

[26] S. C. Kumbharkar; P. B. Karadkar; U. K. Kharul, *J Membr Sci* **2006**, 286, 161.

[27] S. C. Kumbharkar; U. K. Kharul, *J Membr Sci* **2010**, 357, 134.

[28] Y. Yampolskii; I. Pinnau; B. D. Freeman (Eds.), *Material science of membranes for gas and vapor separation*. John Wiley & Sons: Chichester: 2006.

[29] J. D. Wind; D. R. Paul; W. J. Koros, *J Membr Sci* **2004**, 228, 227.

[30] Y. Liu; R. Wang; T.S. Chung, *J Membr Sci* **2001**, 189, 231.

[31] G. Qian; B.C. Benicewicz, *J Polym Sci Part A: Polym Chem* **2009**, 47, 4064.

[32] G. Qian; D. W. Smith Jr; B. C. Benicewicz, *Polymer* **2009**, 50, 3911.

[33] X. Li; G. Qian; X. Chen; B. C. Benicewicz, *Fuel Cells* **2013**, 13, 832.

[34] X. Li, X. Chen, B. C. Benicewicz, *J Power Sources* **2013**, 243, 796.

[35] D.W. van Krevelen; K. te Nijenhuis, *Properties of polymers, 4th edn*. Elsevier: 2009.

[36] A. Bondi, *J Phys Chem - Us* **1964**, 68, 441.

[37] A. M. Striegel, *Carbohyd Polym* **1997**, 34, 267.

[38] A. M. Striegel, *J Chil Chem Soc* **2003**, 48, 73.

[39] C. B. Shogbon; J. L. Brousseau; H. Zhang; B. C. Benicewicz; Y. A. Akpalu, *Macromolecules*, **2006**, 39, 9409.

[40] D. M. D'Alessandro; B. Smith; J. R. Long, *Angew. Chem. Int. Ed.* **2010**. 49, 6058.

[41] L. M. Robeson, *J Membr Sci* **1991**, 62, 165.

CHAPTER 5

POLYBENZIMIDAZOLE BASED RANDOM COPOLYMERS CONTAINING HEXAFLUOROISOPROPYLIDENE FUNCTIONAL GROUPS FOR GAS SEPARATIONS AT ELEVATED TEMPERATURES[4]

[4] R.P. Singh, X. Li, K.W. Dudeck, K.A. Berchtold, B.C. Benicewicz. To be submitted to *Journal of Membrane Science.*

5.1 Introduction

H_2/CO_2 separation plays a critical role in advanced clean energy production schemes from hydrocarbon fuels such as coal, natural gas and bio-mass with integrated carbon capture. Industry standard CO_2 separation techniques such as solvent scrubbing and pressure swing adsorption (PSA) have limited operating regime to achieve high operational efficiencies. These techniques operate at near ambient temperatures and produce a low pressure CO_2 stream, resulting in large energy penalty for CO_2 capture and sequestration.

Membrane-based separation methods are attractive alternatives for large scale H_2 production. With no moving parts, no phase change and extensive process intensification opportunities, membrane-based separation methods can provide economic H_2/CO_2 separation solutions. Polymeric membranes have already been used commercially for H_2 recovery from industrial exhaust stream from hydrogenation and dehydrogenation processes [1]. The high packing density and cheap and established manufacturing practices for polymer membranes are important driving forces for their intended use in large scale H_2 production.

The membrane-based separation process integration in the vicinity of water-gas-shift reactor of advanced hydrocarbon fuel processing scheme is estimated to achieve high process efficiencies. At this stage, the high pressure of synthesis gas (syngas) as well as the high H_2 partial pressure provides a high driving force for efficient membrane operation. The membrane materials and modules comprising of these materials with tolerance to syngas operating conditions (temperature & pressure) and also to chemical impurities present in the syngas provide energy efficient integration routes. However,

commercially available polymeric membranes lack the thermal and chemical tolerance required for energy efficient H_2 separation from fossil fuel derived syngas at elevated temperatures exceeding 150 °C.

Polybenzimidazole (PBI)-based materials are a class of heterocyclic polymers with exceptional thermal and chemical stabilities sufficient for separation applications in syngas operating environments. Owing to its microstructural rigidity imparted by efficient pi-pi stacking and strong hydrogen bonding, PBIs have shown promising molecular sieving characteristics for efficient H_2/CO_2 separation at elevated temperatures [2-4]. Berchtold et al. [2] have tested PBI-metallic composite membranes for typical syngas components in both pure and dry simulated syngas streams at 250 °C, a most attractive temperature for pre-combustion CO_2 separation and clean H_2 production. They reported that PBI-metallic composite membrane's exhibited exceptional long term durability and high H_2/CO_2 selectivity. The H_2 permeance and H_2/CO_2 selectivity of the PBI-metallic composite membrane evaluated in dry simulated syngas feed stream at 250 °C were approximately 7 GPU and 48, respectively. The membrane was also tested for gas permeation at 250 °C for approximately 1 year. During this year-long testing, the membrane maintained a nearly constant H_2 perm-selectivity over other syngas components. This is a pivotal development and demonstration in the polymer membrane field as temperature limitations and intolerance to sulfur compounds often leads to polymer membrane failure.

Appropriate processing ability of PBIs allows fabrication of industrially attractive hollow fiber membranes to achieve high surface-area-to-volume modules for large scale H_2/CO_2 separations. Kumbharkar et al. prepared m-PBI based hollow fiber membranes

fabricated by conventional dry-jet wet spinning technique followed by the solvent exchange process [3]. These PBI fibers showed exceptional H_2/CO_2 separation ability measured in the temperature range of 100-400 °C. Recently, higher performance PBI hollow fibers were reported by Los Alamos National Laboratory (LANL) with H_2 permeance exceeding 150 GPU and H_2/CO_2 selectivity of greater than 20 [5].

Commercially available PBI polymers (m-PBI, poly(2,2'-m-phenylene-5,5'-bibenzimidazole) have demonstrated commercially attractive H_2/CO_2 selectivity; however, their H_2 permeability is low which mandates ultra-thin selective layers to achieve industrial attractive H_2 throughputs [2, 3]. The H_2 permeability of PBI can be improved by structural and chemical manipulations of PBI inducing polymer chain packing disruption and enhancement in polymer free volume architecture. We reported and discussed gas permeation properties of four PBI derivatives (in chapter 4) with main chain structure variations as compared to base m-PBI materials at elevated temperatures [6]. These PBI materials incorporated high localized mobility at high temperatures, contained rigid and bent configurations that frustrated close chain packing, or possessed bulky side groups. We reported that the main chain structural variations effectively disrupted the PBI chain packing resulting in much improved film H_2 permeability (up to 997.2 barrer) compared with m-PBI (76.81 barrer) at 250 °C and 50 psia. However, lower selectivities (5-7 (modified PBI's) versus 23 (m-PBI)) were also measured and reflected the general trade-off between gas permeability and selectivity.

In order to achieve a better balance between H_2 permeability and H_2/CO_2 selectivity within the PBI based materials, in this chapter, a series of PBI-based random copolymers containing bulky and flexible hexafluoroisopropylidene functional groups

were synthesized. High quality free-standing films were prepared from these PBI copolymers and then used for gas permeation measurements at elevated temperatures. By adjusting the concentration of the hexafluoroisopropylidene moieties present in the PBI polymer chains, we expected to achieve a relative control on the polymer chain packing efficiencies, and to eventually achieve a control on the overall H_2/CO_2 separation performance.

5.2 Experimental

5.2.1 Materials

2,2-Bis(4-carboxyphenyl)-hexafluoropropane (6F-diacid, 98.0%) was purchased from TCI America. Isophthalic acid (IPA) was purchased from Amoco Chemicals. 3,3',4,4'-Tetraaminobipheynl (TAB, polymer grade, ~97.5%) was donated by BASF Fuel Cell. Polyphosphoric acid (PPA, 115 %) was purchased from InnoPhos. All the other common solvents such as N,N-dimethylacetamide (DMAc), N-methyl-pyrrolidinone (NMP), and ammonium hydroxide were purchased from Fisher Scientific. The m-PBI used in this study as the benchmark PBI material was obtained from PBI Performance Products, Inc. and used as received. Unless otherwise specified, all chemicals were used without further purification.

5.2.2 Synthesis of 6F/m-PBI Random Copolymers

The general procedure for the synthesis of 6F/m-PBI random copolymers (e.g., 6F:m=50:50, mol:mol) is described as follows: a 100 ml, three-necked, round-bottom flask was equipped with an overhead mechanical stirrer and nitrogen-purge inlet and outlet. TAB (2.681 g, 12.50 mmol), IPA (1.039 g, 6.25 mmol), and 6F-diacid (2.454 g, 6.25 mmol) were added to the reactor in a nitrogen glove box, followed by 124 g of PPA

(Figure 5.1). The reaction mixture was then stirred by the mechanical stirrer set at 50 rpm and purged under flowing N_2. The reaction temperature was controlled by a programmable temperature controller. The typical final polymerization temperatures were 220 °C for approximately 15 h. As the reaction proceeded, the solution became more viscous and developed a dark brown color. At the end of the polymerization, the polymer solution was poured into water, pulverized, neutralized with ammonium hydroxide, and vacuum dried at 110 °C overnight to obtain the polymer powders. Neat 6F-PBI polymer was synthesized according to our previous work [7].

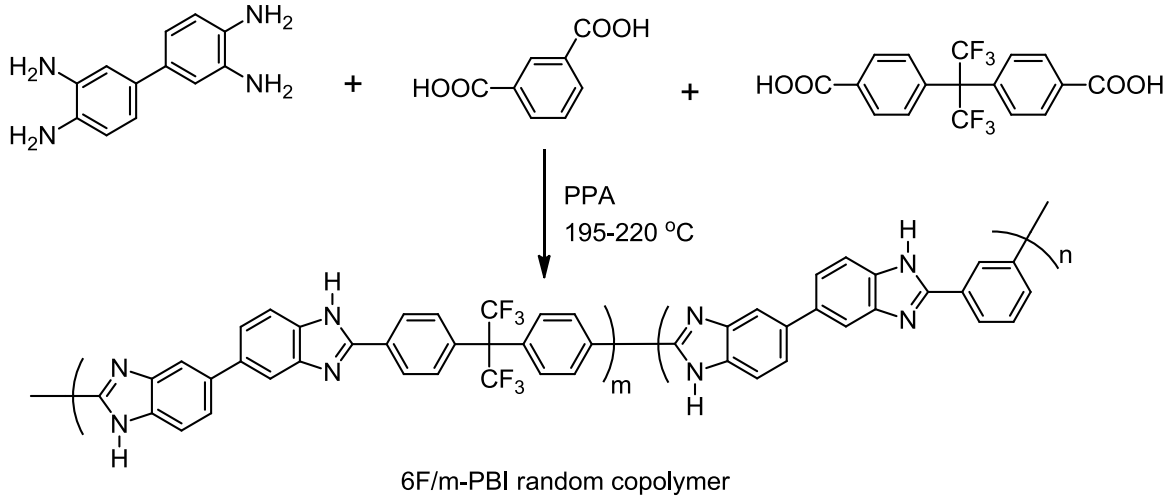

Figure 5.1 Synthetic scheme of 6F/m-PBI random copolymer.

5.2.3 PBI Dense Film Preparation

The optimized PBI dense film preparation procedure [6,8-9] described in our former work (Chapter 4, section 4.3.2) is followed here. In brief, 1.000 g PBI powders were mixed with around 30 ml N,N-dimethylacetamide (DMAc) in a 100 ml round bottom flask and then refluxed for 2-3 hours until most polymers were dissolved. After refluxing, the undissolved polymers, if any, were removed by centrifugation at 6000 rpm

for 0.5 hour to obtain clear PBI solution. Dense PBI films were prepared by solution casting under nitrogen atmosphere. The PBI solutions were transferred to a glove bag and three evacuation/nitrogen purge cycles were applied before casting. The PBI membranes were cast by carefully pouring the solution onto a clean glass substrate. After casting, the wet films were pre-dried under nitrogen atmosphere on a hot plate at approximately 40℃ (hot plate temperature) overnight to remove the solvent. Then the films were dried in vacuum oven at 110℃ overnight.

5.2.4 Characterization

^{1}H NMR spectra were recorded on a Varian Mercury 400 spectrometer. FTIR spectra were recorded on a PerkinElmer Spectrum 100 FT-IR spectrometer with a three reflection diamond/ZnSe crystal. The inherent viscosities (IV's) of the polymer samples were measured with a Cannon Ubbelohde viscometer at a polymer concentration of 0.2 g/dL in concentrated sulfuric acid (96 wt%) at 30℃. Thermogravimetric analysis (TGA) thermograms were obtained using TA Q5000 IR Thermogravimetric Analyzer at a heating rate of 10℃ min^{-1} under nitrogen flow (20 ml/min). The densities of the PBIs were measured by a Micromeritics Accupyc 1330 gas displacement pycnometer using 99.999% purity helium at ambient conditions. The solubility of PBIs was evaluated at both ambient and refluxing conditions. At ambient temperature, the PBIs were mixed with respective solvent and shaken on a Wrist Action shaker for more than 48 hours. At high temperature, the PBI was mixed with respective solvent and then refluxed for 4~6 hours.

5.2.5 Gas Permeation Characterization

The PBI membranes were tested in a custom stainless steel housing using high temperature o-rings in a constant-volume variable-pressure test system. The module was configured for continuous feed gas flow using a dip tube and use of vacuum on the permeate side of the module housing for the permeance measurement. The pure gas permeation experiments were performed with H_2, CO_2, and N_2 at feed pressures and operating temperatures from 20 to 50 psia and 30 to 250 °C, respectively. A 1 °C/min temperature ramp rate was typically used in this work. The upstream and downstream pressures were measured using high accuracy (± 0.25 % FS) pressure transducers (MKS Instruments, Inc.). The permeance (GPU) was calculated from the slope of the linear part of the permeate pressure rise versus time curve using Eq. (1).

$$Permeance, P = 10^6 \frac{dp}{dt} \left(\frac{22400\ V}{R\ T\ \Delta p\ A}\right) \quad (1)$$

where dp/dt (Torr/sec) is the pressure rise; R (62.363 Torr L K^{-1} mol^{-1}) is the universal gas constant, V (L) is the downstream volume; Δp (cmHg) is the pressure difference between membrane upstream and downstream side; T(K) is the permeate temperature; and A (cm^2) is the effective membrane surface area. The material permeability was calculated using the film thickness data obtained on the tested sample using SEM. The ideal selectivity for a gas pair is calculated by taking the ratio of their gas permeances.

5.3 Results and Discussion

5.3.1 Polymer Synthesis

PPA has been widely used in PBI polymerizations since it could be used as both solvent and dehydrating agent and could produce high molecular weight (or IV) polymers [10, 11]. Herein, PPA was also investigated in our study for both homopolymer (6F-PBI)

and random copolymer (6F/m-PBI copolymer) synthesis and the results are shown in Table 5.1. The synthetic details of 6F-PBI homopolymerization in PPA have been studied by several research groups [7,12]. A modified multi-step temperature profile was also applied here and high molecular weight 6F-PBI homopolymer (IV=1.40 dL/g) was produced. A series of 6F/m-PBI random copolymers (6F: m, mol:mol, 50:50-10:90) were also prepared by adjusting the feed ratio of two different diacid monomers (6F-diacid vs. IPA). Since the monomer charge (~8.3 wt%) for a typical m-PBI homopolymerization in PPA is much higher than that for 6F-PBI (~3.0 wt%), the monomer charge for the random copolymerization was gradually increased (from 4.74 wt% to 6.10 wt%) as the increase of the ratio of m-PBI in final random copolymers in order to achieve high reactivity and high polymer molecular weight [7, 13]. High polymerization temperature (220 °C) and long reaction time (> 10 hrs. at 220 °C) were also applied to increase the reaction conversion. All the final copolymer products synthesized exhibited high IV's, indicating relatively high polymer molecular weight.

Table 5.1 Synthetic details of 6F/m-PBI random copolymers.

Polymer	Monomer Charge (wt%)	Polymerization Temperature (°C)	Polymerization Time (h)	IV (dL/g)
6F-PBI	2.89	200; 210; 220	17; 17; 24	1.4
6F/m-PBI (50:50)	4.74	195; 220	17; 15	1.96
6F/m-PBI (25:75)	5.62	195; 220	17; 20	2.22
6F/m-PBI (10:90)	6.1	195; 220	17; 10	1.26

5.3.2 Characterizations

As shown in Figure 5.2, the FTIR spectra of PBI derivatives were recorded and exhibited common absorption at 3500-2800 cm^{-1}, 1600 cm^{-1}, 1430 cm^{-1}, and 1410 cm^{-1}. The broad band at ~3150 cm^{-1} corresponds to the stretching vibration of hydrogen

bonded N-H…H groups. The region 1650-1400 cm^{-1} is the characteristics of benzimidazole and these bands were attributed to the C=C and C=N stretching, in-plane ring vibration of benzimidazole as well as imidazole ring breathing mode. In the spectrum of 6F-PBI homopolymer, broad absorption peaks at 927-969 cm^{-1} and 1104-1268 cm^{-1} were observed, which were attributed to C-F stretching vibration. In case of 6F/m-PBI random copolymers, increasing signal strength at these C-F stretching vibration band were clearly observed with the increasing component ratio of 6F-PBI in final random copolymers. All of the PBIs were also characterized by ^{1}H-NMR and the results were shown in Figure 5.3. Some common proton peaks representing the benzimidazole unit were observed such as imidazole protons (H_4; 12.7-13.5 ppm) and biphenyl protons (H_1, H_2, and H_3; 7.5-8.2 ppm). Decreasing signal strength at one m-PBI characteristic peak (H_7; 9.13 ppm) was clearly observed with the increasing component ratio of 6F-PBI in the whole polymers. All of the characterization confirmed the successful preparation of 6F-PBI and the 6F/m-PBI random copolymers with different component ratios.

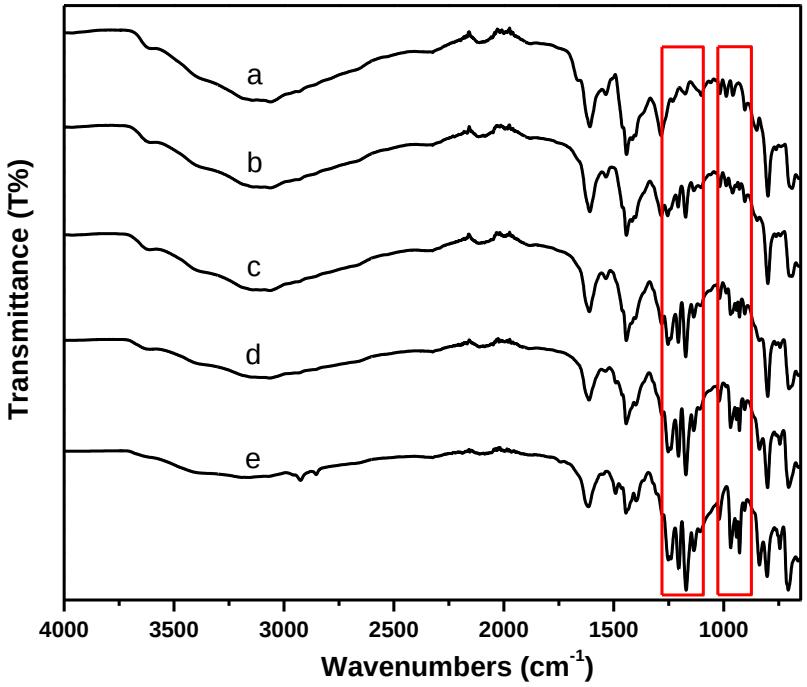

Figure 5.2 FTIR spectra of PBI derivatives (a: m-PBI; b: 6F/m-PBI copolymers (10:90); c: 6F/m-PBI copolymers (25:75); d: 6F/m-PBI copolymer (50:50); e: 6F-PBI).

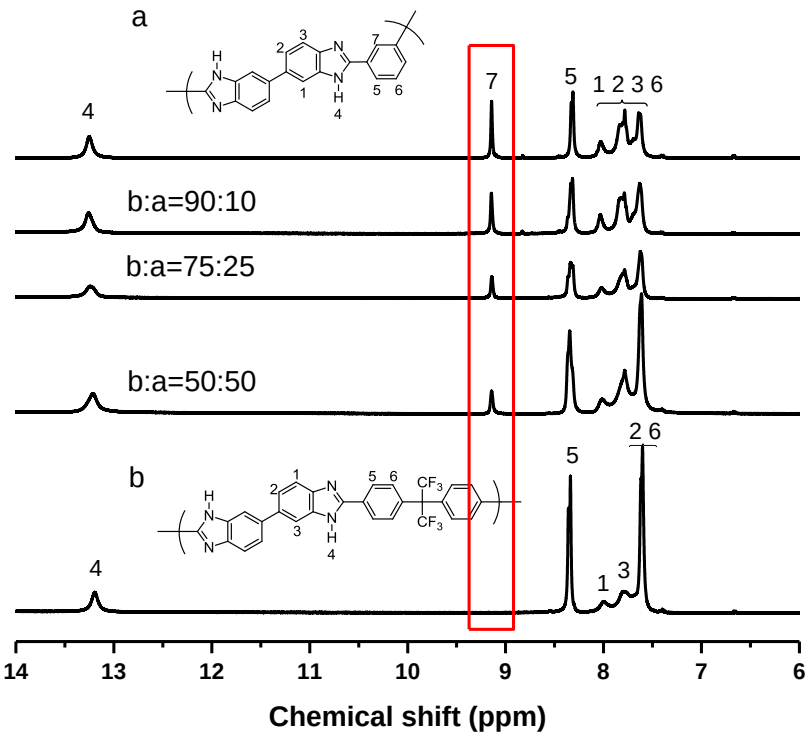

Figure 5.3 ^{1}H-NMR spectra of m-PBI, 6F-PBI, and 6F/m-PBI copolymers (6F:m=10:90, 25:75, 50:50).

The solubility characteristics of the PBIs were determined in two different conditions (a. 1.5 wt% and 5.0 wt% polymer concentrations at ambient temperature; b. 5.0 wt% polymer concentration at reflux temperature) and the results are given in Table 5.2. All the PBIs were soluble in concentrated sulfuric acid at ambient conditions. These polymers also dissolved or partially dissolved in selected polar aprotic solvents such as DMAc and NMP. 6F-PBI was reported to exhibit much better solubility than m-PBI in these solvents, which could be attributed to the introduction of bulky, flexible fluorinated functional groups into the polymer main chain [7,12]. As the molar ratio of 6F-PBI in the random copolymers increased from 50% to 90%, the solubility of corresponded polymers

also slightly increased. All the PBIs were insoluble in common organic solvents such as THF and MeOH.

Table 5.2 Solubility characteristics of PBI derivatives.

Polymer	Inherent Viscosity	Feed Ratio (6F:m)		Ambient temperature								Reflux temperature	
			H_2SO_4	DMAc/LiCl		DMAc		NMP		THF	MeOH	DMAc/LiCl	DMAc
			1.5[a]	1.5[a]	5[a]	1.5[a]	5[a]	1.5[a]	5[a]	1.5[a]	1.5[a]	5[a]	5[a]
m-PBI	1.97	N/A	++	+	+	+	+	+	+	-	-	++	+
6F/m-PBI	1.26	10:90	++	++	++	++	+	++	+	-	-	++	+
6F/m-PBI	2.22	25:75	++	++	++	++	+	++	+	-	-	++	++
6F/m-PBI	1.96	50:50	++	++	++	++	+	++	+	-	-	++	++
6F-PBI	1.40	N/A	++	++	++	++	++	++	++	-	-	++	++

a. Weight percentage of polymer in solvent (wt%).

Thermal stabilities of PBIs were characterized by TGA and the results are shown in Figure 5.4. The initial weight loss of all PBIs in the temperature range of r.t. to ca. 250 °C were due to the moisture (water) absorbed by polymer powders. It can be seen that m-PBI possessed the largest amount of water moisture as compared with other PBI derivatives, which is contributed to the hydrophilic characteristics of benzimidazole ring. As for others, due to the existence of hydrophobic fluorine-containing functional groups (-CF_3), the moisture contents absorbed became smaller. Also, all the polymers are thermally stable up to at least 450 °C (less than 0.1 wt% weight loss), which are ideal for our desired gas permeation testing (testing temperature were up to 250 °C). The thermal stability of m-PBI is the highest among all the candidates, which is due to its rigid structure and strong H-bonding within polymer chains.

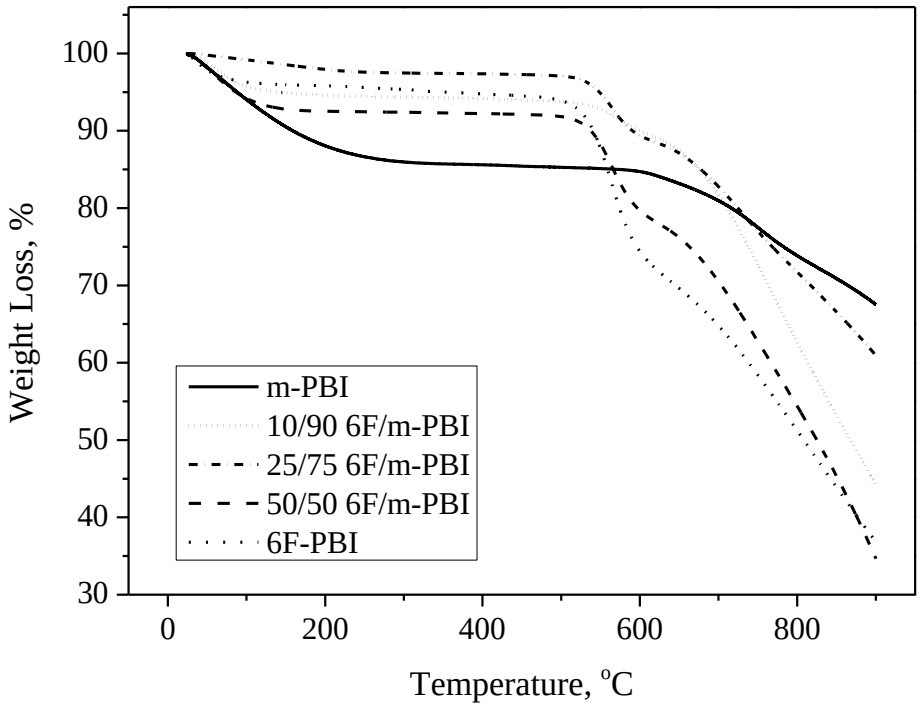

Figure 5.4 Thermal stability of m-PBI, 6F-PBI, and 6F/m-PBI copolymers (6F:m=10:90, 25:75, 50:50) measured by TGA.

5.3.3 Gas Permeation Characterization

5.3.3.1 Gas Permselectivity at Elevated Temperatures

Pure gas permeation data was obtained at varying feed pressures and operating temperatures for the m-PBI, 6F-PBI, and 6F/m-PBI copolymer films. Table 5.3 reports the gas permeation properties of these polymer samples measured at 250 °C and 50 psia. The highest H_2 permeability and lowest H_2/CO_2 and H_2/N_2 selectivities were obtained for 6F-PBI whereas lowest H_2 permeability and highest H_2/CO_2 and H_2/N_2 selectivities were obtained for m-PBI. As the ratio of m-PBI in the 6F/m-PBI copolymers increased from 50 to 90, the H_2 permeability decreased while H_2/CO_2 and H_2/N_2 selectivities increased monotonously. The rigid macromolecular structure of m-PBI with efficient polymer

chain packing is responsible for the polymer's increasing H_2 selectivity over CO_2 and N_2. This tightly packed structure is also responsible for polymer's decreasing H_2 permeability. On the other hand, the presence of bulky $–CF_3$ groups on 6F-PBI can efficiently disrupt the chain packing and significantly improve H_2 permeability, which can be observed from the 6F/m-PBI copolymers. In addition to chain disruption, high rotation mobility of $–C(CF_3)_2$- linkages can also enhance H_2 permeability at elevated temperatures. Figure 5.5 also clearly demonstrates the effect of 6F-PBI ratio (or hexafluoroisopropylidene ratio) in the PBI copolymers on the final gas permselectivity characteristics. In our previous work, incorporation of large high mobility groups in the PBI molecular structure caused significant improvement in H_2 permeability but at the expense of loss in H_2 selectivity over CO_2 and N_2 [6]. Thus, this copolymerization strategy provides a possible solution to control the concentration of these large high mobility groups in the PBI polymers. Then the chain packing efficiencies can be relatively controlled to tune the gas permselectivity within PBI polymers, as evidenced by the trend observed from our gas permeation testing data.

Table 5.3 Molar volume, fractional free volume, gas permeation properties of 6F-PBI, m-PBI, and 6F/m-PBI co-polymers measured at 250 °C and 50 psia.

Polymer	Molar Volume, cm^3/mol	FFV[a]	H_2 Permeability[b], barrer	Selectivity[b]		
				H_2/CO_2	H_2/N_2	CO_2/N_2
6F-PBI	362	0.123	997	5.17	18.7	3.62
6F/m-PBI (50:50)	295	0.121	371	8.21	32.2	3.92
6F/m-PBI (25:75)	250	0.079	219	11.1	45.8	4.11
6F/m-PBI (10:90)	232	0.081	136	13.6	52.7	3.88
m-PBI	236	0.146	76.8	23	98.3	4.26

a. Fractional free volume (FFV) was calculated using polymer density and Bondi's group contribution approach [14,15].
b. Data present were based on pure gas permeation testing.

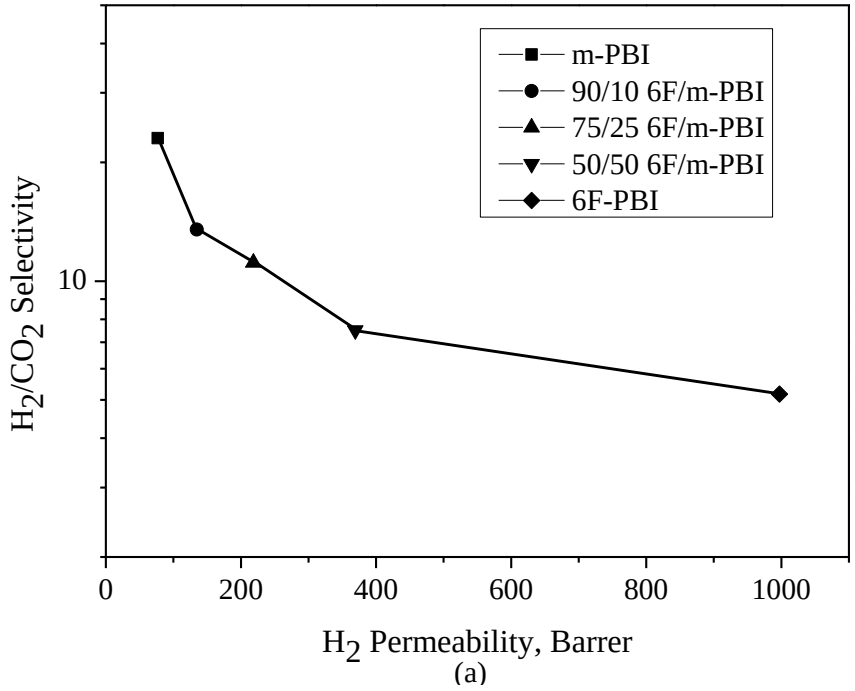

(a)

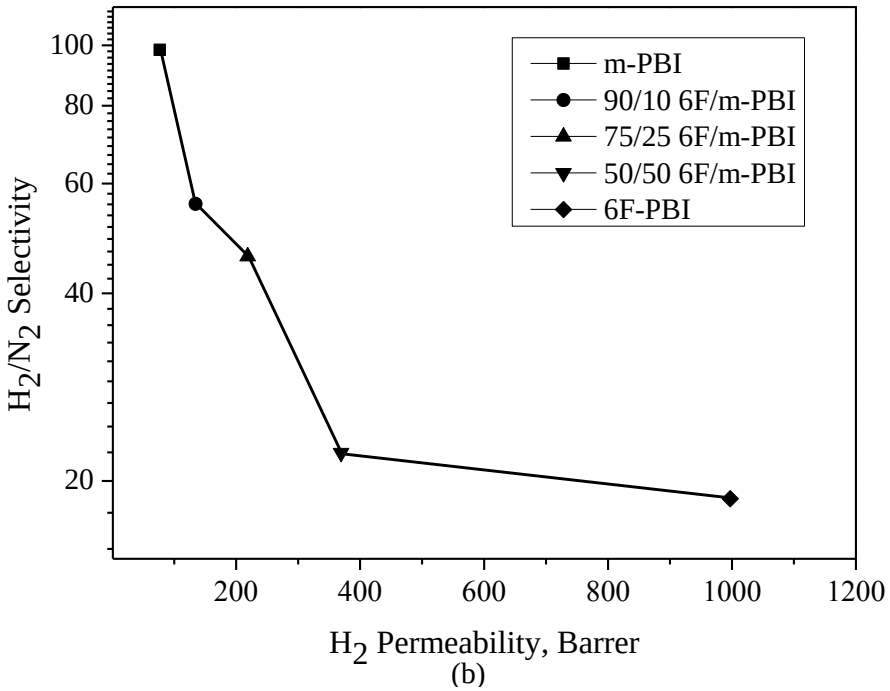

(b)

Figure 5.5 Effect of hexafluoroisopropylidene concentration on gas permselectivity (a. H_2/CO_2 permselectivity; b. H_2/N_2 permselectivity) of PBI derivatives (data was collected at 250 °C and 50 psia).

It is known that free volume concentration and architecture (both size & distribution) within glassy polymers play very important roles in deciding a materials' gas permselectivity characteristics. These data are beneficial for us to understand the change in polymer morphology (or chain packing efficiency) within the PBI polymers and to build up structure-property relationships for the future design of novel PBI materials. Herein, in this work, fractional free volume (FFV) measurement was employed as a quick and easy method to evaluate the free volume concentrations in PBI materials. The FFV's of 6F-PBI, m-PBI, and their random copolymers were calculated based on their molar volume (cm^3/mol) and bulk density (g/cm^3) (measured at ambient conditions) and the final results are shown in Table 5.3. FFV variations were observed within these materials; however, no correlation was found between the FFV data and the measured gas permeation performance. A more accurate free volume measurement method such as positron annihilation lifetime spectroscopy (PALS) would be useful in future to acquire more detailed information on the free volume structure of these materials and correlate them to the PBI chemical structures.

5.3.3.2 Effect of Temperature on Gas Permselectivity

Figure 5.6 shows the H_2 permeability as a function of operating temperature for m-PBI, 6F-PBI and 6F/m-PBI copolymers. The H_2 permeability increased monotonously as operating temperature increased from near ambient to 250 °C. The increase in H_2 permeability as temperature increased from ambient to 250 °C was dependent on the polymer structure and correlated well with the ratio of m-PBI in the copolymers. Quantitatively, the impact of temperature on H_2 permeability can be reflected as activation energy of permeability calculated using Eq. (2).

$$P = P_0 e^{-E_p/RT} \quad (2)$$

where E_p (KJ/mol) is the activation energy for permeability, R (8.314 J/mol) is the universal gas constant and T (K) is temperature. The activation energy for permeability calculated from H_2 permeability versus temperature was shown as follows: m-PBI= -19.35 KJ/mol; 6F/m-PBI (10:90) = -17.07 KJ/mol; 6F/m-PBI (25:75) = -16.02 KJ/mol; 6F/m-PBI (50:50) = -15.23 KJ/mol; and 6F-PBI= -8.36 KJ/mol. This decrease in activation energy shows that the lower energy was required for H_2 diffusion through 6F-PBI than m-PBI. This can be attributed to chain disruption caused by the presence of the hexafluoroisopropylidene groups on 6F-PBI as discussed before.

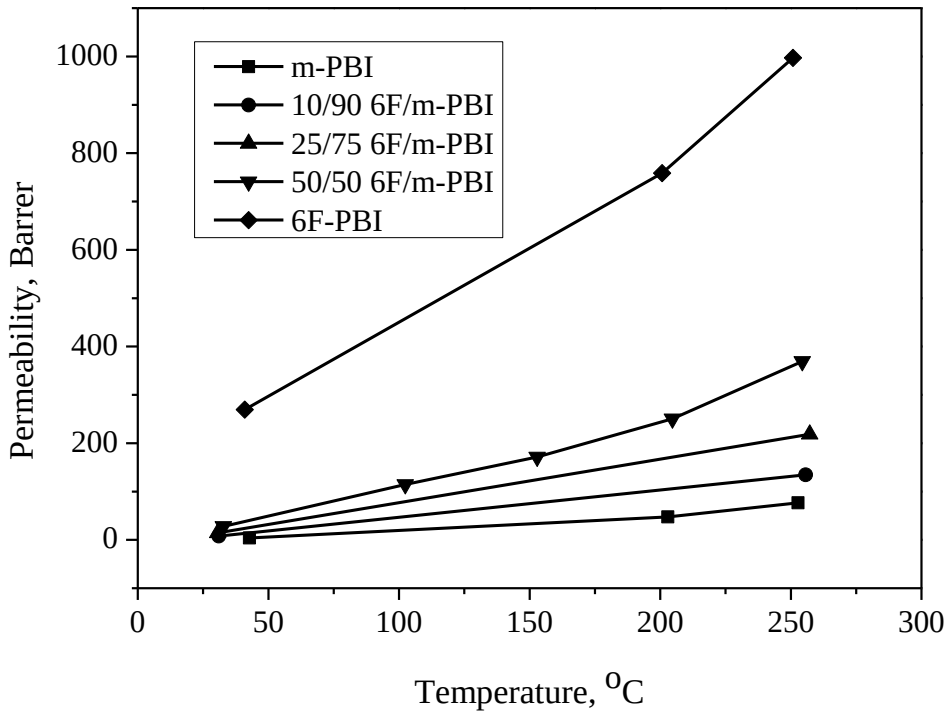

Figure 5.6 H_2 permeability (pure gas) as a function of operating temperature for m-PBI, 6F-PBI and 6F/m-PBI copolymers. Data obtained at feed pressure of 50 psia.

As shown in Figure 5.7 and Figure 5.8, the improvements in H_2 permeability by incorporation of hexafluoroisopropylidene groups in the PBI materials led to decrease in H_2/CO_2 and H_2/N_2 selectivities. The m-PBI is very selective for H_2 over CO_2 and N_2 with selectivities of approximately 23 and 100, respectively at 250 °C. This high H_2 perm-selectivity of m-PBI can be attributed to tight chain packing in rigid m-PBI polymers. Again incorporation of 6F-PBI groups disrupted the chain packing and reduced H_2 selectivities over N_2 and CO_2. Interestingly, H_2/N_2 selectivity decreased with temperature whereas H_2/CO_2 selectivity increased with temperature. Some explanations for that were proposed in our former work [6] based on PBI materials (also discussed in Chapter 4, section 4.3.3.3). However, exact reason for this diffusion behavior is not fully understood at this time.

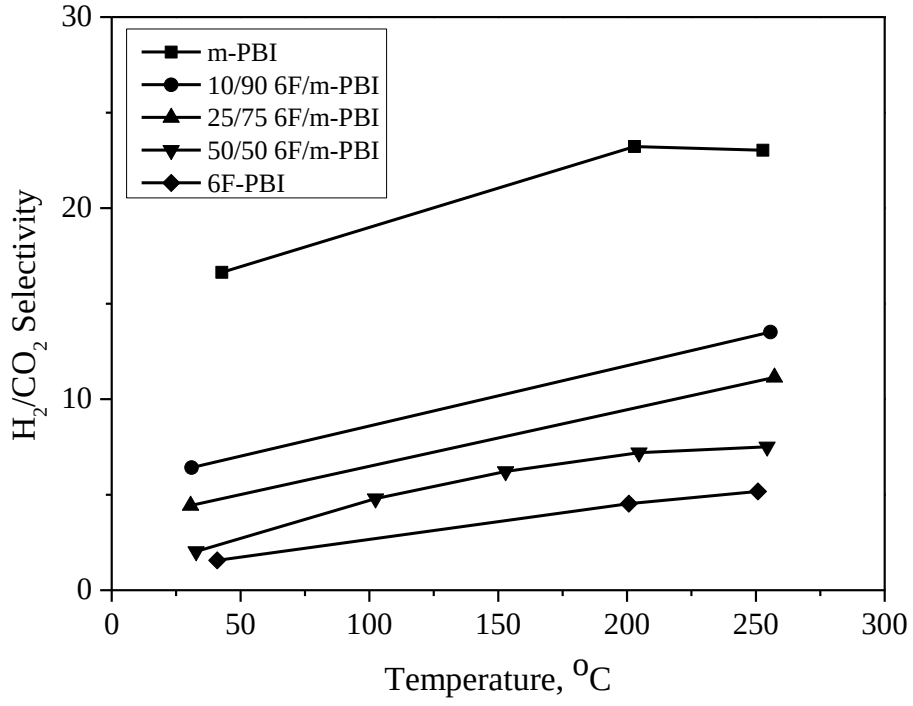

Figure 5.7 H_2/CO_2 selectivity (pure gas) as a function of operating temperature for m-PBI, 6F-PBI and 6F/m-PBI copolymers.

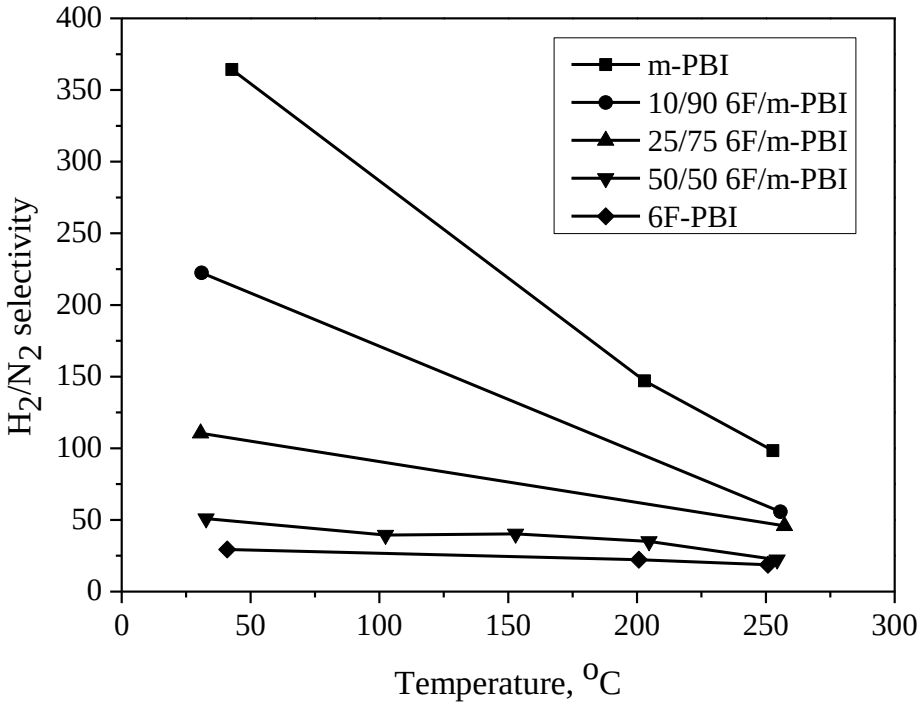

Figure 5.8 H_2/N_2 selectivity (pure gas) as a function of operating temperature for m-PBI, 6F-PBI and 6F/m-PBI copolymers. Data obtained at feed pressure of 50 psia.

5.3.3.3 Effect of Pressure on Gas Permselectivity

Figure 5.9 shows the effect of feed pressure (transmembrane pressure) on H_2 permeability of the m-PBI, 6F-PBI, and 6F/m-PBI co-polymers at 250 °C. The H_2 permeability was constant as a function of pressure for all membranes tested, indicating the absence of viscous flow and correspondingly, defects in the tested dense membranes.

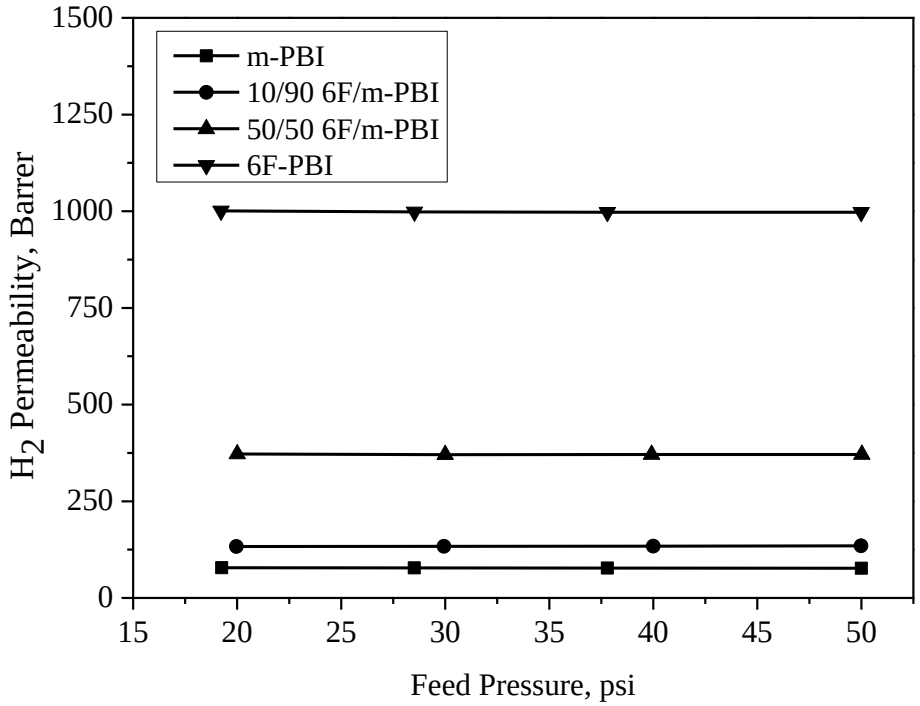

Figure 5.9 H_2 permeability as a function of feed pressure for m-PBI, 6F-PBI and 6F/m-PBI copolymers obtained at 250 °C.

5.3.3.4 Comparison to Other Polymeric Membranes

Tremendous effort has been spent in the past few decades exploring the effect of polymer chemistries on materials' respective gas permselectivity characteristics. These results were collected and organized by Robeson to draw a series of upper bound curves based on different gas pairs [16, 17]. Figure 5.10 shows Robeson's upper bound curve for the H_2/CO_2 gas pair. Materials exhibiting gas permselectivities beyond the upper bound curve (located at the upper right area of the figure) are usually considered as promising candidates for potential industrial uses. It is noteworthy that all of this data collected from the literature presented in the figure was measured at ambient conditions (ca. 35 °C) due to the materials' low tolerance to high temperature testing environments (> 150 °C),

which is not suitable for our proposed applications as discussed in the former section. Also, the gas separation performance of m-PBI, 6F-PBI and their random copolymers measured in this work were incorporated into the Robeson curve (as shown in Figure 5.10). The permselectivities of all PBIs at 250 °C exceeded the upper bound, indicating their great potential as material candidates for industrial H_2/CO_2 separation from syngas at elevated temperatures.

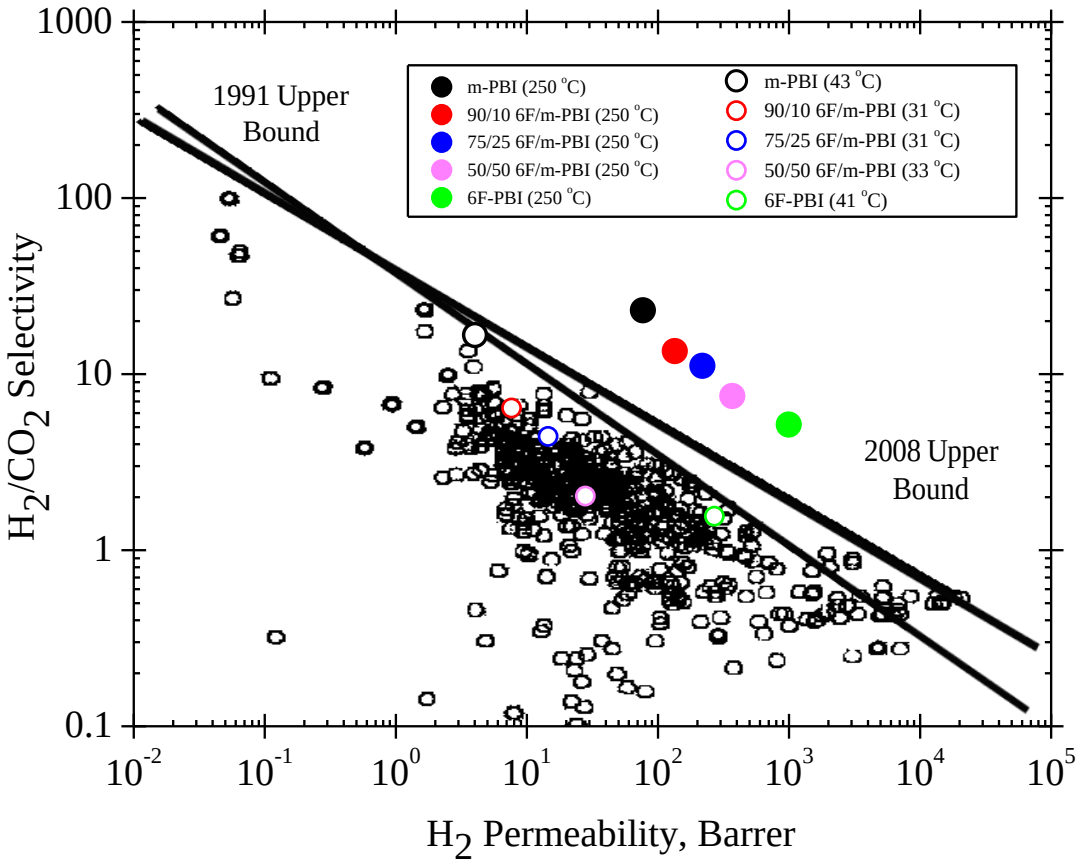

Figure 5.10 Robeson plot comparing the PBI derivative membranes with other polymeric membranes tested for the H_2/CO_2 separation. The lines represent the 1991 and 2008 Robeson upper bounds and the open circle represents literature data for polymeric gas separation membranes [16, 17].

5.4 Conclusions

A series of PBI-based random copolymers containing bulky and flexible hexafluoroisopropylidene functional moieties were successfully synthesized via solution polymerization in PPA in order to compare their gas separation performance (gas permeability and selectivity) with those of commercial m-PBI and formerly synthesized 6F-PBI. Polymerization conditions were carefully optimized in order to achieve high polymer molecular weight. The successful synthesis of these random copolymers was confirmed by FTIR and ^{1}H NMR. It was found that the polymer solubility increased as the increase of 6F-PBI ratio in the copolymer. The gas permeation testing results showed that with the increase of 6F-PBI ratio in the copolymer materials, the H_2 permeability of these materials gradually increased whereas the H_2 selectivity over CO_2 and N_2 decreased, which could be attributed to the increasing concentration of bulky and flexible hexafluoroisopropylidene functional groups. The random copolymerization method was found to be a promising method to achieve better control on the gas separation performance and also a better balance between gas permeability and selectivity of PBI-based materials.

5.5 References

[1] N. W. Ockwig; T. M. Nenoff, *Chem Rev* **2007**, 107, 4078.

[2] K. A. Berchtold; R. P. Singh; J. S. Young; K. W. Dudeck, *J Membr Sci* **2012**, 415, 265.

[3] S. C. Kumbharkar; Y. Liu; K. Li, *J Membr Sci* **2011**, 375, 231.

[4] D. R. Pesiri, B. Jorgensen; R. C. Dye, *J Membr Sci* **2003**, 218, 11.

[5] High temperature polymer-based membrane systems for pre-combustion carbon dioxide capture. http://permalink.lanl.gov/object/tr?what=info:lanl-repo/lareport/LA-UR-13-26453 (accessed January 15, 2014).

[6] X. Li; R. P. Singh; K. W. Dudeck; K. A. Berchtold; B. C. Benicewicz, *J Membr Sci* submitted.

[7] G. Qian; B. C. Benicewicz, *J Polym Sci Part A: Polym Chem* **2009**, 47, 4064.

[8] X. Li; G. Qian; X. Chen; B. C. Benicewicz, *Fuel Cells* **2013**, 13, 832.

[9] X. Li; X. Chen; B. C. Benicewicz, *J Power Sources* **2013**, 243, 796.

[10] L. Xiao; H. Zhang; E. Scanlon; L. S. Ramanathan; E. -W. Choe; D. Rogers; T. Apple, B. C. Benicewicz, *Chem Mater* **2005**, 17, 5328.

[11] S. Yu; H. Zhang; L. Xiao; E. -W. Choe; B. C. Benicewicz, *Fuel Cells* **2009**, 9, 318.

[12] S. -W. Chuang; S. L. -C. Hsu, *J Polym Sci Part A: Polym Chem* **2009**, 9, 318.

[13] H. Zhang, Novel phosphoric acid doped polybenzimidazole membranes for fuel cells. Ph.D. Thesis, Rensselaer Polytechnic Institute, 2004.

[14] D. W. van Krevelen; K. te Nijenhuis, in *Properties of Polymers, 4th Edition*. Elsevier: 2009.

[15] A. Bondi, *J Phys Chem –Us* **1964**, 68, 441.

[16] L. M. Robeson, *J Membr Sci* **1991,** 62, 165.

[17] L. M. Robeson, *J Membr Sci* **2008,** 320, 390.

CHAPTER 6

SUMMARY AND OUTLOOK

Polybenzimidazoles (PBIs), an old class of condensation polymers which were commercialized decades ago, have been recently found to exhibit very interesting and attractive properties in some energy related areas, such as fuel cells and gas separation membranes. Facing the challenge of providing sustainable energy to a growing global population and the increasing concern of environmental protection, it is believed that PBI will experience a renewed vigor of investigation in the near future.

In the first part of this dissertation, two novel PBI derivatives (phenylindane-containing PBI & fluorine-containing PBI) were designed and synthesized for the first time. Conprehensive studies on these new polymers (i.e., monomer synthesis, optimization of polymerization condition, membrane fabrication, acid adsorption behavior, membrane proton conductivities, and fuel cell performance) were performed to evaluate their potential value to be used in the fuel cell industry. Prior to this work our group, as well as research teams around the world, have shown that PBI chemistry and membrane processing methods are determining factors in their ultimate properties in fuel cell applications. Therefore, specific functionalities were designed and incorporated into the PBI backbones in order to improve materials processability (or organo-solubility) and oxidative stability as compared to commercial m-PBI. Additionally, different membrane fabrication methods were explored to achieve acid doped polymer membranes for fuel cells. The traditional acid imbibing method was found to be suitable for high quality membrane fabrication and the resulting membranes exhibited high acid doping levels while maintaining good mechanical properties. Ultimately, by using an optimzied “acid dipping” hot press procedure, these membranes were fabricated into MEAs and were able

to achieve comparable fuel cell performance as the membranes prepared by the "PPA process".

One important concern in polymer based fuel cell membranes is their stabilities and reliabilities for long term uses. For future work, to fully evaluate the potential for these materials in realistic fuel cell applications, long-term fuel cell studies (e.g., voltage loss at constant/variable current densities, stability testing under start-up/shut-down operation cycle, long-term acid loss measurements, and membrane mechanical failure analysis) should be pursued. By obtaining these data, we will be able to understand and compare different PBI chemistries and how they affect membrane's final performance in desired fuel cell applications.

In the second part of this dissertation, the effect of PBI chemistry on a films gas permselectivity characteristics was investigated for the first time in a systematic manner. A series of new PBI materials (homo- & co-polymers) were successfully synthesized, characterized, and fabricated into high quality films, and tested for high temperature gas separation. By tuning the PBI chemistry at a molecular level, we were able to change several of physicochemical properties (e.g., thermal stability, organo-solubility, polymer density) and most importantly, gas separation properties. We were able to effectively suppress the polymer chain packing and largely improve the gas permeability of PBI membranes. This work introduced a new method to tune and control the membrane gas permselectivity behavior, since most of the previous efforts were focused on adjusting these properties by phyical and engineering methods.

In order to fully understand the structure-property relationships in PBI materials and further improve their gas separation performance, future efforts should be considered in the following areas:

1) More accurate and comprehensive free volume measurement techniques are needed to understand the morphology changes within PBI materials, with the understanding that free volume is playing a critical role in deciding the gas permselectivity characteristics of a membrane. One proposed measurement technique is Positron Annhiliation Lifetime Spectroscopy (PALS) since it can provide detailed information of polymer free volume architecture (from concentraion to size and distribution) within polymer materials. Additionally, it can also measure the polymer free volume change derived from temperature, time, and the film thicknesses. By obtaining this information, we will be able to build a better understanding on how to correlate the primary chemical structure to final gas separation performance in PBI materials, which will be valuable for next generation PBI material design.

2) One important conclusion we learned from this work is that PBI chain packing can be effectively supressed by incorporating various bulky, flexible, or frustrated functionalities into polymer main chains. However, it is also realized that high gas permeabilities were achieved at the expense of gas selectivities. Therefore, a new approach could be envisioned which effectively controls the polymer morphology to achieve slightly disrupted chain packing structure which may be important to ultimately improve PBI's gas separation performance. Random copolymerization provides a possible route to achieve a better control on the final gas separation properties of polymers. Instead of using co-monomers containing bulky flexible functional groups

(such as hexafluoroisopropylidene as discussed in Chapter 5), another proposed method would be incoporating rigid aromatic monomers. It is expected the slight difference in symmetry of polymer repeat units induced by copolymerization will produce a slightly disrupted chain packing and then produce high gas permeabilities without lossing too much selectivity. Some preliminary work has already been performed on this research and the results will be presented in future publications.

3) Although PBI-based membranes possess several advantages over conventional separation techniques, their further development has been constrained by a performance tradeoff between the gas permeability and selectivity. One possible solution is the Mixed Matrix Membranes (MMMs, polymer matrix mixed with inorganic fillers), which synergistically combine polymer processability with superior separation characteristics of inorganic fillers and exhibit very promising gas separation performance. So far, very little work has been done on investigating PBI-based MMMs for hydrogen separation applications. The future work will focus on introducing novel synthetic approaches to modify both polymer and inorganic fillers in order to improve the compatibility of organic and inorganic interface of MMMs and to achieve improved hydrogen production performance. For instance, a series of inorganic fillers such as zeolite with different sizes, shapes, and porosities could be selected as candidates to tune the gas perm-selectivity of corresponding membranes.

In conclusion, it is reasonable to expect additional efforts to fully explore the PBI polymers and to obtain more comprehensive structure-property-performance understanding of these materials would result in considerable property improvements. With a better and more accurate control of PBI film or membrane properties, it is

expected that researchers will provide potential cost-effective solutions for both fuel cell and gas separation related applications.

APPENDIX A – PERMISSION TO REPRINT

Title: Synthesis and properties of phenylindane-containing polybenzimidazole (PBI) for high-temperature polymer electrolyte membrane fuel cells (PEMFCs)

Author: Xin Li,Xiaoming Chen,Brian C. Benicewicz

Publication: Journal of Power Sources

Publisher: Elsevier

Date: 1 December 2013

Order Completed

Thank you very much for your order.

This is a License Agreement between Xin Li ("You") and Elsevier ("Elsevier"). The license consists of your order details, the terms and conditions provided by Elsevier, and the payment terms and conditions.

Get the printable license.

License Number	3307981136949
License date	Jan 14, 2014
Licensed content publisher	Elsevier
Licensed content publication	Journal of Power Sources
Licensed content title	Synthesis and properties of phenylindane-containing polybenzimidazole (PBI) for high-temperature polymer electrolyte membrane fuel cells (PEMFCs)
Licensed content author	Xin Li,Xiaoming Chen,Brian C. Benicewicz
Licensed content date	1 December 2013
Licensed content volume number	243
Number of pages	9
Type of Use	reuse in a thesis/dissertation
Portion	full article
Format	both print and electronic
Are you the author of this Elsevier article?	Yes
Will you be translating?	No
Title of your thesis/dissertation	Stucture-property relationships in benzimidazole materials for fuel cells and gas separation applications
Expected completion date	Mar 2014
Estimated size (number of pages)	170
Elsevier VAT number	GB 494 6272 12
Permissions price	0.00 USD
VAT/Local Sales Tax	0.00 USD / 0.00 GBP
Total	0.00 USD

ORDER MORE... CLOSE WINDOW

Title:	Synthesis and Characterization of a New Fluorine-Containing Polybenzimidazole (PBI) for Proton-Conducting Membranes in Fuel Cells
Author:	X. Li,G. Qian,X. Chen,B. C. Benicewicz
Publication:	Fuel Cells
Publisher:	John Wiley and Sons
Date:	Aug 30, 2013

Order Completed

Thank you very much for your order.

This is a License Agreement between Xin Li ("You") and John Wiley and Sons ("John Wiley and Sons"). The license consists of your order details, the terms and conditions provided by John Wiley and Sons, and the payment terms and conditions.

Get the printable license.

License Number	3307980840760
License date	Jan 14, 2014
Licensed content publisher	John Wiley and Sons
Licensed content publication	Fuel Cells
Licensed content title	Synthesis and Characterization of a New Fluorine-Containing Polybenzimidazole (PBI) for Proton-Conducting Membranes in Fuel Cells
Licensed copyright line	Copyright © 2013 WILEY-VCH Verlag GmbH & Co. KGaA, Weinheim
Licensed content author	X. Li,G. Qian,X. Chen,B. C. Benicewicz
Licensed content date	Aug 30, 2013
Start page	832
End page	842
Type of use	Dissertation/Thesis
Requestor type	Author of this Wiley article
Format	Print and electronic
Portion	Full article
Will you be translating?	No
Total	0.00 USD

ORDER MORE... CLOSE WINDOW